

QUANTIFYING CONFINEMENT EFFECTS
IN
ICE IMPACT LOADS

by

©Dan Oldford, B.Eng, P.Eng

A thesis submitted to the School of Graduate Studies
In partial fulfillment of the requirements for the degree of
Master of Engineering

Faculty of Engineering and Applied Science
Memorial University of Newfoundland

May 2016

St. John's

Newfoundland and Labrador

Canada

Page intentionally left blank

Abstract

Ships and offshore structures, that encounter ice floes, tend to experience loads with varying pressure distributions within the contact patch. The effect of the surrounding ice adjacent to that which is involved in the contact zone has an influence on the effective strength. This effect has come to be called confinement. A methodology for quantifying ice sample confinement is developed, and the confinement is defined using two non-dimensional terms; a ratio of geometries and an angle. Together these terms are used to modify force predictions that account for increased fracturing and spalling at lower confinement levels. Data developed through laboratory experimentation is studied using dimensional analysis. The characteristics of dimensional analysis allow for easy comparison between many different load cases; provided the impact scenario is consistent. In all, a methodology is developed for analyzing ice impact testing considering confinement effects on force levels, with the potential for extrapolating these tests to full size collision events.

Acknowledgements

If I were to list all the individuals who helped me with this work, this thesis would have to be considerably longer, and considering I have aimed at keeping this a relatively short and concise document I first extend a general thank you to everyone at ABS and MUN (Memorial University of Newfoundland).

I would like to thank my father, he was a constant driver for all of us to get more education. He never got to see me obtain a degree but without the motivation he provided I would not have earned an undergraduate and definitely would not have made it to this level. And of course I have to thank my mother, who never let me forget my father's attitude towards education. Thank you.

A special thank you must be extended to several individuals whom especially helped me in this effort.

Dr. Bruce Colbourne, was my principal academic supervisor on this master's degree. He was always willing to offer help in hashing out ideas or pulling a trick or two out of his hat to solve some of the more pesky problems.

Mathew Curtis, was a lab technician at MUN during the experimentation. He helped set up the pendulum initially, offered advice and experience on how to conduct the testing, and always knew where to find tools and equipment that seems to wander off during a testing program.

Dr. Claude Daley, his energetic personality and enthusiasm for this type of research was part of the initial draw to continuing this master's degree. Dr. Daley was also very good to consult and brain storm with to come up with new ideas.

Dr. Han-Chang Yu and James Bond, Manager of ABS Harsh Environment Group and Director of ABS Shared Technology, respectively. Without their help and support this thesis may never have been realized. Dr. Yu encouraged me to push forward and get through it, and both gentlemen made the project time available for me to conduct this required research.

Regina Sopper who was a fellow graduate student at Memorial University was also a co-author on the ICETECH 2014 paper.

Last but certainly not least is Katherine Scott. Her assistance in making this a legible piece of work was truly invaluable. I also thank her for her patience with me to put up with the extended period it took me to complete this work and humoring me those nights I wished to discuss the ice testing experiments of the day.

Contents

Abstract.....	iii
Acknowledgements.....	iv
Nomenclature and Abbreviations.....	xi
1 Introduction	1
1.1 Scope and Objectives	3
1.2 Literature Review	3
1.2.1 Ice Making.....	4
1.2.2 Ice Crushing.....	4
1.2.3 Confinement	7
1.2.4 Dimensional Analysis	8
1.2.5 Summary of Literature Review	9
2 Ice Crushing Experiments.....	10
2.1 Test Apparatus	12
2.1.1 Double Pendulum	12
2.1.2 Release Angle and Contact Velocity.....	15
2.1.3 Load Cells and Associated Mounting	18
2.1.4 Power Supply / Coupler	24
2.1.5 Adjustment and Calibration	26
2.1.6 Ice Holders	30
2.1.7 Data Acquisition System	31
2.1.8 High Speed Camera	32
2.1.9 Indenters	33
2.2 Ice Samples	34
2.2.1 Ice Production	34
2.2.2 Processing of Samples for Tests:.....	35
2.3 Testing Procedure	38
2.4 Phase 1 Test plan	39
2.4.1 ICETECH 2014 Dataset.....	39
2.4.2 September 26, 2014 Dataset	40

2.5	Round 1 Results	40
3	Analysis	42
3.1	Mass	42
3.2	Velocity	43
3.3	Ice Strength	44
3.4	Confinement	47
3.4.1	Confinement Angle	47
3.4.2	Radial Confinement.....	48
3.5	Dimensional Analysis Set-up.....	49
3.5.1	Examination of C_0	52
3.5.2	Examination of ζ	53
3.6	Analysis of Data.....	53
3.7	Force Estimation	57
3.8	Confinement Angle Effects on Results.....	59
3.9	Phase 2 Tests.....	66
3.10	Comparison to Published Results	70
3.11	Predicting Full Scale Loads	75
4	Conclusions and Recommendations	78
4.1	Conclusions	78
4.2	Recommendations	79
4.2.1	Recommendations for Repeat or Expanded Pendulum Testing.....	79
4.2.2	Recommendations for Further work	80
1	References	82
	Appendix 1	86
	Appendix 2	89
	Appendix 3	107
	Appendix 4	111

List of Figures

Figure 2-1. Level of Confinement.....	12
Figure 2-2. Double Pendulum	13
Figure 2-3. Rendering of Double Pendulum	15
Figure 2-4. Pendulum Angle.....	16
Figure 2-5. Clinometer Screenshot	16
Figure 2-6. Pendulum Swing	18
Figure 2-7. Load Cell.....	19
Figure 2-8. Preload Schematic of Sensor, from (Dytran Instruments, 2001).....	20
Figure 2-9. Load Cell Sandwich	21
Figure 2-10. Small Carriage Face Plate.....	24
Figure 2-11. Power Supply/Amplifier - Front.....	25
Figure 2-12. Power Supply/Amplifier – Back	25
Figure 2-13. First calibration apparatus.....	27
Figure 2-14. Calibration run with MTS machine - Time constant = 10 seconds	28
Figure 2-15. Calibration with MTS machine - Time constant = 0.1 seconds.....	29
Figure 2-16. CAD rendering of 5cm tall ice holders	30
Figure 2-17. LabVIEW SignalExpress Voltage to Force ratio	32
Figure 2-18. Spherical Indenters	34
Figure 2-19. Ice holder, mold, and insulation	35
Figure 2-20. Weighing a 25 cm diameter X 30 cm deep ice sample.....	38
Figure 3-1. Confinement Angle	48
Figure 3-2. ζ Vs. Coefficient for first 41 tests	53
Figure 3-3. ζ Vs. Coefficient for first 41 tests - Regular Scale.....	54
Figure 3-4. Line fit to data.....	55
Figure 3-5. Values for e	56
Figure 3-6. Bounds of First 41 Data Points.....	57
Figure 3-7. Data without Confinement Angle.....	60
Figure 3-8. Prediction Spread	63
Figure 3-9. Difference	64
Figure 3-10. Predicted Forces - With and Without Confinement Angle – 35 cm Diameter samples	65
Figure 3-11. Predicted Forces - With and Without Confinement Angle – 25 cm Diameter samples	65
Figure 3-12. Predicted Forces - With and Without Confinement Angle – 15 cm Diameter samples	66
Figure 3-13. Data points including Phase 2 Tests	68

Figure 3-14. Data points including Phase 2 Tests - Transformed	69
Figure 3-15. Comparison to Other Data Points Published – 40 cm ice diameter	72
Figure 3-16. Comparison to Other Data Points Published – 100 cm ice diameter, $\sigma = 2$ MPa	74
Figure A2-1. Test No. 24 - Frame 389	95
Figure A2-2. Test No. 24 - Frame 390	96
Figure A2-3. Test No. 24 - Frame 391	97
Figure A2-4. Test No. 24 - Frame 392	98
Figure A2-5. Test No. 24 - Frame 393	99
Figure A2-6. Test No. 24 - Frame 394	100
Figure A2-7. Test No. 24 - Frame 395	101
Figure A2-8. Test No. 24 - Frame 396	102
Figure A2-9. Test No. 24 - Frame 397	103
Figure A2-10. Test No. 24 - Frame 398	104
Figure A2-11. Test No. 24 - Frame 399	105
Figure A2-12. Test No. 24 - Frame 400	106
Figure A3-1. Test No. 44 - Frame 361	108
Figure A3-2. Test No. 44 - Frame 362	109
Figure A3-3. On Screen measurement.....	110

List of Tables

Table 2-1. Load Cell Placement.....	23
Table 2-2. Power Supply/Coupler settings.....	26
Table 2-3. Round 1 results	41
Table 3-1. Test# 24 - Force Time History	46
Table 3-2. Summary of Pressures	47
Table 3-3. Values for e	56
Table 3-4. Sample Inputs	61
Table 3-5. Comparison: With or Without Confinement Angle	62
Table 3-6. Example 2 With or Without Confinement Angle	62
Table 3-7. Phase 2 tests	68
Table 3-8. Example Transformations	69
Table 3-9. Differences Timco-Frederking to Oldford	70
Table 3-10. Full Scale Prediction	76
Table 3-11. Additional Assumptions	76

Nomenclature and Abbreviations

A	Cross Sectional Area
a	Acceleration [m/s^2]
C_0	Coefficient – Ratio of impact force to possible impact energy. Shown as “ γ ” in plots.
D	Dimension
E	Youngs Modulus
e	Exponent
F	Force [N]
g	acceleration due to gravity (9.81 m/s^2)
h	height [m]
K	Constant
k	Stiffness
L_e	Effective Length
M, m	Mass [kg]
n	Number of test runs
R_i	Radius of ice sample [cm]
R_s	Radius of indenter [cm]
r	Length of Pendulum Arm
S	Standard Deviation
V	Velocity [m/s]
X	See ζ
\bar{X}	Data point value
\bar{X}	Mean
γ	See C_0
∇_s	Volume of Sphere [m^3]
ϕ	Angle from vertical – pendulum arm
σ_i	Ice strength term [Pa]
θ	Confinement Angle [Degrees]
ζ	Coefficient – Ratio of kinetic energy to ice strength, Shown as “X” in plots

1 Introduction

Ice crushing experiments have been conducted for many years to gain improved understanding of the material. Ice is simply solid water but even at a cool temperature of -20°C (253K) ice is at about 93% of its melting temperature. In comparison, steel perhaps one of the best known materials in the present day engineering toolbox melts around 1500°C (1773K), at 93% of its melting point (1375°C), the properties of steel would be much less predictable. Steel at 1375°C (1648K) would definitely not be described as brittle as ice is. This brittle material, ice, is frequently present in northern waters where shipping and offshore activities have occurred, and will occur in the future.

Ice impacts on marine structures often occur over small localized areas in larger ice features. In other words, typical ice impacts are localized to the structure-ice interface; which is usually only a small portion of the ice floe. The effect of the ice surrounding the point of impact has an influence on the effective strength of the ice. This influence on effective strength has come to be called confinement. Although conceptually simple, parameters to define the extent or the effect of ice confinement have not been postulated.

The question of estimating forces during a collision between ice and an indenter has been the motivator of much ice mechanics research. The force (or pressure) generated in collisions between ice and rigid structures is of great practical interest as this is the primary means by which marine structures or ships are damaged by ice and thus an

important design case for arctic ships and structures. The ultimate goal of most laboratory experimentation is to estimate full scale forces by conducting small scale tests. One of the identified issues in translating lab scale results to full scale is quantifying and determining the appropriate level of confinement of the ice being tested. Some research into the effects of confinement has been done in recent years, (Gagnon, 1998), (Barrette, Pond, Li, & Jordaan, 2003) but very rarely is the study done using dynamic impact testing and even rarer is a dimensional analysis applied.

The concept of dimensional analysis has been used to analyze complex problems for decades but appears to have received relatively little application to the field of ice mechanics. The concept of fundamental physical dimensions to explain the universe was introduced by J. Fourier in 1822 (Fourier, 1822). In the early part of the 20th century several mathematical scientists began work on the use of dimensional analysis. One of these was Lord Rayleigh (Rayleigh, 1915) and another is Edgar Buckingham with his well-known Buckingham Pi theorem (Buckingham, 1914).

In this thesis I have applied dimensional analysis to a specific ice impact scenario; one of a spherical indenter into a flat ice surface. The dimensional analysis is used as a tool to analyze various parameters affecting the forces. A set of novel parameters for defining confinement by means of a ratio and an angle are presented and analyzed herein.

1.1 Scope and Objectives

In this work I have taken a number of ice geometry conditions (representing different levels of confinement), subjected the samples to impacts at differing energy levels, and analyzed them using a set of dimensionless coefficients. This has allowed the data to be more consistently grouped and has allowed the effects of geometry as a proxy for confinement to be analyzed. The use of a dimensional analysis framework allows results to be used to estimate ice impact loads on spherical indenters for various impact speeds and dimensions. The analysis procedures developed in this thesis may also be used to establish coefficients for other geometries. This work presents and validates a means of quantifying confinement by means of a ratio of geometric parameters and an angle. The method of dimensional analysis is used allowing comparison between varied input parameters as well as allowing for prediction of loads on full scale scenarios. At present this work only considers one class of geometries and a limited range of the remaining variables. Further validation would be required to extend the method to different sizes, masses, velocities, and geometries.

1.2 Literature Review

Elements of this research found in literature include ice sample manufacturing, ice crushing experiments, effects of confinement, and dimensional analysis.

1.2.1 Ice Making

The STePS² project (Sustainable Technology for Polar Ships and Structures) at Memorial University developed a technique for ice sample manufacturing. This process produced samples that maintain a reasonably consistent material that will produce reliable and repeatable experiments. From within the STePS² project, a laboratory manual (STePS², 2013) was developed that gives detailed process instructions including photographic references as to how to make ice samples. The process was also summarized in S. Bruneau et al., 2011 (S. E. Bruneau, Dillenburg, & Ritter, 2011).

1.2.2 Ice Crushing

Crushing is the initial failure mode in most real-life ice-structure interactions and thus the ice crushing test has become a standard experimental procedure. In the field, this is often done by a hydraulically driven machinery, such as the Borehole jack tests (Frederking, Johnston, & Centre, 2002), the medium scale tests reported on in (Sodhi, Takeuchi, Nakazawa, Akagawa, & Saeki, 1998), or the tests that were analyzed by Gagnon in his 1998 paper (Gagnon, 1998). There is even more laboratory experimentation with the use of hydraulic driven test machines such as described in (S. Bruneau et al., 2013). Testing in the aforementioned paper (S. Bruneau et al., 2013) utilized conical shaped ice samples which creates an ideal method for using load and displacement to produce a nominal pressure area relationship. The testing in this thesis was conducted using the same apparatus used in some of the testing in the S. Bruneau 2013 paper. In (Kim, Golding, Schulson, Løset, & Renshaw, 2012) reported on tests where small spherical indenters are

driven into freshwater ice with and without the use of lateral confinement. It is difficult to directly compare the work done in Kim's paper and the work done in this research but it is a good reference point for spherical indenters using hydraulic test machinery. Jordaan in his 2004 paper (Li, Jordaan, & Barrette, 2004) also experimented with spherical indenters using a hydraulic test machine. In ice crushing experiments the measured force is usually the primary output. Most authors also present their results for ice crushing experimentation in terms of a pressure area relationship as it would then be possible to establish a force for other scenarios if the contact area is known. One of the things that is apparent when reading the literature referenced above (S. Bruneau et al., 2013) is that rate of indentation plays a role in the loads supported by the ice.

The earliest account of impact testing on ice that could be found in available literature is (Kurdyumov & Kheisin, 1976). In this work steel balls were dropped onto an ice surface. The balls were 156 kg and 300 kg castings, and dropped from various heights to give impact speeds between 1 and 6 m/s. The authors observed the layer of crushed ice in way of the contact surface. Seeing this they hypothesized that the thin crushed layer of ice in front of the indenter flows as a viscoplastic fluid. This would create a smooth pressure curve from the center of the indenter to the edge of nominal contact. Later as further testing was conducted it became apparent that this model failed to explain the regions of high pressure that were observed such as those presented in (Gagnon, 1998). (Jordaan & McKenna, 1988), provides a good review of testing conducted and reported on, from the 1960's to the 1980's. As with the S. Bruneau paper, this book covers both impacts and

forced indentations, with impact testing commencing in the 1970s. The authors use an energy balance to define the ice crushing processes and produce a comparative list of results with impact energy and specific energy (energy per volume of crush iced) as the basis for comparison. (Daley, 1999) introduces an approach with fundamentals linked back to (Popov, Faddeev, Kheisin, & Yakovlev, 1969). Daley's method takes the energy based method and expands it to representative ship geometries. These geometries penetrating into the ice produces energy inputs that can be related back to the overall vessel motion using Popov's method. Daley's work presented in his 1999 paper was evolved into a spreadsheet based solver called DDePS (Direct DDesign of Polar Ships). DDePS was tested in (Oldford, Sopper, & Daley, 2014) using the test apparatus described herein.

In 2012 a thesis from the MUN STePS² project, Clarke (Clarke, 2012) used a double pendulum apparatus. Clarke crushed conical ice samples into various flat steel plates. Clarke's use of the pendulum apparatus was referenced during this laboratory experimentation.

Other researchers have utilized various indenter geometries in their ice crushing research. One such reference is a combination of both spherical indenters with impact testing, (G. W. Timco & Frederking, 1993). In this paper tests are conducted with three indenters, spherical (20cm diameter), wedge, and flat into either an ice edge or onto a flat surface

and varying C-Axis directions. This 1993 paper is the closest dataset to the present results, found in the literature review and will be examined further, later in this thesis.

Timco and Frederking also published a number of similar papers in the early 1990s. One paper, (Gold, Timco, & Frederking, 1991), describes spherical indenters used on level sheet ice of various thicknesses. The data presented in this paper can be generally compared with the data obtained in the experiments presented in this thesis but the data is not directly compared as the necessary details for each test are not provided.

1.2.3 Confinement

Many articles, such as (Clarke, 2012), (G. W. Timco & Frederking, 1993), (Dragt & Bruneau, 2013) on ice mechanics attribute higher ice loads to confinement of the ice. The basic idea of confinement is that the ice adjacent to the ice being crushed in the contact zone acts to restrain the spalled ice pieces. The spalled ice pieces are held in place by the surrounding ice and forced to fail by crushing thus increase the supported load during the crushing event. Unconfined ice samples tend to spall off large pieces, therefore reducing the contact area and therefore reducing the contact force. In the (S. Bruneau et al., 2013) paper, ice cones are employed as a method of including natural ice confinement in the tests. The cone shape produces a growing nominal contact area as indentation occurs. In the early 1980s several experiments were conducted to quantify confinement such as (G. Timco, 1983), where he conducts confined compression testing on sea ice harvested from the Beaufort Sea. As expected the completely confined samples sustained pressures over

60% higher than unconfined samples. In a 2003 PERD report (Barrette et al., 2003) various tests were conducted in confined and unconfined conditions. The confinement conditions established in this report are similar to the confinement cases studied in this thesis.

1.2.4 Dimensional Analysis

The principal reference used for dimensional analysis is (Sharp, 1981). This is a text book titled “Hydraulic Modelling” that covers fundamental dimensional analysis techniques effectively for use in other fields such as in ice mechanics in this thesis. In Hydraulic Modelling a chapter on Snow and ice models is included (chapter 10) which describes different aspects of application of dimensional analysis to ice loads. The first and perhaps the most obvious is the application of a dimensional analysis in relation to model testing ice breakers in an ice model basin. The other is the application to ice covered rivers and bodies of water with an interest as to how the floating solid flows down a river, through a spill way, over a dam, or through a seaway lock. The equations developed later in this thesis are similar to Sharp’s equations for resistance on an ice breaker but Sharp considers variables that have no bearing on the results of the tests conducted herein.

(Arunachalam, 2005), examines ice test results reported by others but does so using dimensional analysis. In his conclusions he makes the statement “...it is useful and necessary to express experimental data for ice-induced pressure in dimensionless form rather than in dimensional form, as a function of dimensionless independent

parameters.” This concept is one that is used and followed in this thesis although Arunachalam’s approach is somewhat different than the one taken here.

1.2.5 Summary of Literature Review

In summary, a lot of research has been conducted on ice, for example the forces it can produce on an indenter or structure, and even some research into the relative forces of a confined sample as compared to an unconfined one. Although confinement can be defined in terms of an applied pressure, such as that used in a tri-axial test, it is not clear what level of pressure would be equivalent in a natural ice sample of a given geometry. Thus there is no means to quantify the effects of confinement on effective strength of ice for natural cases where the geometry or extent of the interaction might be known, but the internal confining pressure cannot be determined. The work proposed in this thesis will seek to address that gap by establishing a geometrically based methodology for quantifying the confinement for a simple geometry in which the indenter and ice sizes are varied systematically.

2 Ice Crushing Experiments

To define a methodology of quantifying confinement, various ice sample arrangements were established. These arrangements allow for controlled levels of confinement from a low level up to a high level. Testing also had to be similar enough to practical, real-world collisions for the dimensional analysis to be applicable. This means that geometries had to be similar and a test apparatus with specified mass and velocity for a collision had to be used. During a real world collision, the ships mass and velocity are basically the available energy. Some energy is provided by the propulsion system but the majority of the impulse energy is from mass and velocity. A test apparatus that closely mimics this available energy for a collision was selected for this experimentation. The experiments are designed to approximate ship ice collision speeds, between about 4 knots (2 m/s) up to almost 10 knots (5 m/s). The mass is also intended to be controllable to a degree.

The indenter geometry representing the ship structure was selected as a sphere because appendages such as azimuthing propulsion units often use spherical geometries. A range was selected from a large sphere with a diameter matching the smallest holder diameter, and one that was half the diameter for the large sphere. Some supplemental testing is done on an even smaller sphere (5cm) but mostly as a means of validation. More detail on holders is given in 2.1.6 Ice Holders and more detail on the spheres is given in 2.1.9 Indenters.

The testing apparatus that was selected as the main tool for the experiments has a physical limit to the size of sample it can take. The maximum diameter holder that could fit was selected as the large sample, 35 cm. A significant supply of 25 cm diameter holders existed in the MUN laboratories as they were developed and used by other researchers. This was selected as the medium diameter holder. In order to keep the experimentation dimensionally linear the diameter of the smallest holder was selected to be 15 cm. The largest ice sample (35 cm) offered the largest radial confinement possible, whereas the smallest sample gave a very low radius of ice offering low radial confinement.

Ice depth was another ice parameter that was varied. The low depth was dictated by the depth of the ice holders (11 cm). The deep samples were selected to be 30 cm. This was driven by size limitations of the pendulum.

Together the ice depth and diameter of the restraining ring are used to define the level of confinement. The concept of dimensionally varying level of confinement is graphically shown in Figure 2-1. Deeper samples with more overhanging ice results in a lower level of confinement. Changing the sample diameter results in a different range of confinement level.

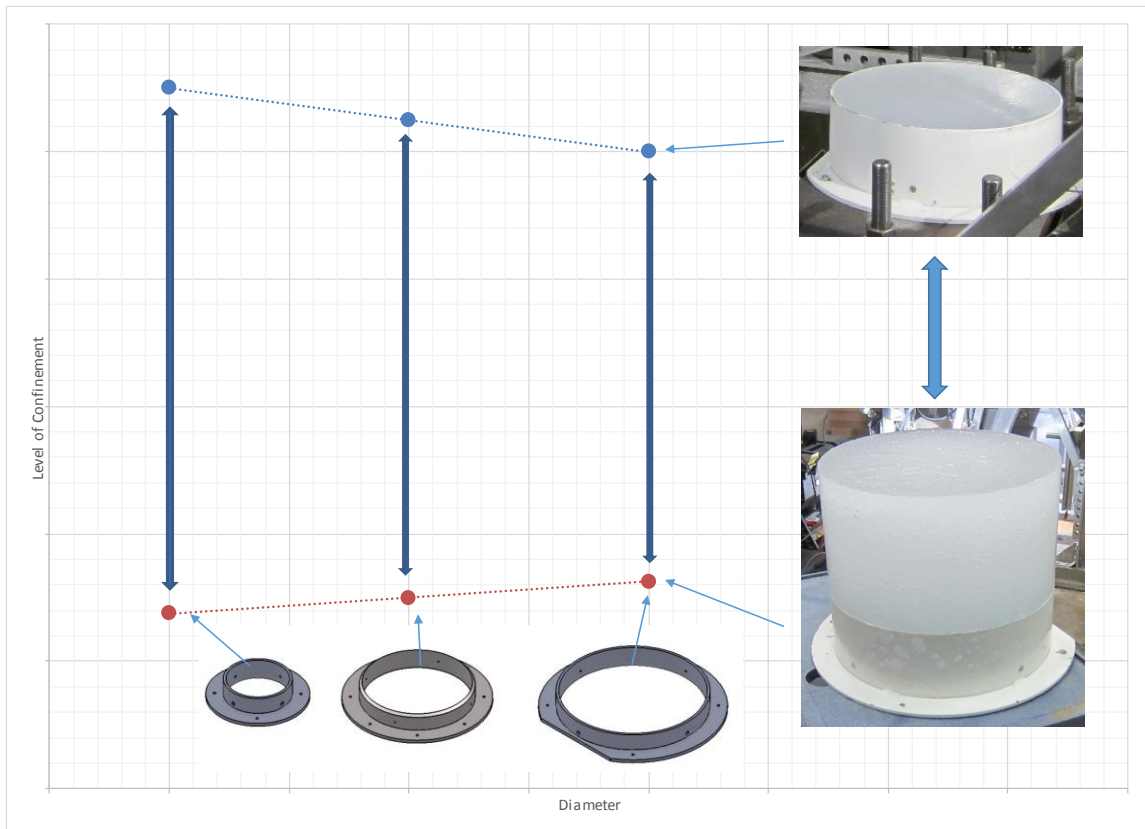


Figure 2-1. Level of Confinement

2.1 Test Apparatus

2.1.1 Double Pendulum

This test apparatus shown in Figure 2-2 & Figure 2-3 was the same double pendulum apparatus first described in (Clarke, 2012) and again in (Oldford et al., 2014). The apparatus is essentially a 1 meter cube aluminum structure with two opposing carriages. Each carriage hangs on a series of four parallel arms with bearings on both ends. This

parallel arm arrangement ensures the centerlines of the carriages remain horizontal throughout the swing, and ensures there is zero rotational velocity at the point of impact.

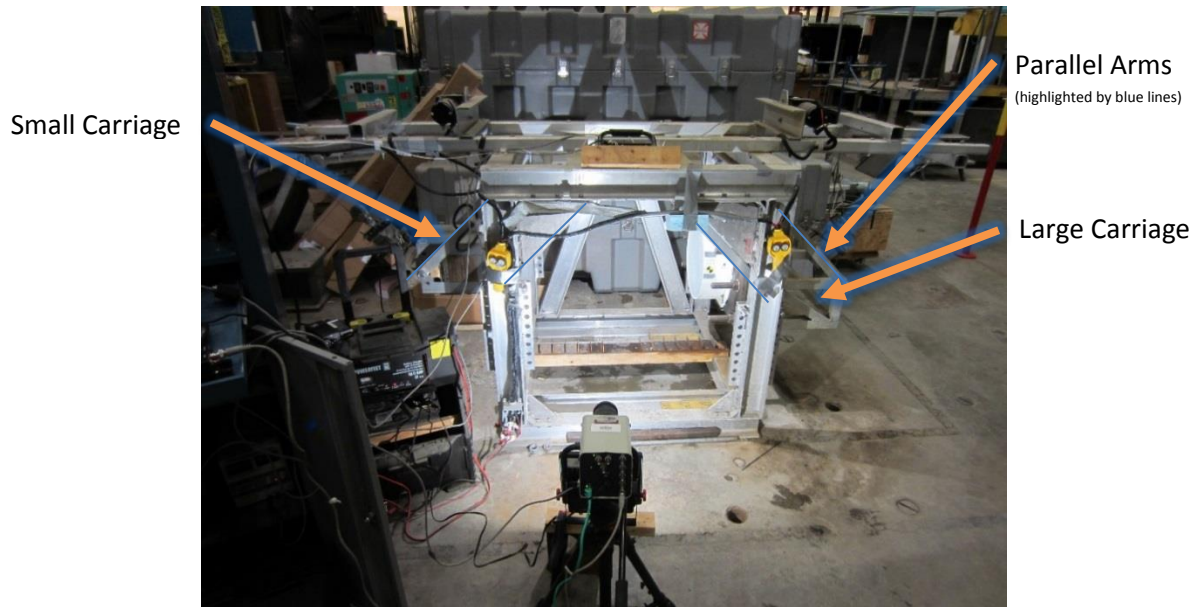


Figure 2-2. Double Pendulum

The smaller carriage is where the load cells and indenter are mounted. The three load cells are sandwiched between two steel plates that are connected by means of three high strength bolts. The hemispherical indenters are mounted to the face plate by means of a 2" diameter screw positioned equidistantly between the three load cells. The other plate of the load cell sandwich is a solid steel plate that is bolted to the carriage body. Further explanation of load cells and the arrangement is given later in 2.1.3 Load Cells. Behind the load cell sandwich plate arrangement, ballast plates for the small carriage are contained. A large bolt runs the length of the carriage in the center of the void behind the load cell backing plate. Ballast weights are cut from steel plates with a hole in the middle. This hole goes over the central bolt in the center of the carriage. When there is sufficient room

between the ballast plates and the back of the carriage a nut is installed to hold the ballast plates securely in place. When additional ballast is required and there is insufficient room to install the nut, wooden wedges are driven in between the last ballast plate and the frame of the carriage. This arrangement proved satisfactory as the wood's flexibility kept the plates secure for multiple tests.

The larger carriage carries the ice sample. No instrumentation was used on this carriage for these experiments. The carriage arrangement was significantly modified for the testing reported in (Oldford et al., 2014) and that same arrangement was used for these tests with some slight additional modifications. The large carriage consists of an aluminum framed structure with a 12 mm (1/2") thick aluminum face plate. This plate has two 25 mm (1") thick aluminum blocks on either side. Six large steel bolts are threaded into these aluminum blocks. The six bolts are used to secure a 19 mm (3/4") steel plate. The steel plate is machined with mounts for the various ice holders.

The large carriage is capable of being ballasted by using steel plates in the carriage structure. Each plate has a hole in the middle and through this hole passes a threaded rod. The rod is threaded into a plate in the carriage then the ballast weights are held in place by tightening a nut on the threaded rod.

Each carriage is raised to a specified angle by means of 12 V electric winches. The winch cables run through a series of pulleys with 110 volt electro magnets at the ends. The two magnets (one for each carriage) are driven by a common power supply. This power supply

can easily be disengaged using a simple electrical switch. Disengaging both magnets at the same time ensures a simultaneous release of both carriages.

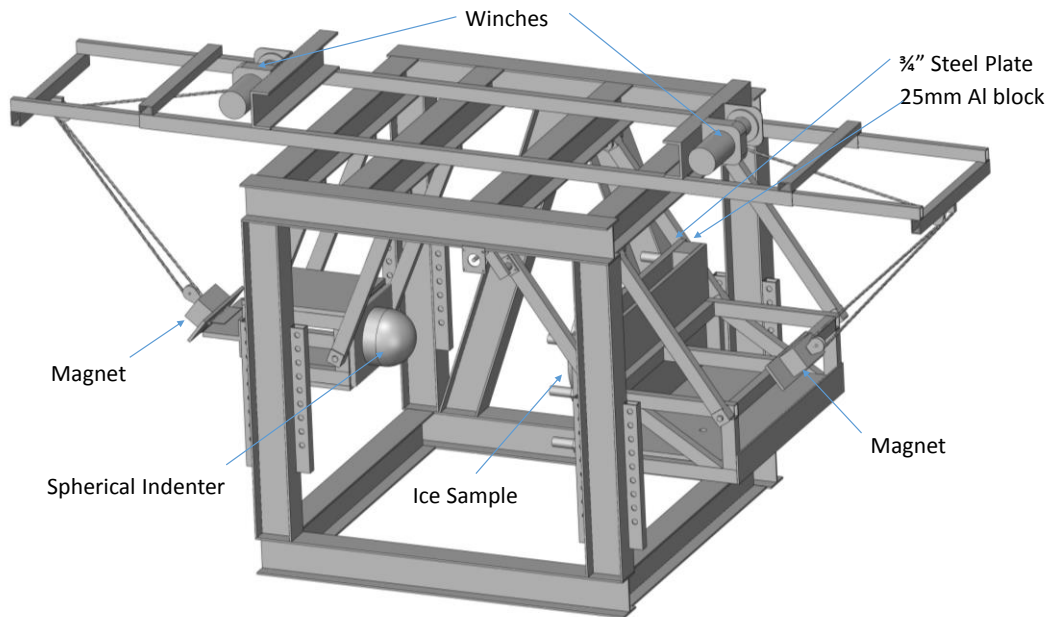


Figure 2-3. Rendering of Double Pendulum

2.1.2 Release Angle and Contact Velocity

All angles mentioned in this thesis are relative to vertical as shown in Figure 2-4. This convention results in a more intuitive result, the larger the release angle the higher the speed. For example an angle of 60 degrees will yield higher contact speeds than a 30 degree release angle.

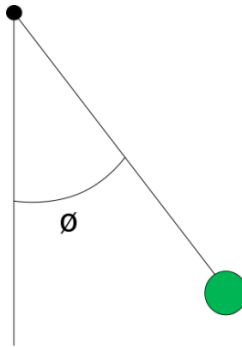


Figure 2-4. Pendulum Angle

Both carriages are pulled back to the same angle. Therefore when a release angle of 45 degrees is stated this means that both carriages were pulled back until the arms on both carriages were at 45 degrees from the vertical. Measurement of this angle was performed using both a calibrated angle measurement tool in the laboratory as well as with a modern day mobile phone and a program (application) called Clinometer developed by Plaincode™ from Sternstr. 5, 83071 Stephanskirchen, Germany. The version used was 2.2 with a screenshot included in Figure 2-5. The mobile phone and app proved to be just as good as the dedicated digital angle measurement tool and was used for the majority of the tests.



Figure 2-5. Clinometer Screenshot

Impact velocity is controlled by varying release angle. Impact velocities are simply calculated using a simple energy balance.

$$E_{Potential} = mgh \quad \text{Equation 2-1}$$

$$E_{Kinetic} = \frac{1}{2}mV^2 \quad \text{Equation 2-2}$$

Since the carriage is initially at rest, all the initial energy is in the form of gravitational potential energy, Equation 2-1. At the bottom of the pendulum swing, all the energy is in the form of kinetic energy, Equation 2-2 therefore:

$$mgh = \frac{1}{2}mV^2 \quad \text{Equation 2-3}$$

Mass of the carriage does not change before the point of impact, therefore mass cancels out. Solving for velocity gives:

$$V = \sqrt{2gh} \quad \text{Equation 2-4}$$

Applying simple trigonometry the release height can be linked to the release angle and the length of the pendulum arm.

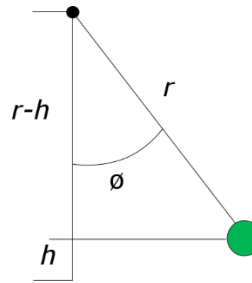


Figure 2-6. Pendulum Swing

$$\cos \phi = \frac{r - h}{r}$$

$$h = r - r \cos \phi$$

Equation 2-5

Inserting Equation 2-5 into Equation 2-4 gives:

$$V = \sqrt{2g(r - r \cos \phi)}$$

Equation 2-6

Noting that this is for one carriage, so this would only give half of the collision velocity.

Also noting that both carriages are set to the same release angles therefore the collision velocity can be estimated with Equation 2-7 assuming frictionless and perfect angles.

$$V = 2\sqrt{2g(r - r \cos \phi)}$$

Equation 2-7

The actual contact velocities was measured using a high speed camera that will be detailed later in 2.1.8 High Speed Camera.

2.1.3 Load Cells and Associated Mounting

The load cells shown in Figure 2-7 used for this experimentation are described by the manufacturer as Low Impedance Voltage Mode (LIVM) Piezoelectric Ring Type Force Sensors. Specifically three Dytran Instruments Inc. model 1203V5 were used. To simply

explain the basic principle of these load cells they can be imagined as being like a sponge wrapped in a sleeve. The power supply/coupler, (described further below in 2.1.4 Power Supply / Coupler), fills the crystals with a charge; like water in a sponge. But the sponge is wrapped in a tight sleeve. When the load cells are subject to compression the crystals are squeezed, which in turn produces a voltage directly proportional to the amount of force. Likewise with the wrapped sponge, when squeezed, pressure rises proportionally to the squeeze.



Figure 2-7. Load Cell

The three load cells used for these experiments were all shipped with calibration certificates stating a non-preloaded sensor sensitivity of 0.51 mV/lbf. Meaning that the sensor as it was shipped without the bolt will output 0.51 mV for every pound of force applied to the sensor. The maximum measurable load for these sensors is 10,000 lbf (~44

kN). Preloading reduces the sensitivity of these units at a ratio of the stiffness of the load cell to the stiffness of the bolt preloading it and the maximum load possible is the rated load minus the preload. This is illustrated below in Figure 2-8.

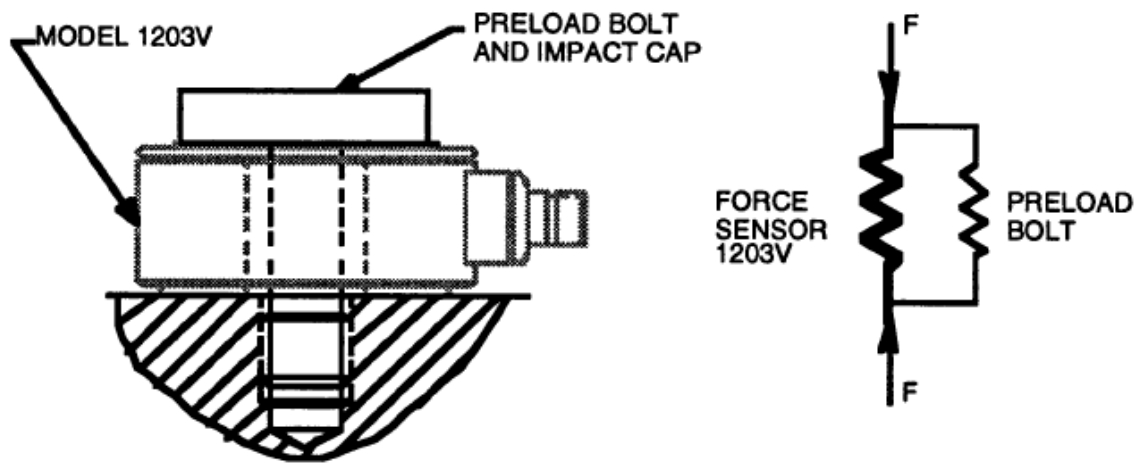


Figure 2-8. Preload Schematic of Sensor, from (Dytran Instruments, 2001)

The small carriage of the double pendulum has three load cells sandwiched between two steel plates. The plates are held together via three bolts passing through the load cells (one bolt through each load cell). This is graphically demonstrated in Figure 2-9. This load cell sandwich plate system is designed so that it can be assembled, calibrated then mounted onto the small carriage of the pendulum.

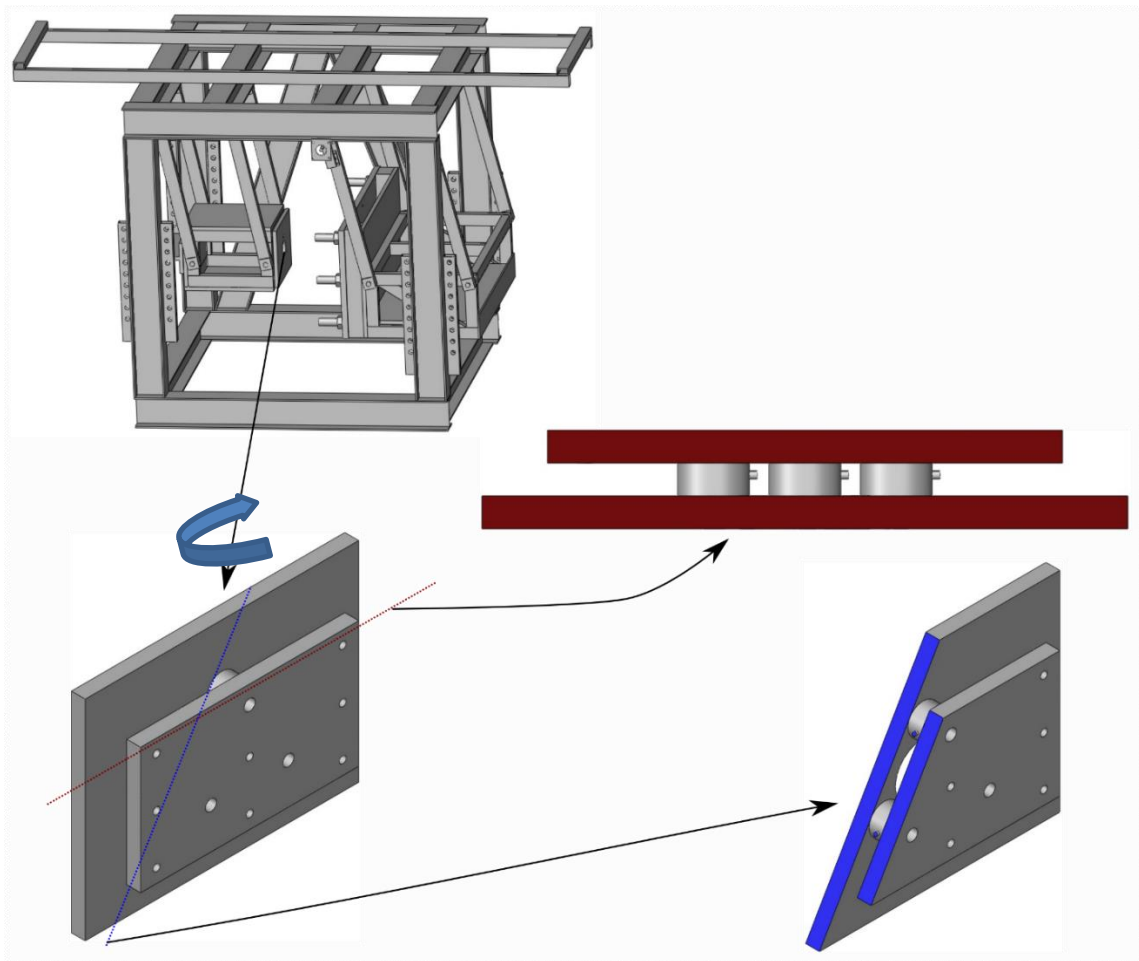


Figure 2-9. Load Cell Sandwich

The bolts used for this experimentation were Black-Oxide Alloy Steel Flat-Head Socket Cap Screws obtained from McMaster-Carr. The bolts were 5/16"-24 thread size and 1-1/2" long. McMaster-Carr was contacted requesting information on the stiffness of the bolts but replied stating that they only know the minimum tensile strength of the bolts is 145,000 psi. In the white paper, (Anderson, 2010) the authors give a bolt stiffness formulation of:

$$k = \frac{A \times E}{L_e}$$

Equation 2-8

Where: A = Cross sectional area of the bolt, E is Young's Modulus, and L_e is the bolt's effective length.

A and L_e are both determined by the bolts chosen and the plate arrangement. E is roughly consistent at 207 GPa for plain carbon and low alloy steels (William D. Callister, 1997), therefore the stiffness can be estimated. The stiffness of the load cells is given by the manufacturer as 3.46 kN/ μ m, see Appendix 1.

The bolt length is taken as half the height of the head (7 mm / 2 = 3.5 mm) + the thickness of the load cell (12.7 mm) + half the thickness of the plate the bolt is threaded into (12.7 mm / 2 = 6.35 mm)

Therefore: $L_e = 22.55$ mm

The bolt diameter is taken as 5/16" which is 7.9375 mm. This gives a cross section area of 49.5×10^{-6} m².

Therefore the bolt's calculated stiffness is 454×10^6 N/m or 0.454 kN/ μ m.

The sensitivity of the load cell is reduced by the ratio of the stiffness's according to:

$$\text{System Sensitivity} = \text{Sensor Sensitivity} \times \left(1 - \frac{\text{Bolt Stiffness}}{\text{Sensor Stiffness}}\right)$$

$$\text{System Sensitivity} = 0.51 \times \left(1 - \frac{0.454}{3.46}\right) = 0.443 \text{ mV/lbf}$$

The value of 0.443 mV/lbf was entered into the power supply/coupler as a starting point for the calibration process. Further calibration and adjustment of this value will be described below in the section, 2.1.5 Adjustment and Calibration.

To ensure that all three load cells are equally preloaded, the bolts are set into place in the load cell sandwich using a torque wrench. The torque setting was 35 inch-lbs, then the bolts were carefully turned 1/12 of a rotation (30 degrees). This careful preloading using bolt rotation rather than bolt torque alone gives much more accurate control over equal preload of each sensor as is described in (Anderson, 2010).

Load cells were installed in positions shown in Table 2-1 and Figure 2-10:

Table 2-1. Load Cell Placement

Position	Serial Number
Left	1634
Middle	1620
Right	1631

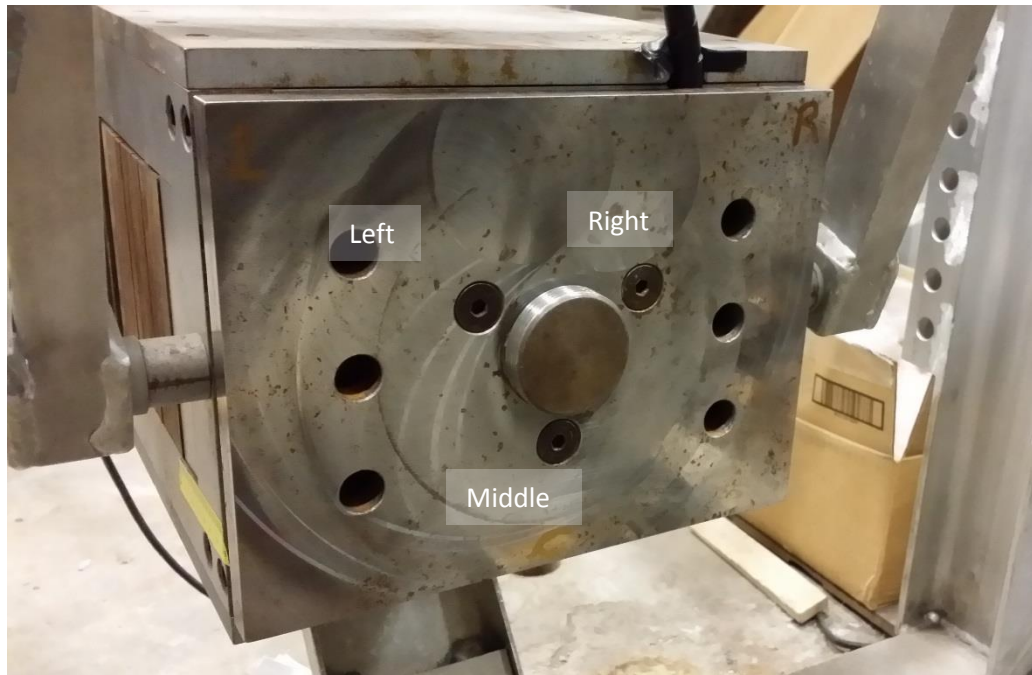


Figure 2-10. Small Carriage Face Plate

2.1.4 Power Supply / Coupler

The power supply / coupler does two jobs with the load cells; it charges the crystals as well as measures the potential output during a loading event on the cells. The coupler then sends the measured signal out to the data acquisition system.

For the experiments performed in this thesis a Kistler Type 5134B was used and is shown in Figure 2-11 and Figure 2-12.



Figure 2-11. Power Supply/Amplifier - Front



Figure 2-12. Power Supply/Amplifier – Back

Channels 1, 2, and 3 were wired to load cells right, middle and left. The power supply/coupler is a four channel instrument and in Figure 2-12 the reader will notice that channel 4 is connected to a wire. In initial testing this channel was used for an accelerometer attached behind the ice sample. This accelerometer was not used for any testing conducted in this thesis with the exception of a few early tests presented in the ICETECH 2014 paper. The subject power supply / coupler has several settings for each channel, but only channels 1 through 3 will be discussed here. The values given herein are the settings used in the experimentation after calibration. If repeat testing is to be done these settings (shown in Table 2-2) are recommended to be used.

Table 2-2. Power Supply/Coupler settings

Description	Channel 1	Channel 2	Channel 3
Sensitivity [mV/lbf]	0.38	0.38	0.38
Range 10V [lbf]	10,000	10,000	10,000
Gain	2.63	2.63	2.63
Low Pass Filter	Bypass	Bypass	Bypass
Time Constant [s]	10	10	10
Overload Threshold	100% FSO	100% FSO	100% FSO
Curr/Bias [mA/V]	4/9.3	4/9.2	4/9.2

2.1.5 Adjustment and Calibration

The assembled load cell sandwich plate system was subject to a multitude of calibration and cross checking. With a sensitivity setting of 0.44 mV/lbf the load cell plate was installed in a manually powered hydraulic test platform. The test platform consisted of a rectangular frame a load cell, hydraulic jack, manual pump and data acquisition system as shown in Figure 2-13. This test apparatus is commonly used to load simply supported beams such as during model bridge building competitions. The load cell plate was installed in the apparatus and pressure was applied using the manual pump. The loads from the test apparatus data acquisition system and the pendulum load cell sandwich plate were compared. During this calibration it was realized how significant the time constant setting on the power supply / coupler is. Using the manual pump arrangement, accurate loading could not be done rapidly. A 0.1 second constant resulted in the measured output forces decaying before the test apparatus could register load. This made it impossible to compare the loads. The time constant was adjusted to 10 seconds and found to be much easier to compare. An informational paper from Dytran Inc. (Rosenberg, 2007) contains information supporting this approach; the documentation

suggests using a longer time constant for quasi-static calibration. During this first phase of calibration testing it was discovered that the sensitivity of the load cells needed to be adjusted as the loads were not equal. By trial and error it was found that a setting of 0.38 mV/lbf resulted in a better calibration.



Figure 2-13. First calibration apparatus

The second series of calibration testing was performed in the MUN cold room in the S.J. Carew building's Thermodynamics Lab. Within this cold room was an electro-hydraulic materials test machine capable of applying load much quicker and more accurately than the manual machine shown in Figure 2-13. The testing machine is produced by Materials Testing Systems (MTS), therefore the machine is known as the MTS machine. The load cells Data Acquisition system was programmed to operate in the range of 0 N up to 44,482 N, corresponding to 0 to 10,000 lbf that the load cells are rated for. Considering the load

cells preloading and the 3 X 44 KN capacity, peak loads were carefully restricted to less than 80 KN. It was quickly discovered that this upper level was giving high values. Several tests were conducted on the load cell sandwich plate system, tuning the maximum force value until the systems reported nearly identical forces such as the comparison plot shown in Figure 2-14. Adjustments at this calibration stage were done within the Data Acquisition System's computer controller. This was found to be easier to adjust between calibration runs and finer adjustment could be made as compared to adjusting the sensor sensitivity in the power supply/coupler. Optimal results were obtained by selecting a 10 volt output equal to 39,962 N. This equates to a loss in maximum capacity of 4,520 N. This loss is attributed to the preloading of the sensors.

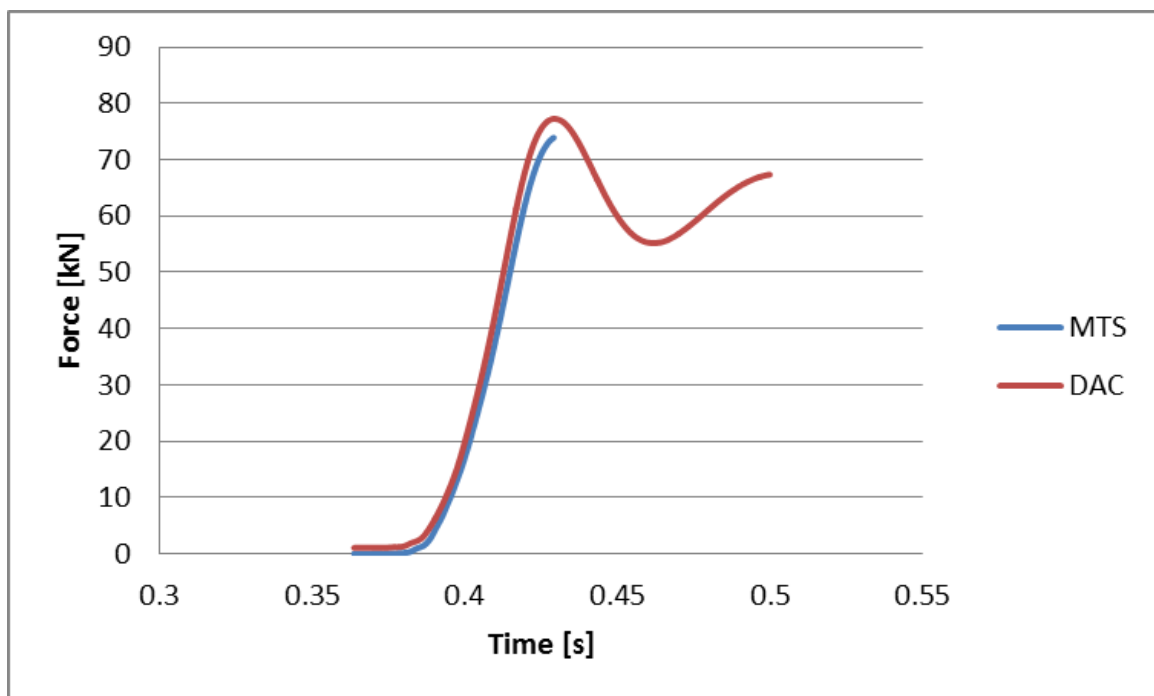


Figure 2-14. Calibration run with MTS machine - Time constant = 10 seconds

As with the manual test machine, if the time constant was set any lower than 10 seconds the load cells output would begin decaying before the MTS machine load was established. This is evidenced in Figure 2-15 that was done using exactly the same settings as Figure 2-14, only with a time constant to 0.1 seconds.

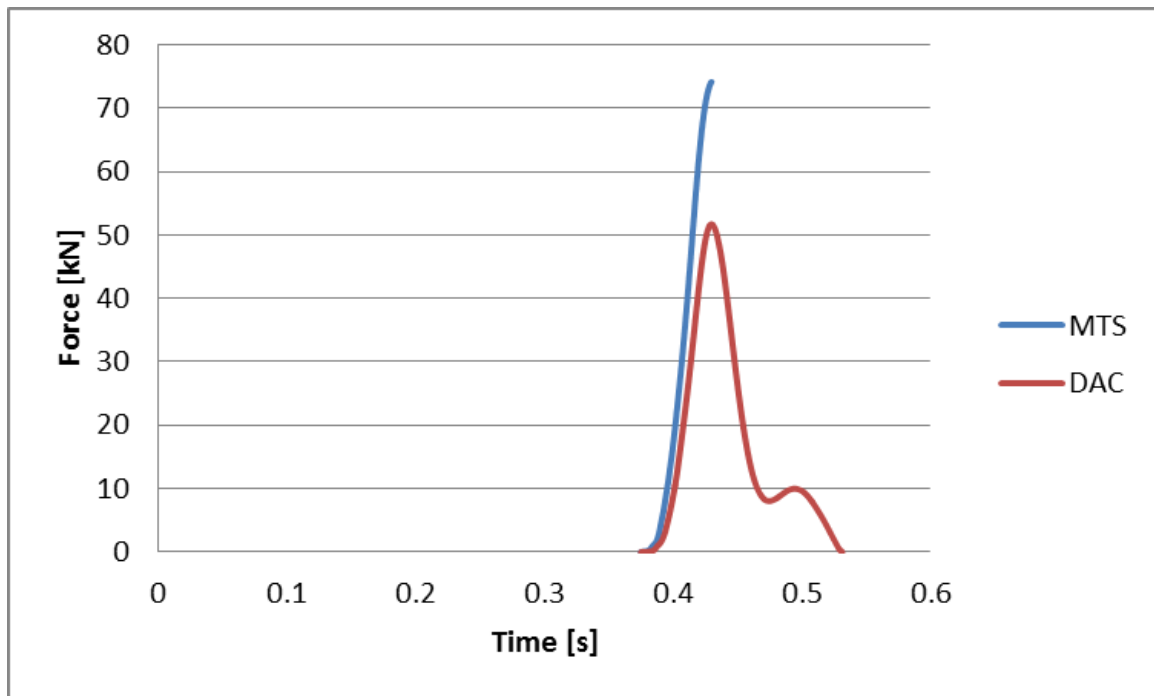


Figure 2-15. Calibration with MTS machine - Time constant = 0.1 seconds

In addition to the two hydraulic test machine calibrations, Memorial University has an impulse hammer that is often used to measure loads on utility poles. This hammer was used to apply impact loads to the load cell sandwich plate system. The loads for these two instruments were close but the calibration of the hammer could not be verified and was therefore only used as an additional level of confidence.

All final calibration, including the impulse hammer, was done with a time constant setting of 10 seconds. Since the desired output from the tests was only the peak impulse force, the time constant of 10 seconds was used for all tests conducted for this thesis.

2.1.6 Ice Holders

Six different ice holder designs are employed in this experimentation, three diameters and two heights. All holders are basically the same style consisting of a flange ring that is used to mount the holder onto the pendulum, a cylindrical ring that is in contact with the circumference of the ice sample, and a series of four screws that are frozen into the ice sample. The screws act as additional means of securing the ice sample in the holder. The short holders are graphically shown in Figure 2-16 and a tall holder is shown in Figure 3-1. The largest diameter holder, shown in Figure 2-16 on the right, was at the extreme limit of the pendulum's size capacity. The flange would have protruded below the bottom of the large carriage if a complete circle was retained. Therefore a section was cut from the bottom of the flange as is shown in the figure.

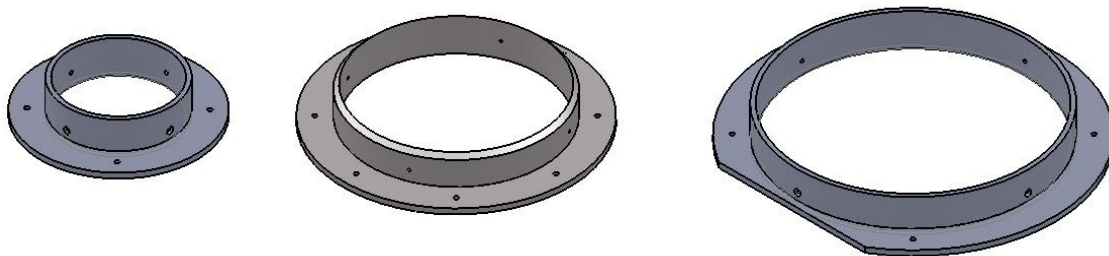


Figure 2-16. CAD rendering of 5cm tall ice holders

2.1.7 Data Acquisition System

The data acquisition system is the instrument that takes the output from the power supply / coupler as a voltage then produces and records it in a manner that is useful for analysis. In this case the instrument used is a National Instruments NI eDAQ-9174 running an NI 9239 module. The NI 9239 module was wired directly into the power supply / coupler outputs. The eDAQ-9174 is connected to a National Instruments industrial controller, which is basically a simplified computer, by means of a USB cable. The controller was running a dated but effective operating system, Windows XP. The software used to interface with the eDAQ was LabVIEW SignalExpress. The inputs were voltages ranging from 0 to 10 Volts. In accordance with the calibration procedure described in 2.1.5 Adjustment and Calibration, a value of 0 N was assigned to 0 V and a force of 39,962 N was assigned to the 10V output. The program linearly interpolates between these values as shown in Figure 2-17.

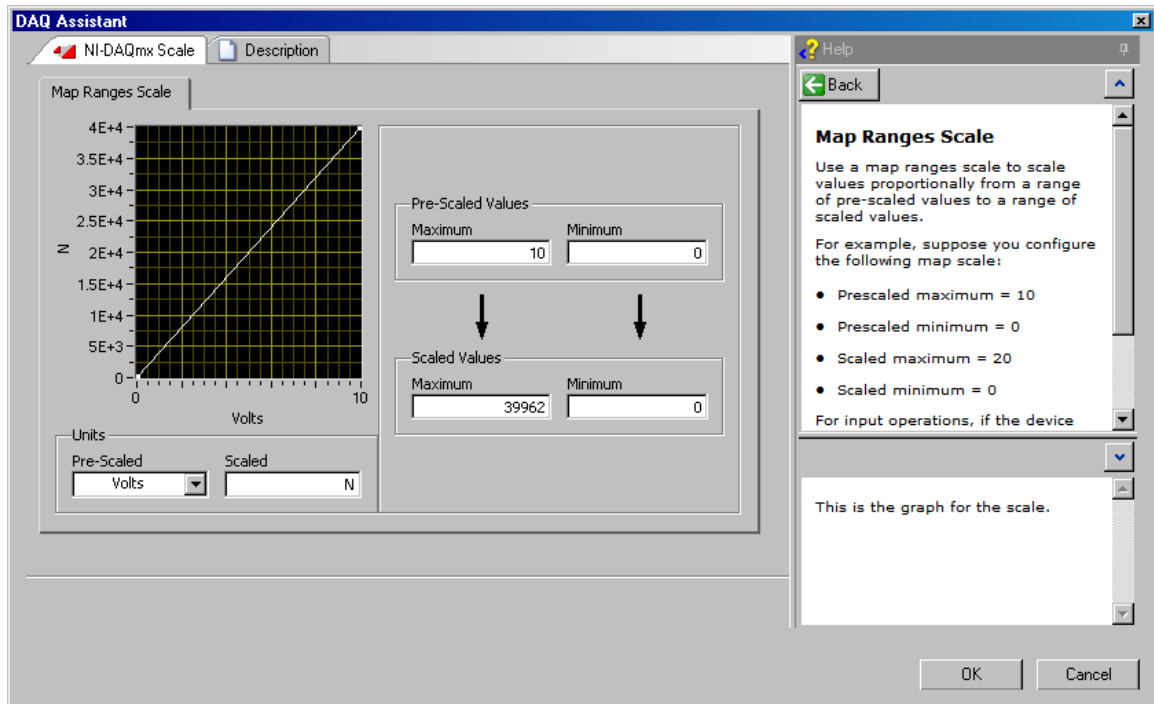


Figure 2-17. LabVIEW SignalExpress Voltage to Force ratio

2.1.8 High Speed Camera

A high speed camera and DC powered LED lights were used to record the collisions. The video is the principal means of determining the actual contact velocity of ice and indenter. Additionally the video can be used to explain any abnormal results. The camera used was a Mega Speed 55KS2B4, manufactured by Canadian Photonic Labs Inc. in Minnedosa, MB. Optics for the camera is a relatively simple 58mm Nikon lens, with zoom ranging from 70 to 28 mm and f Stop range of 16 to 2.8. The camera required significant light levels to obtain a clear image, therefore an f Stop of 2.8 was selected to maximize the aperture opening. To keep the camera safely away from flying ice debris the maximum zoom was selected. To adjust the focus for this set up the camera was aimed at the pendulum and using the connected computer, digitally zoomed in by 400%. The marker circle and

associated scale with numbers were the objects used to maximize the focus so that reading these during data analysis would be as easy as possible. The camera settings were set to 1,000 frames per second, Exposure time = 900 μ s, Gain = 900, Offset = 8. These settings were established early in the testing and found satisfactory, therefore were not altered through the test program.

Lighting was provided by two large LED construction lights. As purchased, the lights were driven by 110 V through a built in transformer/rectifier but it was quickly established that the AC power from the grid showed excessive flashing on the high speed video. The transformer/rectifiers were removed in favor of an external clean DC power source. Voltage was brought up to about 30 V and the lights produced bright steady light on high speed video.

2.1.9 Indenters

A series of three spherical indenters shown in Figure 2-18 are used in this experimentation. All three are machined from aluminum alloy round stock with diameters, 5 cm, 7.5 cm, and 15 cm. Each indenter was machined with a 2 inch threaded hole in the base to screw onto the pendulum carriage. This threaded hole is the reason for the “shoulders” on the smallest indenter.



Figure 2-18. Spherical Indenters

2.2 Ice Samples

2.2.1 Ice Production

In S. Bruneau et al., 2011 (S. E. Bruneau et al., 2011), an ice making methodology was proposed. The process is covered in great detail in the STePS²: Manual of Laboratory Procedures (STePS², 2013). The method of ice production was used with one exception. The STePS² methodology included a further process of shaping the ice into a cone which was not employed for the purpose of this research.

The method used here was one where the water is purified through distillation, de-ionization, and then de-aeration. Commercially available bagged ice cubes are crushed and then sieved to below 10 mm and above 2 mm.

Ice holders are placed into steel buckets (mold) and wrapped with insulation, see Figure 2-19. This assembly is then hung from a purpose built chest freezer lid. This arrangement has only the bottom of the bucket directly exposed to the low temperature in the freezer, and insulated elsewhere.



Figure 2-19. Ice holder, mold, and insulation

Ice chips or seeds are poured into the ice holder/bucket arrangement then the purified water is poured into the ice seeds, and constantly stirred as the water is poured to release as many air bubbles as possible.

Samples grown following this procedure produces relatively fine grained ice samples with no principal crystal orientation, resulting in a very strong material close to multiyear ice.

2.2.2 Processing of Samples for Tests:

Following the above production technique produces controlled grain sized samples that assumed the exact size and shape of the mold in which they were created. This was not perfect for the intended testing because there was always some ice protruding beyond

the top of the holder. Therefore some pre-test processing of the samples was required. This processing followed in a series of steps that slightly varied based on sample size.

1) Remove sample from mold:

The molds were steel buckets that tightly fit around the holder ring. To release the bucket from the ice sample, a splashing of cool water was applied to the outer surface of the steel mold. This would create a slight surface melting and allow the mold to be slid off. The releasing of the molds was aided by prying on the edge of the mold with two pry bars (one on either side of the holder)

2) Melt back surface flush with holder:

The surface of the ice sample in the holder near the mounting flange would often protrude up out of the holder due to the expansion of the water as it froze. To ensure that the base of the holder would mount flush with the pendulum carriage, the ice protruding from the holder was melted away using thick aluminum plates. Sliding the ice sample over the plate until the holder flanges made contact proved to be sufficient.

3) Cut sample at depth or flush with holder ring:

The upper surface of the sample also required processing as the molds were all slightly deeper than the holder rings or deeper than was needed for testing. The smaller samples (15 cm and 25 cm diameter) were cut using a band saw located in the MUN cold room. The larger samples (35 cm diameter) would not fit in the band saw and were therefore cut to size using a chain saw.

4) Smooth testing surface:

Cutting the samples creates a rough surface. This surface is the one to be impacted with the spherical indenters therefore they were smoothed using the same aluminum plate used for the back of the sample. The surface was made parallel with the bottom by melting the sample to the top of the holder ring (completely confined samples) or by using a limiting spacer between the melting plate and the holder flange.

5) Weigh sample:

After processing was complete the samples were all weighed, for accurate weight inputs into the pendulum calculations. This was done using a digital scale as shown in Figure 2-20. The foam insulation underneath the ice sample is to prevent contact with the warm surface of the scale which could cause unwanted melting. The scale was zeroed with the foam on the scale surface.



Figure 2-20. Weighing a 25 cm diameter X 30 cm deep ice sample

6) Store Samples:

After processing and preparation, samples were stored in the cold room at -10°C . Due to the cold room's humidity control systems, ice samples were wrapped tightly in a plastic bag to prevent possible sublimation in the event that the samples had to be stored for several days.

2.3 Testing Procedure

The procedure established for the testing was first and foremost focused on safety. No injuries were reported during this testing and it is desirable that any confirmation or follow up testing be performed without incident. The procedures are recommended to ensure experimentation consistency, efficiency and above all, safety of those involved.

The testing procedure followed the checklist given in Appendix 4. The key points were to ensure that no one got in harm's way, the instrumentation was all calibrated and functioning prior to installation of ice, and that all systems were engaged before conducting the testing. Some of the large ice samples produced projectile debris upon impact that could potentially harm someone if they were struck. For this reason, no one was permitted within approximately 3 meters of the pendulum during testing.

2.4 Phase 1 Test plan

The initial test plan was one which covered all the variables that will be identified later in 3.5 Dimensional Analysis Set-up, giving one sample at each variable level. A release angle of 45 degrees was chosen for this phase of the testing because this was the highest angle that the electro magnets could hold the 35 cm diameter X 30 cm deep sample. Also 45 degrees is an angle in the middle of the release angles used in two previous data sets (the ICETECH 2014, and Sept 25th datasets) that were incorporated into this study.

For the phase 1 testing, in order to maintain a consistent mass for the large carriage, steel plates are used for ballast. Starting with the largest, 35 cm \varnothing X 30 cm sample, no plates were loaded. Subsequent test samples became smaller and lighter, and thus ballast plates were added as needed to maintain the mass equal to the largest sample.

2.4.1 ICETECH 2014 Dataset

In the winter of 2013/2014 a series of 16 tests were conducted using the same double-pendulum apparatus described in this thesis. The results of those tests were presented

in (Oldford et al., 2014). These results are well in line with the test plan established herein and are therefore used in conjunction with the phase 1 results established in Table 2-3, Round 1 results.

2.4.2 September 26, 2014 Dataset

As part of the early planning of this research a series of samples were prepared. These samples were prepared using the same techniques as described in this thesis. The samples were being stored in a refrigerated container unit when a mechanical failure of the unit prompted the unit to be cleared out so that it could be repaired. Seven 25cm diameter samples were prepared for testing but the test plan was not fully established. It was decided to test these samples in a similar manner as the ICETECH 2014 samples were tested. The results of this testing is also included in round 1 data set.

2.5 Round 1 Results

A summary of the data is given below in Table 2-3. The “Group” column identifies source of the data with “Phase 1” indicating testing that was conducted here. An analysis will follow in the next section. Test Nos. 19 and 22 had a failure of the video. As they were the same release angles as test Nos. 18 and 21 respectively, the same velocities were used. Test No. 41 contained a few pre-test fractures. The results of this test are included in the analysis, but it is noted that this run does exhibit lower forces for a nearly identical test run No. 32.

Table 2-3. Round 1 results

Test #	Group	Indenter Diameter [cm]	Ice Diameter [cm]	Holder Height [cm]	Ice Depth [cm]	Release Angle [deg]	Small Carriage Mass [kg]	Large Carriage Mass [kg]	Contact Speed [m/s]	Force [N]
1	ICETECH	15	25	11	11	30	105.647	106.215	2.13	32,591
2	ICETECH	15	25	11	11	60	105.647	106.215	4.106	51,707
3	ICETECH	15	25	11	11	30	105.647	106.215	2.126	34,476
4	ICETECH	15	25	11	11	60	105.647	106.215	3.874	51,161
5	ICETECH	15	25	11	11	30	105.647	106.215	2.197	43,002
6	ICETECH	15	25	11	11	60	105.647	106.215	2.088	33,092
7	ICETECH	15	25	11	11	30	105.647	106.215	4.305	45,659
8	ICETECH	15	25	11	11	60	105.647	106.215	2.05	29,623
9	ICETECH	15	25	11	11	30	105.647	106.215	4.34	51,906
10	ICETECH	15	25	11	11	60	105.647	106.215	2.322	32,144
11	ICETECH	15	25	11	11	30	105.647	106.215	4.752	37,992
12	ICETECH	15	25	11	11	60	105.647	106.215	3.445	40,573
13	ICETECH	15	25	11	11	45	105.647	106.215	3.311	39,767
14	ICETECH	5	25	11	11	45	102.148	106.215	2.22	15,089
15	ICETECH	5	25	11	11	30	102.148	106.215	3.506	21,060
16	Sep. 26	15	25	11	11	60	105.647	106.215	4.95	39,321
17	Sep. 26	15	25	5	11	60	105.647	104.903	5.083	29,146
18	Sep. 26	15	25	11	11	60	105.647	106.215	2.152	21,174
19	Sep. 26	15	25	5	11	60	105.647	104.903	2.152	24,294
20	Sep. 26	15	25	11	11	60	105.647	106.215	4.605	29,989
21	Sep. 26	15	25	5	11	60	105.647	105.229	4.275	31,330
22	Sep. 26	15	25	5	11	60	105.647	105.229	4.275	37,482
23	Phase 1	15	35	11	30	45	111.24	127.48	3.334	35,836
24	Phase 1	15	35	11	11	45	111.24	127.43	3.423	49,130
25	Phase 1	15	35	5	11	45	111.24	127.5	3.62	37,259
26	Phase 1	7.5	35	11	30	45	111.48	127.48	3.279	21,108
27	Phase 1	7.5	35	11	11	45	111.48	127.43	3.37	33,259
28	Phase 1	7.5	35	5	11	45	111.48	127.5	3.696	27,949
29	Phase 1	15	25	11	30	45	111.24	127.49	3.508	29,695
30	Phase 1	15	25	11	11	45	111.24	127.5	3.633	35,395
31	Phase 1	15	25	5	11	45	111.24	127.53	3.655	33,007
32	Phase 1	7.5	25	11	30	45	111.48	127.49	3.54	22,307
33	Phase 1	7.5	25	11	11	45	111.48	127.5	3.673	31,506
34	Phase 1	7.5	25	5	11	45	111.48	127.53	3.705	30,099
35	Phase 1	15	15	11	30	45	111.24	127.44	3.419	7,212
36	Phase 1	15	15	11	11	45	111.24	127.43	3.67	48,618
37	Phase 1	15	15	5	11	45	111.24	127.49	3.656	12,293
38	Phase 1	7.5	15	11	30	45	111.48	127.44	3.52	7,953
39	Phase 1	7.5	15	11	11	45	111.48	127.43	3.563	23,458
40	Phase 1	7.5	15	5	11	45	111.48	127.49	3.588	12,469
41	Phase 1	7.5	25	11	30	45	111.48	127.49	3.411	16,502

3 Analysis

Following the method set forth in Sharp, 1981 (Sharp, 1981) a dimensional analysis can be conducted. The primary factors are considered to be:

M: Mass: [kg]

V: Velocity: [m/s]

D: Dimension [m] {R_s: Radius of Sphere, R_i: Radius of Ice}

σ_i: Ice strength: [Pa]

θ: Confinement angle: [deg] – Non Dimensional

3.1 Mass

Mass in the case of this analysis is taken as being the effective mass for the collision in accordance with Newton's laws. Mass m_1 will be for one of the pendulum carriages and mass m_2 will be for the other carriage, their respective accelerations are a_1 and a_2 . Also applying Newton's third law the forces between the carriages are equal and opposite, therefore we can write the familiar equation:

$$F_{12} = m_1 a_1 \text{ and } F_{21} = m_2 a_2 \quad \text{Equation 3-1}$$

$$F_{12} = -F_{21} \quad \text{Equation 3-2}$$

Therefore:

$$m_1 a_1 = -m_2 a_2 \Rightarrow a_2 = -\frac{m_1}{m_2} a_1 \quad \text{Equation 3-3}$$

Relative acceleration between the two carriages can be given by:

$$a_{rel} = a_1 - a_2 \quad \text{Equation 3-4}$$

Combining Equation 3-3 and Equation 3-4 gives:

$$a_{rel} = a_1 - \left(-\frac{m_1}{m_2} a_1\right) = \left(1 + \frac{m_1}{m_2}\right) a_1 \quad \text{Equation 3-5}$$

Using Equation 3-4 in Newton's second law gives:

$$F = m_{eff} a_{rel} \quad \text{Equation 3-6}$$

Which must also equal Equation 3-1. Therefore:

$$F_{12} = m_1 a_1 = m_{eff} a_{rel}$$

$$m_1 a_1 = m_{eff} \left(1 + \frac{m_1}{m_2}\right) a_1$$

$$m_{eff} = \frac{m_1 \frac{1}{m_1}}{\left(1 + \frac{m_1}{m_2}\right) \frac{1}{m_1}}$$

$$m_{eff} = \frac{1}{\frac{1}{m_1} + \frac{1}{m_2}} \quad \text{Equation 3-7}$$

3.2 Velocity

Velocity is measured by on-screen pixel counting using high speed photography; as was done in (Oldford et al., 2014). This procedure is offered in more detail in Appendix 3. The

principle behind the velocity estimates is that using pixels and known distances on screen, a relative displacement from one frame to another can be established. Knowing the frame rate for the video (1,000 fps) a distance over time is established. This process was repeated multiple times for each carriage and averaged to produce an estimated velocity for each carriage. The two carriage velocities are added to give a speed at impact.

For experimental set up, a velocity relative to release angle is estimated using Equation 2-7. For example if a speed of 3 m/s is desired, the angle of release would be set to:

$$V = 2\sqrt{2g(r - r \cos \emptyset)}$$

$$\emptyset = \cos^{-1} \left(1 - \frac{1}{2gr} \left(\frac{V}{2} \right)^2 \right)$$

$$\emptyset = \cos^{-1} \left(1 - \frac{1}{2 \times 9.81 \times 0.5} \left(\frac{3}{2} \right)^2 \right) = 39.6^\circ$$

3.3 Ice Strength

Ice strength was not measured for each sample, rather it was determined for one sample and assumed constant for all the test runs. The value used was cross-referenced with results obtained from other laboratory experiments conducted at Memorial University and found to be comparable with respect to ice strength values. (S. Bruneau et al., 2013), (S. E. Bruneau et al., 2011)

The sample chosen to be the representative for all the test runs needed to offer the most favorable characteristics. The optimal test would maximize the ice surface and also use

the large sphere to maximize crushing. The sample would also need to be radially bound to minimize large spalls. The test chosen was run 2 in the Phase 1 Test plan (Test# 24 of Table 2-3).

For this test run the high speed photography was used to estimate the moment of contact and the moment of final indentation (end of positive motion). The frames between contact and final indentation were examined to establish indentation at each frame through the crushing event. These indentations were then compared to the force data from the load cells. The load cells operated at a rate of 25,000 measurements per second whereas the high speed camera filmed at a rate of 1,000 frames per second. This resulted in 25 force measurements per frame of video. The moment of contact in the video was visually established. This is simply done by scrolling frame by frame until signs of impact can be seen. The moment of impact in the force time history was established by examining the force levels. The moment at which the forces began to rise was selected. In the case of this test run the force time history is given below in Table 3-1, with line 4 (highlighted) selected as the moment of impact.

Table 3-1. Test# 24 - Force Time History

Time*	Total Force
19.83124	74.8
19.83128	69.4
19.83132	75.8
19.83136	70.4
19.8314	147.2
19.83144	485.9
19.83148	1229.4
19.83152	2,426.5
19.83156	4,373.0
19.8316	7,288.5

Every 25th row from the highlighted line was selected to correspond with each consecutive frame in the video up until the end of indentation. Using the video a measurement of movement of both carriages was made and combined to develop an indentation for each frame. Also knowing the indentation and the geometry of the indenter (spherical) a nominal cross-sectional area was calculated. This nominal area and the highest force recorded in the last 25 lines of data gives a nominal pressure that was assigned to the frame in the video. Then an average of all “frame” pressures was made to give an average pressure for the indentation event. This average pressure is taken as the compressive strength for the ice. A summary of the pressures is given below in Table 3-2, as well as a complete presentation in Appendix 2.

Table 3-2. Summary of Pressures

Time *	Total Force									
		Frame #	Small Carriage Movement [mm]	Large Carriage Movement [mm]	Total Indentation [mm]	Radius for normal area	Nominal contact area [mm ²]	Nominal contact area [m ²]	Peak force [N]	Nominal Pressure [Pa]
19.83	75.80									
19.83	70.37	390	0.00	0.00	0.00	0.00	0.00	0.00		
19.83	22322.09	391	1.84	1.43	3.27	21.90	1506.55	0.00	23934.66	15,887,100
19.83	39980.75	392	2.78	3.26	6.05	29.50	2734.49	0.00	40170.65	14,690,370
19.83	46236.47	393	3.90	3.66	7.56	32.81	3382.04	0.00	46236.47	13,671,190
19.84	39135.55	394	4.85	4.06	8.91	35.46	3949.62	0.00	49130.09	12,439,180
19.84	27905.64	395	5.57	4.69	10.26	37.87	4505.34	0.00	40674.53	9,028,066
19.84	24025.92	396	5.79	5.68	11.47	39.85	4990.04	0.00	30746.91	6,161,652
19.84	22941.59									
19.84	22011.81								Average pressure:	11,979,592

3.4 Confinement

Confinement of the ice is one of the key parameters under investigation in this thesis. Two aspects of confinement are considered: First is the “confinement angle” or the depth of ice before the edges become confined. Second is the “radial confinement”, or the radius of ice from point of impact out to the confining ring or ice edge.

3.4.1 Confinement Angle

Confinement angle is one of the two proposed measures of ice sample confinement defined in this thesis. Upon impact the ice will tend to split and spall with many fractures propagating from the point of impact. The confinement angle is visualized by imagining a cone of ice within the sample. The tip is the point of impact and the base is the upper edge of the confining holder. Below in Figure 3-1 a 35 cm diameter ice sample with a

depth of 30 cm is shown to demonstrate the concept of confinement angle using an 11 cm tall holder.

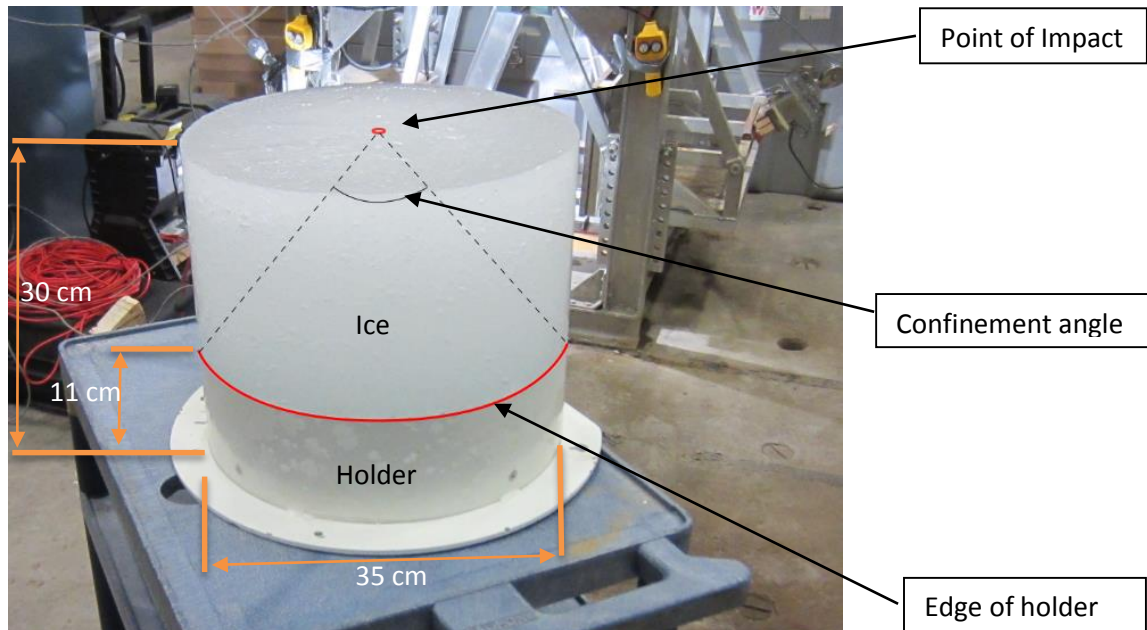


Figure 3-1. Confinement Angle

3.4.2 Radial Confinement

In many rules for structural loads, such as the IACS Polar Class rules (*IACS POLAR CLASS Rules, 2011*), an ice sheet is assumed to be of infinite horizontal extent. In order to simulate an infinite sheet some researchers encase the ice in some form of holder. In some cases the holder is manufactured to be extremely strong and assumed to be rigid in relation to the ice (Kim et al., 2012), (G. Timco, 1983).

In this research three different diameter ice samples were selected, 15 cm, 25 cm, and 35 cm diameter. The ice diameter relative to the indenter diameter is one way of characterizing the difference in ice sizes. A small radius ice sample with a large diameter

indenter results in very little ice (radially) to resist the collision, where as a large diameter ice sample and a small indenter offers a lot more ice (radially) to resist the energy of the collision. These provide relative measures of confinement that can give insight into scale effects or relative size effects.

3.5 Dimensional Analysis Set-up

$$F = \phi(M, V, D, \sigma_i, \theta) \rightarrow F = KM^a V^b D^c \sigma_i^d \quad \text{Equation 3-8}$$

Note that θ is left out of the equation for now due it being non-dimensional.

$$\frac{[M][L]}{[T]^2} = K[M]^a \left(\frac{[L]}{[T]}\right)^b [L]^c \left(\frac{[M]}{[L][T]^2}\right)^d \quad \text{Equation 3-9}$$

Where:

M = Mass
L = Length
T = Time
K = A Constant

$$[M]: 1 = a + d \Rightarrow d = 1 - a \quad \text{Equation 3-10}$$

$$[L]: 1 = b + c - d \quad \text{Equation 3-11}$$

$$[T]: -2 = -b - 2d \Rightarrow b = 2 - 2d \quad \text{Equation 3-12}$$

Using Equation 3-10 in Equation 3-12 gives:

$$b = 2 - 2(1 - a) \Rightarrow b = 2a \quad \text{Equation 3-13}$$

Using Equation 3-10 and Equation 3-13 in Equation 3-11 gives:

$$\begin{aligned}
1 &= 2a + c - 1 + a \\
2 &= 3a + c \\
c &= 2 - 3a
\end{aligned}$$

Equation 3-14

Using Equation 3-10, Equation 3-13, and Equation 3-14 into Equation 3-8 gives:

$$F = KM^a V^{2a} D^{2-3a} \sigma^{1-a}$$

$$F = \frac{KM^a V^{2a} D^2 \sigma}{D^{3a} \sigma^a}$$

$$F = K\sigma D^2 \left(\frac{MV^2}{D^3 \sigma} \right)^a$$

The exponent 'a' is combined into the general function ϕ to give Equation 3-15.

$$\frac{F}{K\sigma D^2} = \phi \left(\frac{MV^2}{D^3 \sigma} \right)$$

Equation 3-15

Including the non-dimensional terms for confinement angle and ratio of ice radius to sphere radius by compounding gives:

$$\frac{F}{K\theta\sigma D^2} \left(\frac{R_i}{R_s} \right)^e = \phi \left(\frac{MV^2}{D^3 \sigma} \right)$$

Equation 3-16

Where e is some exponent that will be derived from the data. Multiplying the non-dimensional fraction inside the function from the right hand side to the non-dimensional

term on the left hand side of Equation 3-16 through the principal of non-dimensional term compounding generates a third non-dimensional term.

$$\frac{F}{K\theta\sigma D^2} \left(\frac{D^3\sigma}{MV^2} \right) \left(\frac{R_i}{R_s} \right)^e = \phi \left(\frac{MV^2}{D^3\sigma} \right)$$

$$\frac{FD}{K\theta MV^2} \left(\frac{R_i}{R_s} \right)^e = C_0$$

Equation 3-17

Where:

$$C_0 = \phi \left(\frac{MV^2}{D^3\sigma} \right)$$

Equation 3-18

Re-writing Equation 3-17 to solve for F gives:

$$F = \frac{K\theta MV^2 C_0}{D} \left(\frac{R_s}{R_i} \right)^e$$

Equation 3-19

Using the Dimension “D” in Equation 3-19 as the Radius of the Sphere, R_s , than Equation 3-19 becomes:

$$F = \frac{K\theta MV^2 C_0}{R_s} \left(\frac{R_s}{R_i} \right)^e$$

Equation 3-20

Which can also be solved for C_0 :

$$C_0 = \frac{FR_s}{K\theta MV^2} \left(\frac{R_s}{R_i} \right)^e = \frac{F}{K\theta MV^2 / R_s} \left(\frac{R_s}{R_i} \right)^e$$

Equation 3-21

It is noted that in Equation 3-18 D^3 is a characteristic volume and applying the sphere radius and multiplying by $4/3\pi$ will make D^3 the volume of the spherical indenter.

Therefore we re-write Equation 3-18 as:

$$C_o = \phi \left(\frac{MV^2}{\frac{4}{3}\pi R_s^3 \sigma} \right)$$

$$C_o = \phi \left(\frac{MV^2}{\nabla_s \sigma} \right)$$

Equation 3-22

Where ∇_s is the volume of the spherical indenter. For simplicity in explanation we take the term inside the brackets in Equation 3-22 to be ζ such that:

$$\zeta = \frac{MV^2}{\nabla_s \sigma}$$

Equation 3-23

3.5.1 Examination of C_o

Equation 3-21 is the multiplication of two non-dimensional terms. Considering the ratio of radii first; this ratio gives a ratio for the ‘sharpness’ of the indenter over the amount of ice required to be fractured to create a spall. Smaller indenters tend to penetrate more easily and form a wedge to create fractures in the ice sample. The other term in the equation is a ratio of energies. The kinetic energy for the collision to the energy absorbed during the collision.

3.5.2 Examination of ζ

This zeta term is fundamentally a ratio of kinetic energy over ice strength. The numerator is essentially a function of Equation 2-3, kinetic energy. The denominator is the volume of the indenter multiplied by the ice strength, giving an energy required to crush the ice with the given indenter. Another way of thinking about this ratio is that it is the resistance of the ice to the indenter's kinetic energy.

3.6 Analysis of Data

To begin the analysis a plot of ζ vs. C_0 is developed and presented in Figure 3-2 on a Log-Log scale for the first 41 tests. It is noted that for this plot e is initially taken as -1, and $K = 1$.

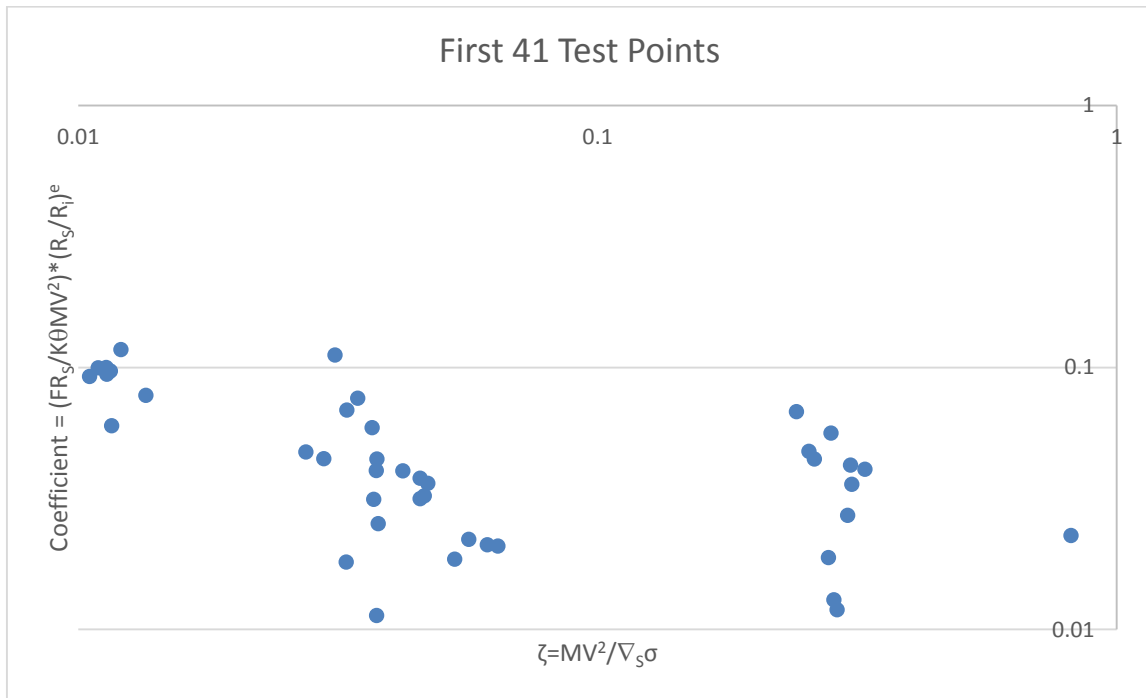


Figure 3-2. ζ Vs. Coefficient for first 41 tests

In order to simplify the statistical confidence intervals, a logarithm of the data is taken and the plot regenerated on a normal scale as follows in Figure 3-3.

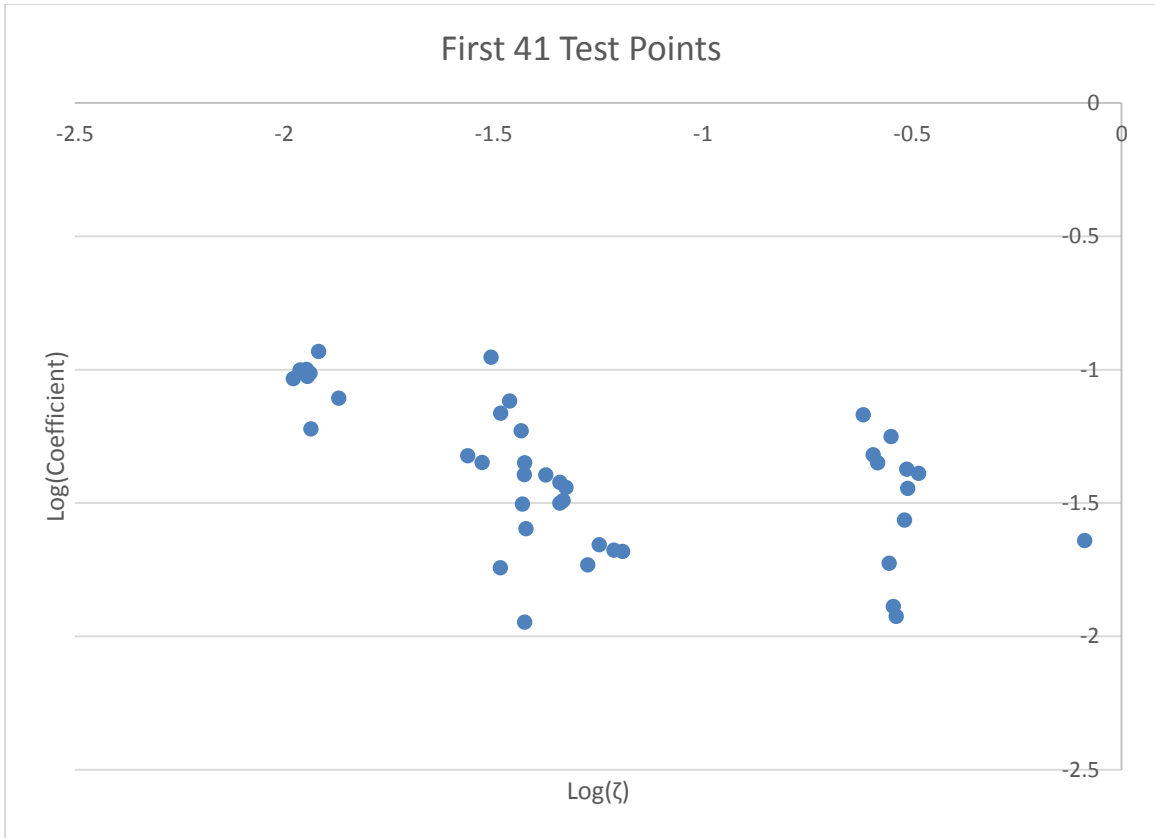


Figure 3-3. ζ Vs. Coefficient for first 41 tests - Regular Scale

To do this Equation 3-23 is re-written as:

$$\zeta' = \log \left[\frac{MV^2}{\nabla_s \sigma} \right] \quad \text{Equation 3-24}$$

and Equation 3-21 is re-written as:

$$C_o' = \log \left[\frac{FR_s}{K\theta MV^2} \left(\frac{R_s}{R_i} \right)^e \right] \quad \text{Equation 3-25}$$

This results in a force prediction formula of:

$$10^{c'_o} = \frac{FR_s}{K\theta MV^2} \left(\frac{R_s}{R_i}\right)^e$$

$$F = \frac{K\theta MV^2 10^{c'_o}}{R_s} \left(\frac{R_i}{R_s}\right)^e$$

Equation 3-26

A line can be fit to these points using a simple linear regression. This line (shown in Figure 3-4) is found using the built-in trend line function in Microsoft Excel® 2013 and selecting the “linear” option.

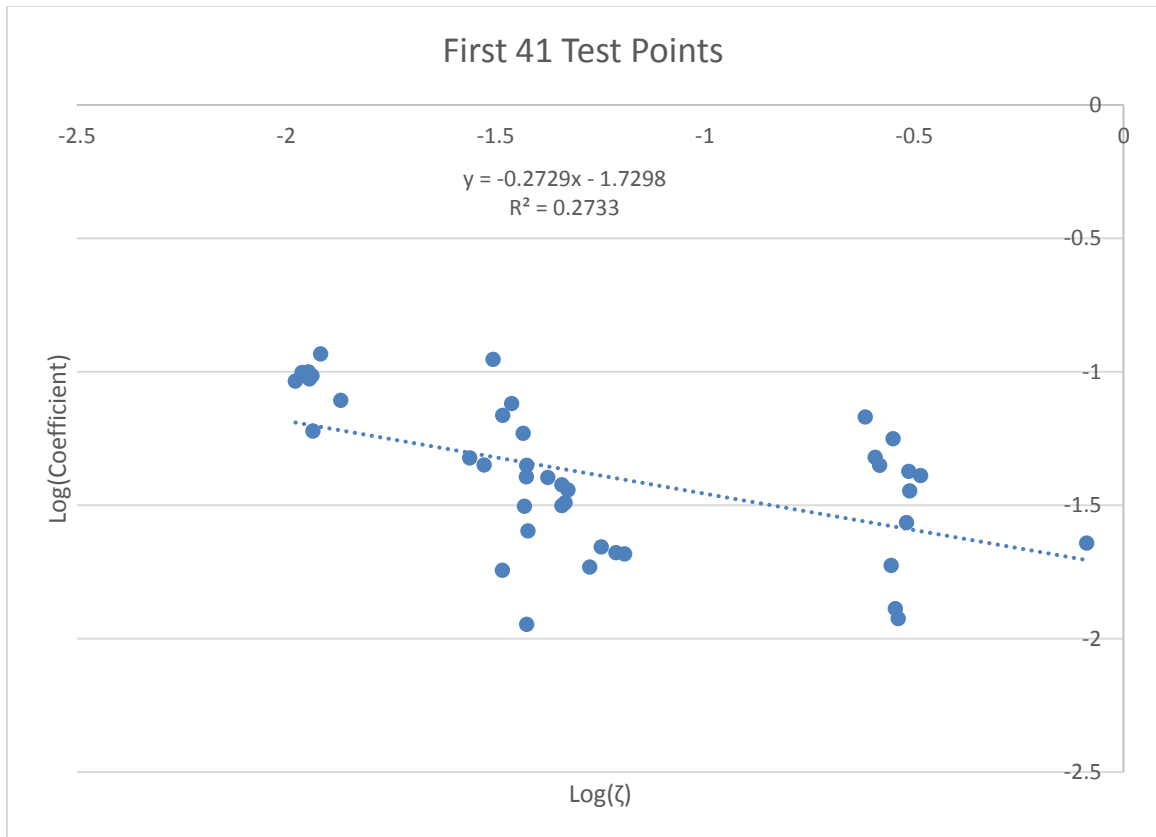


Figure 3-4. Line fit to data

The value of e can be adjusted to minimize the spread of the data. Using the R^2 value of the trend line as the optimizing value the following is found. The values are presented in Table 3-3 as well as graphically in Figure 3-5.

e	R^2
-1	0.2733
-0.1	0.7673
-0.01	0.7993
-0.001	0.8022
0	0.8025
0.001	0.8028
0.01	0.8057
0.1	0.8323
1	0.9238
1.1	0.9224
1.2	0.92
1.5	0.9081

Table 3-3. Values for e

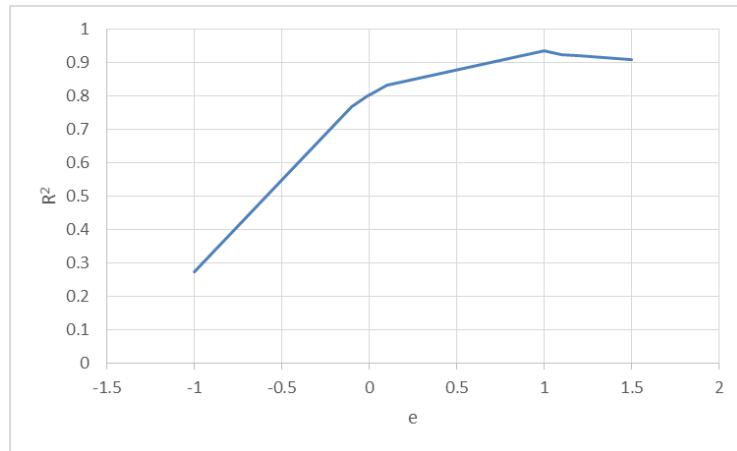


Figure 3-5. Values for e

The R^2 for e peaks at a value of 1, therefore we take $e = 1$.

An upper and lower boundary for the data set can be established as shown in Figure 3-6.

This is done by 2 standard deviations above and below the mean line (the line shown in Figure 3-4).

An alternative way of looking at the upper bound is that if the data is spread about the trend line in a normal distribution, 95% of all the data points are below this upper bound.

The method of establishing the standard deviation in this case is the method described in (Walpole, Myers, & Myers, 1998) and presented in Equation 3-27:

$$S = \sqrt{\frac{\sum_{i=1}^n (X_i - \bar{X})^2}{n - 1}}$$

Equation 3-27

Where:

n = number of test runs (data points)

X_i = Data point value

\bar{X} = Mean

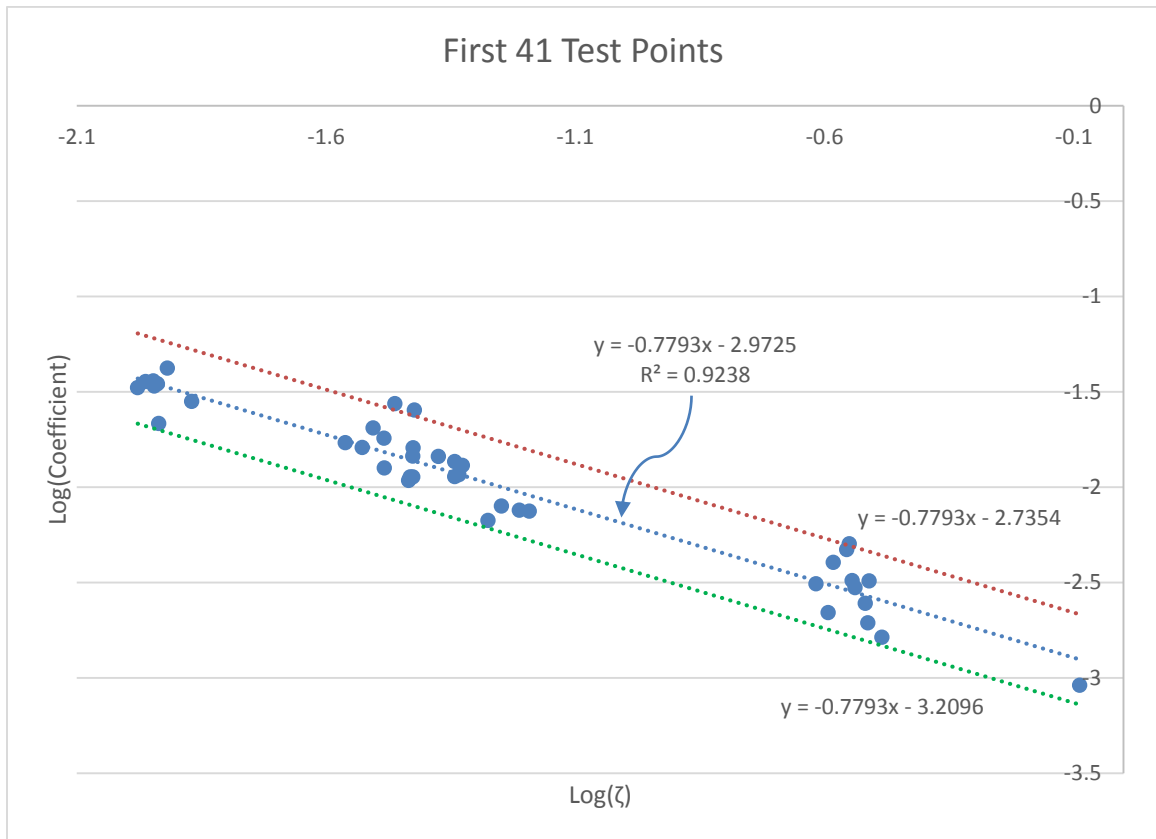


Figure 3-6. Bounds of First 41 Data Points

3.7 Force Estimation

Values for the variables on the x-axis (ζ) of the above plots can be controlled to some extent. The mass is the easiest to closely control with an explanation of equivalent mass

given in 3.1 Mass. Velocity is also explained earlier in 3.2 Velocity. Although velocity can be controlled it is slightly more difficult to tightly control than mass. The volume of the sphere is extremely well controlled by using machined aluminum spheres, and the ice strength is controlled as closely as possible using the ice making techniques defined in 2.2 Ice Samples. Adjusting these values to determine a value for ζ , and entering that into the line equations given in Figure 3-6 yields a value for the coefficient. Inside the coefficient, all the variables except for force can be controlled in the laboratory which will give an estimate for force.

For example conducting tests with an equivalent mass of 59.48 kg (small carriage mass = 111.48 kg, large carriage mass = 127.52 kg), a release angle of 45 deg ($V \sim 3.39$ m/s), using the 7.5 cm diameter sphere ($\nabla_s = 220.9 \times 10^{-6}$ m³) and an ice strength of 11,979,591 Pa, ζ can be calculated as follows:

$$\zeta = \log \frac{MV^2}{\nabla_s \sigma} = \log \frac{59.48 \times 3.39^2}{220.9 \times 10^{-6} \times 11,979,591} = -0.5878$$

Then using the equation for the line in Figure 3-6 the following coefficient value can be calculated:

$$y = -0.7793 \times X - 2.9725 = -0.7793 \times -0.5878 - 2.9725 = -2.5144$$

Using the 35 cm diameter ice sample that is cut flush with the holder (radially confined) the force can be estimated as:

$$F = \frac{K\theta MV^2 10^{C_o}}{R_s} \left(\frac{R_s}{R_i}\right)^e = \frac{1 \times 180 \times 59.48 \times 3.39^2 \times 10^{-2.5144}}{0.0375} \left(\frac{0.0375}{0.175}\right)^1 = 46,843 \text{ N}$$

Using a similar technique the upper bound can be calculated to be 80,865 N.

3.8 Confinement Angle Effects on Results

Given that the idea of confinement angle is a new concept that attempts to quantitatively capture the effect of ice confinement and the purpose of this work was to test the idea, the data was analyzed to measure the utility of the angle by looking at the overall data set, with and without the confinement angle as a variable. By looking at certain data measures both with and without the inclusion of the confinement angle it is intended to demonstrate the effectiveness of the concept.

The data from Figure 3-6 is compared with the same data presented without the confinement angle considered. The data without confinement angle is plotted in Figure 3-7. The standard deviation for the data with confinement angle considered (Figure 3-6) is 0.1469, whereas without confinement angle (Figure 3-7) the standard deviation is 0.1937. This represents approximately a 25% decrease in standard deviation when confinement angle is considered.

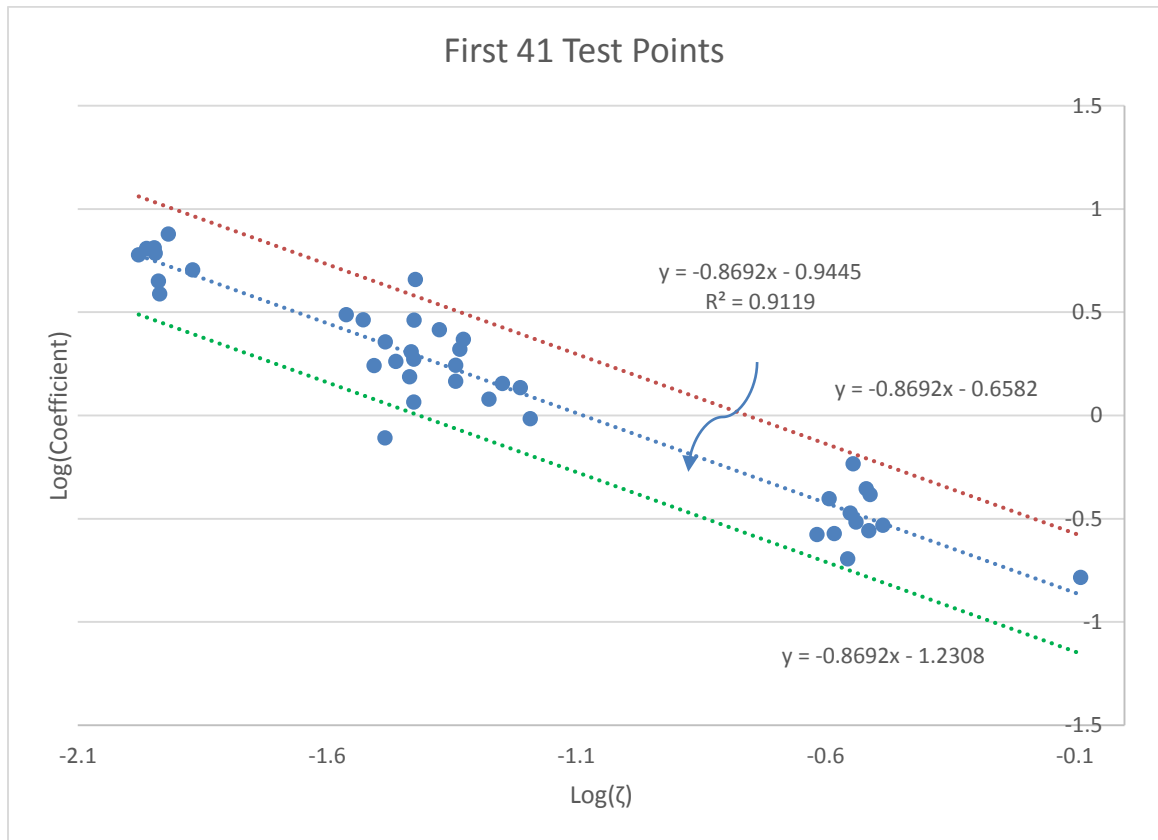


Figure 3-7. Data without Confinement Angle

These two plots appear very similar but the R^2 without confinement angle drops by a percentage point from 92.38% to 91.19%, meaning the data spread increased with the loss of confinement angle and thus the inclusion of the confinement angle explains a small portion of the variability in the data. This reduced spread alone is sufficient to judge if the confinement angle is a valued attribute for making the data coalesce. But a better way of examining the difference is to examine the predicted loads from the same data set.

Applying the same examples given above in 3.7 Force Estimation, the force prediction using the plots in Figure 3-7 would give the following:

$$\zeta = \log \frac{MV^2}{\nabla_s \sigma} = \log \frac{59.48 \times 3.39^2}{220.9 \times 10^{-6} \times 11,979,591} = -0.5878$$

$$y = -0.8692 \times X - 0.9445 = -0.8692 \times -0.5878 - 0.9445 = -0.43358$$

$$F = \frac{KMV^2 10^{C_o}}{R_s} \left(\frac{R_s}{R_i} \right)^e = \frac{1 \times 59.48 \times 3.39^2 \times 10^{-0.43358}}{0.0375} \left(\frac{0.0375}{0.175} \right)^1 = 31,348 \text{ N}$$

Likewise the upper bound gives a force estimate of 60,604 N. This is a spread of predicted forces of 60,604 – 31,348 = 29,256 N whereas considering the confinement angle gives a load prediction spread of 33,807 N. This represents about a 13.5 % increase in predicted envelope when considering the confinement angle.

The above example only considers a fully confined ice sample, i.e. angle = 180 deg. An unconfined sample, where the confinement angle will have a greater effect on the results, is considered next. The inputs used for this case are given in Table 3-4.

Table 3-4. Sample Inputs

Large Carriage Mass =	127.48	kg
Small Carriage Mass =	111.24	kg
Release Angle =	45	deg
Sphere Diameter =	15	cm
Ice Diameter =	35	cm
Ice Depth =	30	cm
Holder Height =	11	cm

Yields the values in Table 3-5.

Table 3-5. Comparison: With or Without Confinement Angle

Effective Mass =	59.4		kg
Estimated Contact Speed =	3.39		m/s
$\zeta = \text{Log}[MV^2/(4/3)\pi r^3 \sigma]$ =	-1.49096		nd
Confinement Angle =	85.29		deg
	With Confinement Angle		Without Confinement Angle
Upper Bound Force =	48,417	N	92,329 N
Predicted Force =	28,047	N	47,758 N

In Table 3-5 it is very clear that the analysis without the confinement angle yields a huge difference in values and spread, about 54% increase in spread without the confinement angle considered. It is also worth noting that test number 23 was in line with these parameters and a force of 35,836 N was measured. Another example in between the two given above is presented in Table 3-6.

Table 3-6. Example 2 With or Without Confinement Angle

Large Carriage Mass =	127.52		Kg
Small Carriage Mass =	111.48		Kg
Release Angle =	45		Deg
Sphere Diameter =	15		Cm
Ice Diameter =	25		Cm
Ice Depth =	11		Cm
Holder Height =	5		Cm
Effective Mass =	85.7		Kg
Estimated Contact Speed =	5.08		m/s
$\zeta = \text{Log}[MV^2/(4/3)\pi r^3 \sigma]$ =	-1.4909		Nd
Confinement Angle =	128.7		Deg
	With Confinement Angle		Without Confinement Angle
Upper Bound Force =	52,206	N	65,960 N
Predicted Force =	30,241	N	34,119 N

This example (Table 3-6) shows that a sample with a medium confinement angle still has about a 31% tighter range when considering the confinement angle. A study of the confinement angle vs the predicted spread is given below using the same input values as Table 3-6 but varying ice diameter, depth and holder height.

In Figure 3-9 the difference is defined as:

$$Difference = 1 - \left(\frac{Prediction\ Spread\ With\ Angle}{Prediction\ Spread\ Without\ Angle} \right)$$

Where:

$$Prediction\ Spread = Upper\ Bound\ Force - Predicted\ Force \text{ (See Figure 3-8)}$$

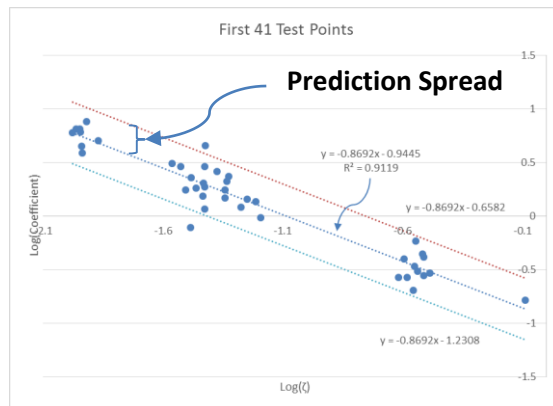


Figure 3-8. Prediction Spread

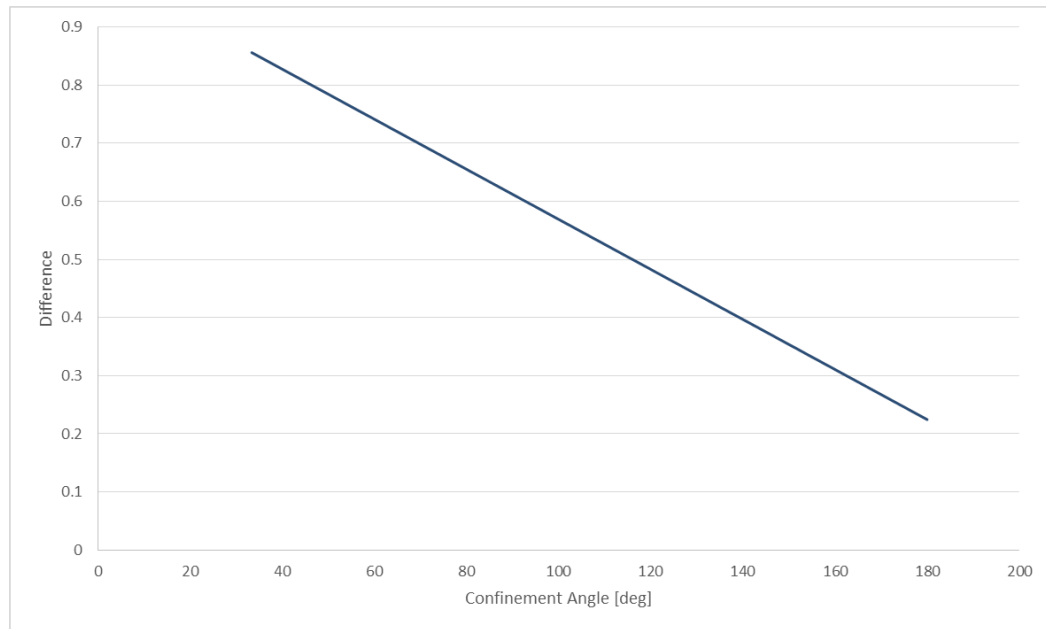


Figure 3-9. Difference

This can also be examined in a slightly different way by plotting the predicted forces as compared to confinement angle (Figure 3-10, Figure 3-11, & Figure 3-12). In these plots it is clear that the difference is reduced at lower confinement angles (cases where the sample is more fully confined).

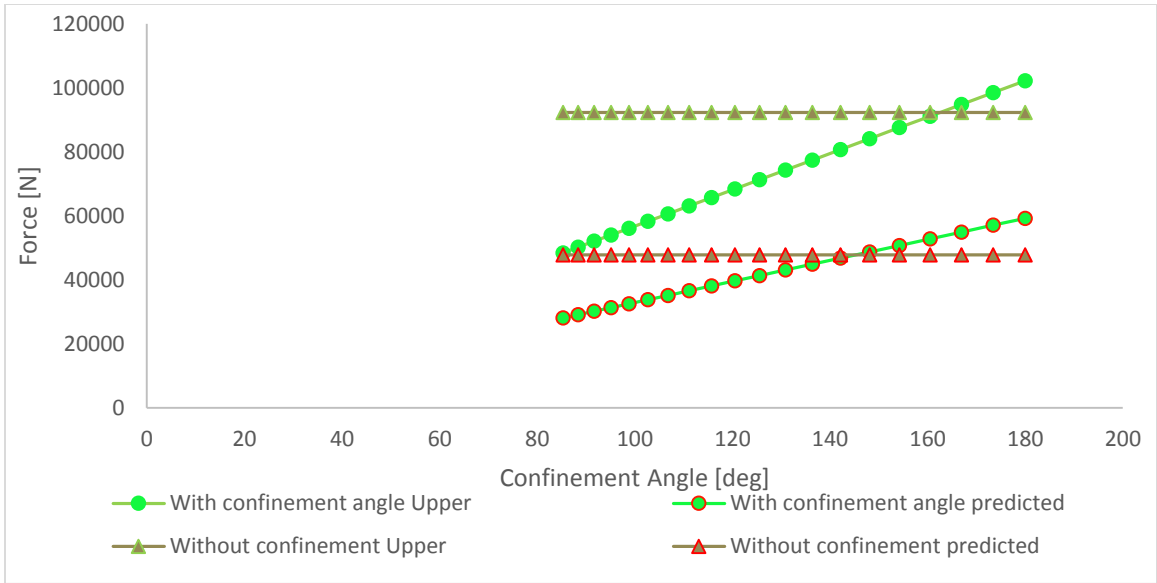


Figure 3-10. Predicted Forces - With and Without Confinement Angle – 35 cm Diameter samples

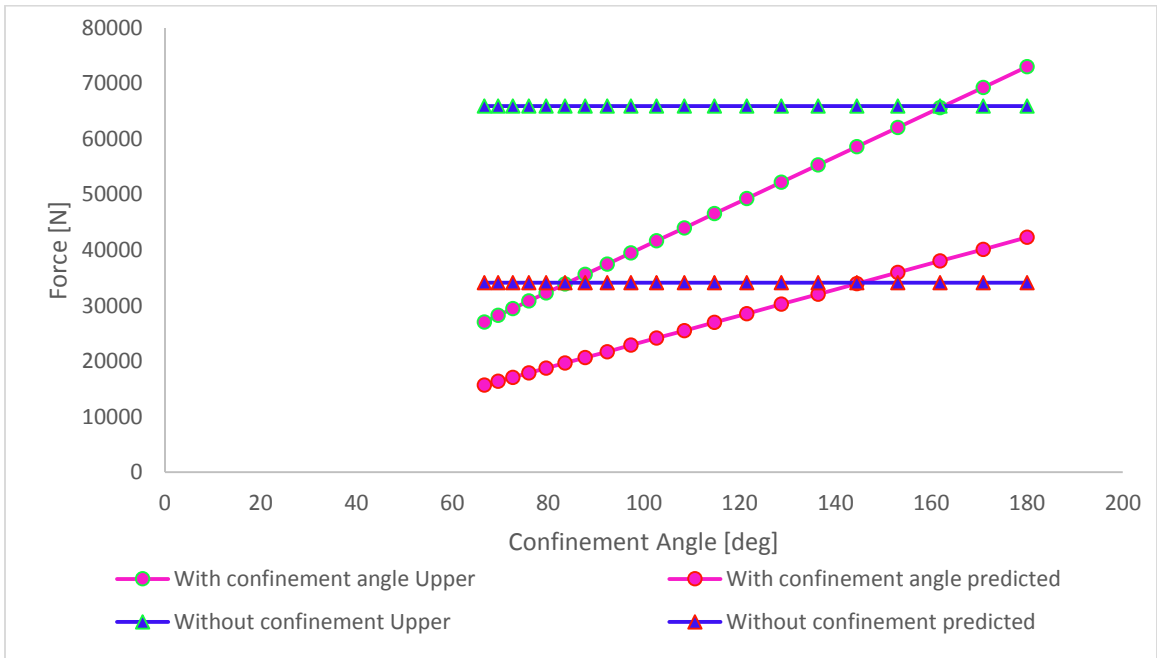


Figure 3-11. Predicted Forces - With and Without Confinement Angle – 25 cm Diameter samples

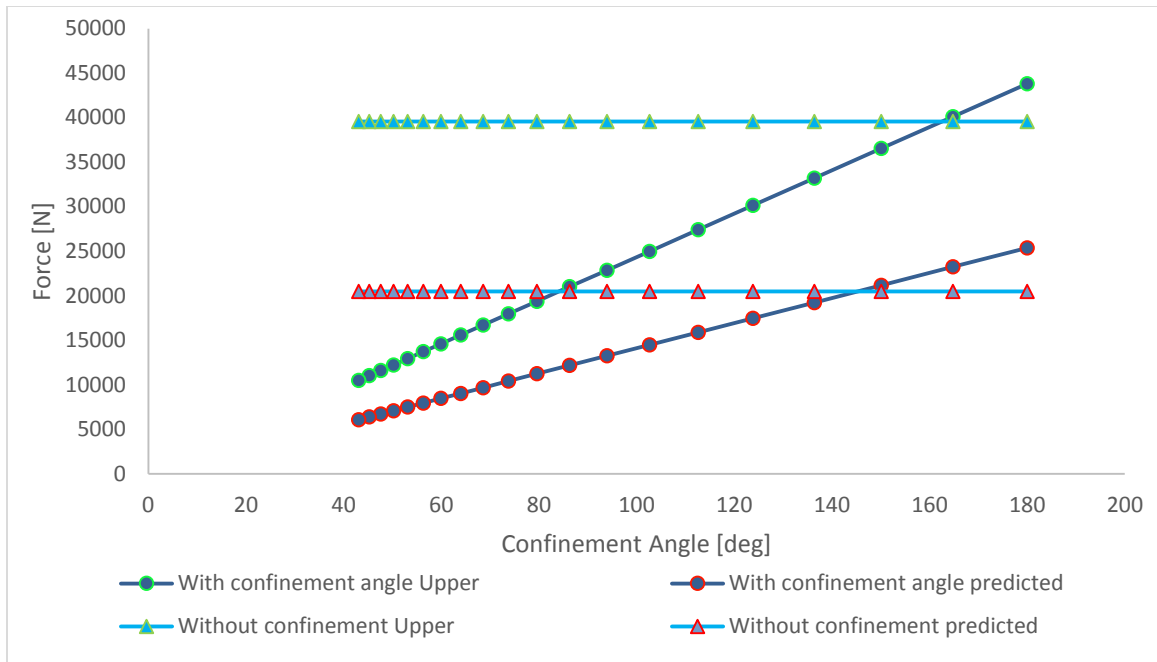


Figure 3-12. Predicted Forces - With and Without Confinement Angle – 15 cm Diameter samples

The significance of Figure 3-10, Figure 3-11, & Figure 3-12 is that when the ice becomes less confined, i.e. lower angles, predicted force values become lower. This can be rationalized by considering what the confinement angle represents. At 180 degrees the indenter is impacting on a smooth surface with the outer sides bound by a steel ring. An angle smaller than 180 means some value of the ice edge is unconfined, or protruding out of the holder. Unconfined ice is free to fail in fracture and reduce loads by spalling, whereas confined ice is forced to fail primarily by crushing.

3.9 Phase 2 Tests

The Phase Two tests consist of verification of the force estimates produced using the formulations from Round 1 tests. Two tests are conducted with an aim of checking the force prediction in a region where the prediction is expected to be reliable. For these

tests, parameters consistent with those of the third cluster of points from the left (see Figure 3-6) was selected ($\text{Log}(\zeta)$ between -0.6 and -0.5). The tests are number 42 and 43 and are detailed in Table 3-7 and shown in Figure 3-13. Two tests were conducted near the furthest right point in Figure 3-6 as only one data point was obtained in that area in phase 1, these tests are numbers 44 and 45. Additionally tests were conducted to land in between the clusters in Figure 3-6. These tests are numbers 46 and 47, also with details in Table 3-7 and Figure 3-13. Test No. 47 was deliberately done using a different depth than any other test, to get an untested confinement angle. This sample was grown just like the 30 cm deep samples but during processing was cut approximately in the middle. This difference was introduced into the test to ensure that the confinement methodology developed herein would work with a sample not perfectly in-line with other samples from the previous phase of tests. In addition to the varied depth dimension for sample 47, both samples 46 and 47 were created using a slightly different method. Neither of these samples were seeded, they were simply created by freezing distilled, de-ionized, and de-aerated water in the molds. Because an alternative ice making process was used the strength of these samples is determined using the technique described in 3.3 Ice Strength and test No. 46. In the case of tests 46 and 47 the ice strength term is valued at 9.2 MPa.

Table 3-7. Phase 2 tests

Test #	Group	Indenter Diameter [cm]	Ice diameter [cm]	Holder Height [cm]	Ice depth [cm]	Release angle [deg]	Small Carriage Mass [kg]	Big Carriage Mass [kg]	Contact Speed [m/s]	Force [N]
42	Phase 2	7.5	35	11	11	45	111.48	127.52	3.44	31,354
43	Phase 2	7.5	35	11	11	45	111.48	127.45	3.362	23,115
44	Phase 2	5	35	11	11	45.3	107.36	109.44	3.225	23,430
45	Phase 2	5	15	11	11	46.6	107.36	98.89	3.316	15,316
46	Phase 2	7.5	15	11	11	35.0	107.34	98.899	2.309	19,972
47	Phase 2	7.5	15	11	18.7	32.0	107.34	100.207	2.407	12,635

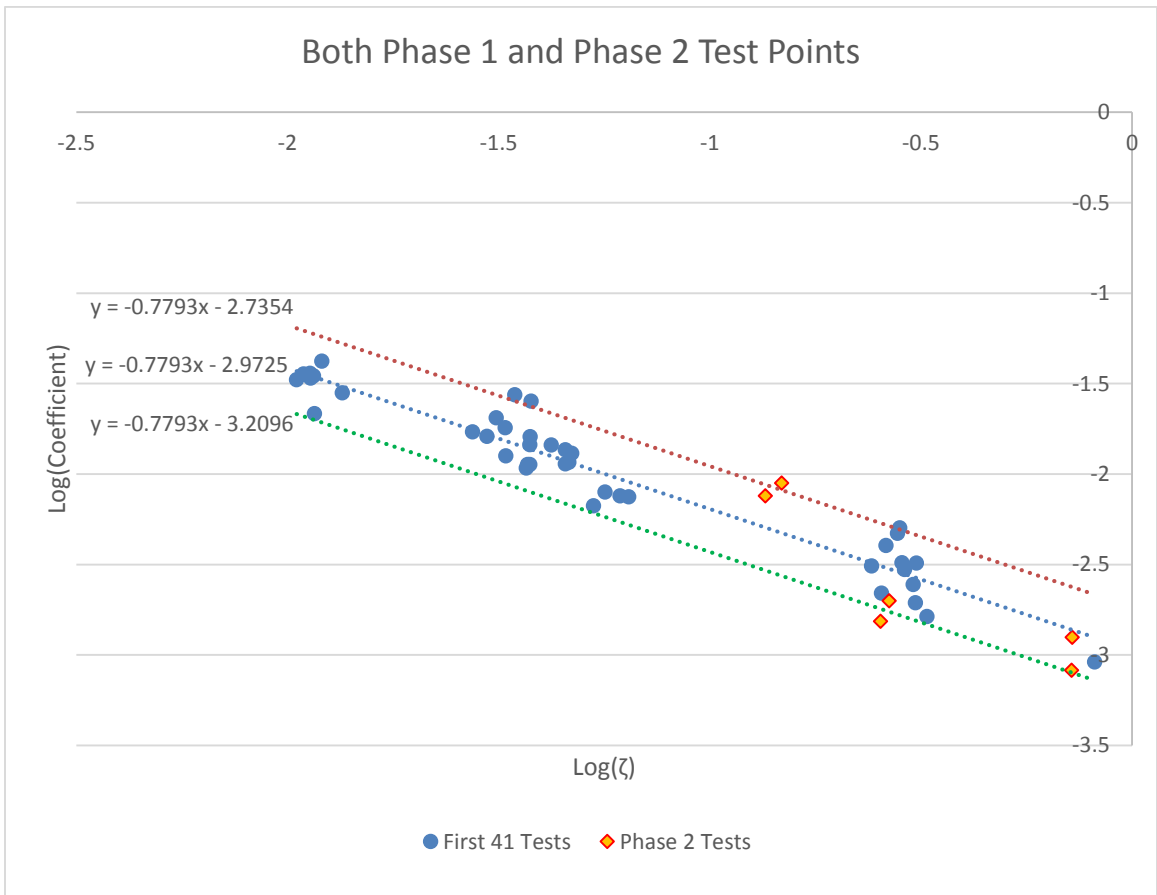


Figure 3-13. Data points including Phase 2 Tests

To obtain an alternative look at the data plotted in Figure 3-13, a transformation of the data is conducted to remove the Logarithmic scales. The altered representation is plotted in Figure 3-14 on a linear scale. The mean line and bounding lines are transformed simply

taking all points as 10^{ζ} . For example the mean line is given as an equation in Figure 3-13

as:

$$y = -0.7793X - 2.9725$$

Or more properly:

$$C_o = -0.7793\zeta - 2.9725$$

A couple of example points are transformed in Table 3-8.

Table 3-8. Example Transformations

ζ	C_o (Mean Line)	10^{ζ}	10^{C_o} (Mean Line)
-1.945	$-0.7793(-1.945) - 2.9725 = \mathbf{-1.457}$	$10^{-1.945} = \mathbf{0.0114}$	$10^{-1.457} = \mathbf{0.0349}$
-1.334	$-0.7793(-1.334) - 2.9725 = \mathbf{-1.933}$	$10^{-1.334} = \mathbf{0.0463}$	$10^{-1.933} = \mathbf{0.0117}$

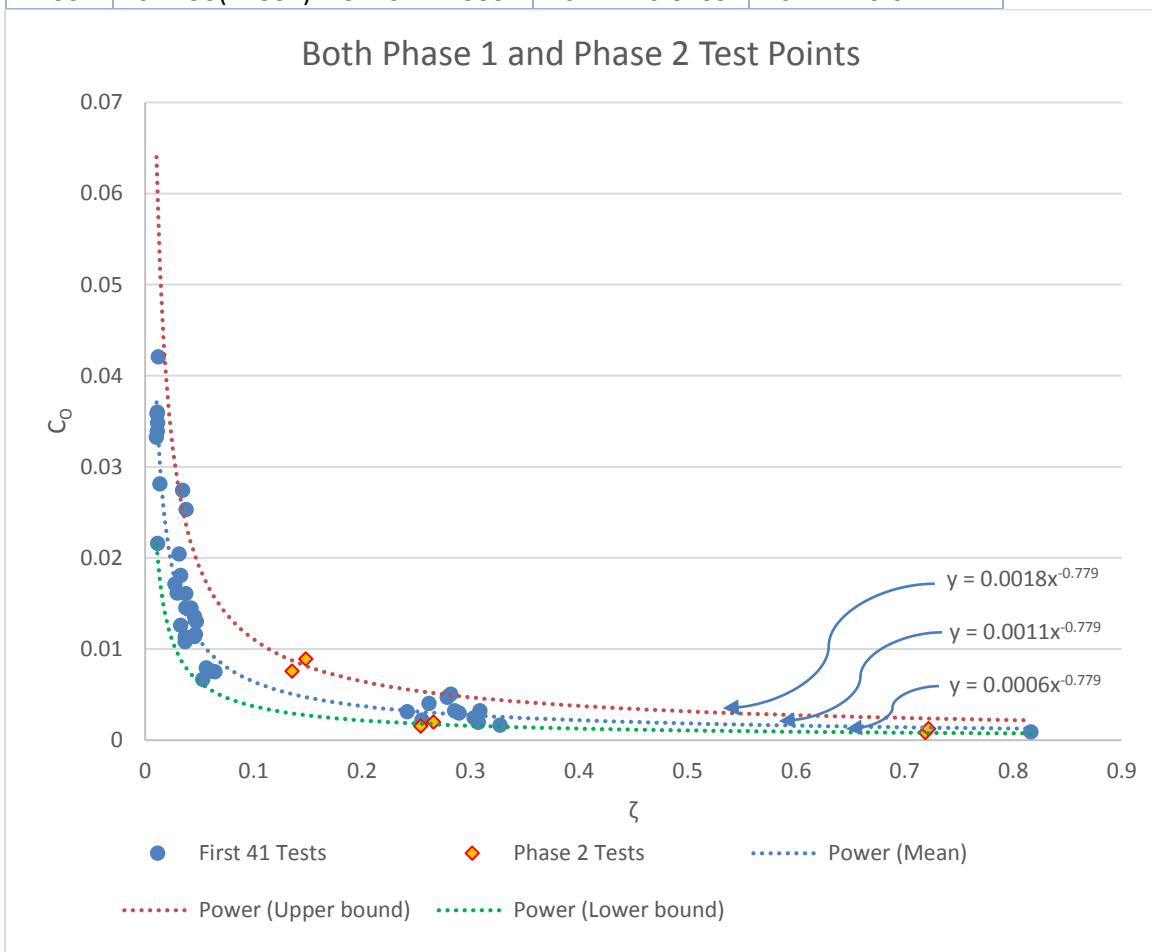


Figure 3-14. Data points including Phase 2 Tests - Transformed

3.10 Comparison to Published Results

In Timco & Frederking, 1993 (G. W. Timco & Frederking, 1993) a series of results for impact testing using a spherical indenter is presented. The testing conducted in this paper involves ice sheets of various thicknesses, indented using a 20cm diameter spherical indenter and varying the mass of the projectile. The contact speed in the paper is calculated rather than measured.

Data presented in the Timco & Frederking paper has some significant differences from the experimentation conducted for this thesis. The notable differences are given in Table 3-9.

Table 3-9. Differences Timco-Frederking to Oldford

Difference	Timco & Frederking	Oldford
Backing/Foundation	Water backing	Steel plate backing
Holder	No holder	Defined diameter holder
Ice	Freshwater lake ice – naturally grown	Laboratory grown

Looking at Table 3-9 the identified differences could result in Timco-Frederking forces being lower than those in this research. A rigid steel backing verses a water foundation would be expected to yield a higher shock load. The ice sheet can move to some extent on the water foundation whereas the sample in the pendulum is supported by a near rigid backing. The holder diameter is expected to have a small effect on the predicted loads. The confinement angle and ratio used in this thesis should accommodate that difference provided an appropriate “holder diameter” is used for the lake ice tests. The ice produced

for this thesis was intended to be as strong as possible. Following the processes described in 2.2 Ice Samples, the ice is a very pure material with strengths at the high end of what would be found in nature.

To perform this comparison several assumptions for the Timco-Frederking data was required. These assumptions are:

- The holder height for the Timco-Frederking data is 0 cm.
- The actual speed for the Timco-Frederking results is the calculated impact speed.
- “Holder Diameter” is between twice and five times the indenter diameter.

Figure 3-15 shows a comparison of the data from this thesis and the Timco-Frederking data.

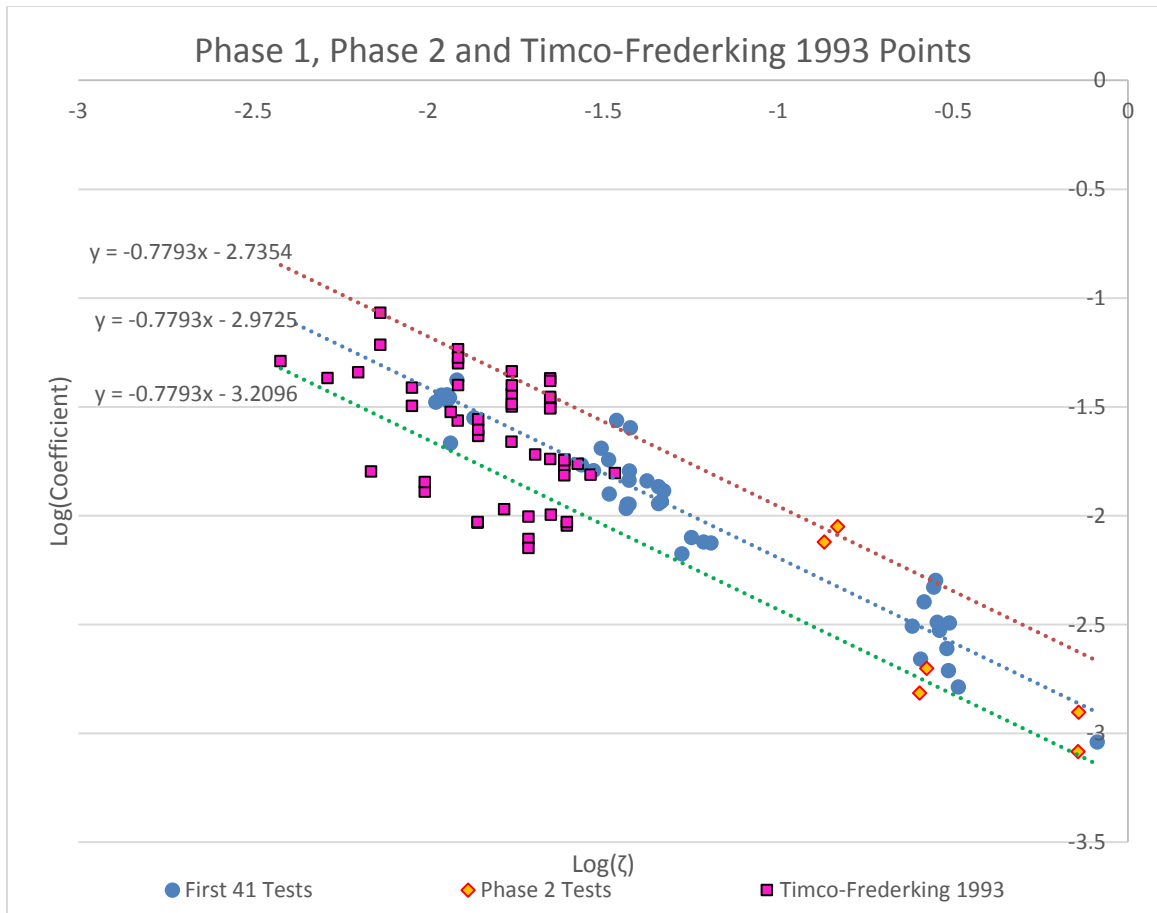


Figure 3-15. Comparison to Other Data Points Published – 40 cm ice diameter

A question likely to be raised is on the selection of 40 cm as the relevant confinement diameter for the Timco-Frederking values. This value represents an ice confinement diameter that is twice as large as the 20 cm indenter used in their experiments. This value provides the best overlap between the in-situ data and the laboratory data and perhaps gives some insight into the effective equivalence between an infinite sheet and ring-confined laboratory data. On the extreme end (test No. 14 and 15) the ratio was 1/5 in the experimentation conducted herein. Using this ratio an ice diameter of 100cm (20 cm indenter X 5) should be used. Applying an ice diameter of 100 cm or higher causes the

Timco-Frederking points to shift down the y-axis away from the data points from this experimentation.

Examination of the Y-axis formula gives insight into this. Restating Equation 3-25:

$$C_o = \log \left[\frac{FR_s}{K\theta MV^2} \left(\frac{R_s}{R_i} \right)^e \right] \quad \text{Equation 3-28}$$

Increasing ice diameter (R_i) will result in a decreased coefficient which naturally lowers the data points on the plot. Through experimentation it was found that at an R_s/R_i of approximately $\frac{1}{2}$ the Timco-Frederking results lined up optimally with the assumed coefficients. The key coefficient that makes these data sets difficult to compare is the ice. In their paper Timco and Frederking reported measuring a peak pressure of 42 MPa. This represents a peak force over a very small sensor. The σ term used in this work is an average pressure over the entire crushing event. The natural grown ice in the Timco-Frederking paper likely has a lower σ than the finely controlled laboratory grown ice from this experimentation. If we assume the ice strength term is 2 MPa and retain the 100 cm diameter sample size, the data points shift back into correlation with the results reported herein. This is shown in Figure 3-16.

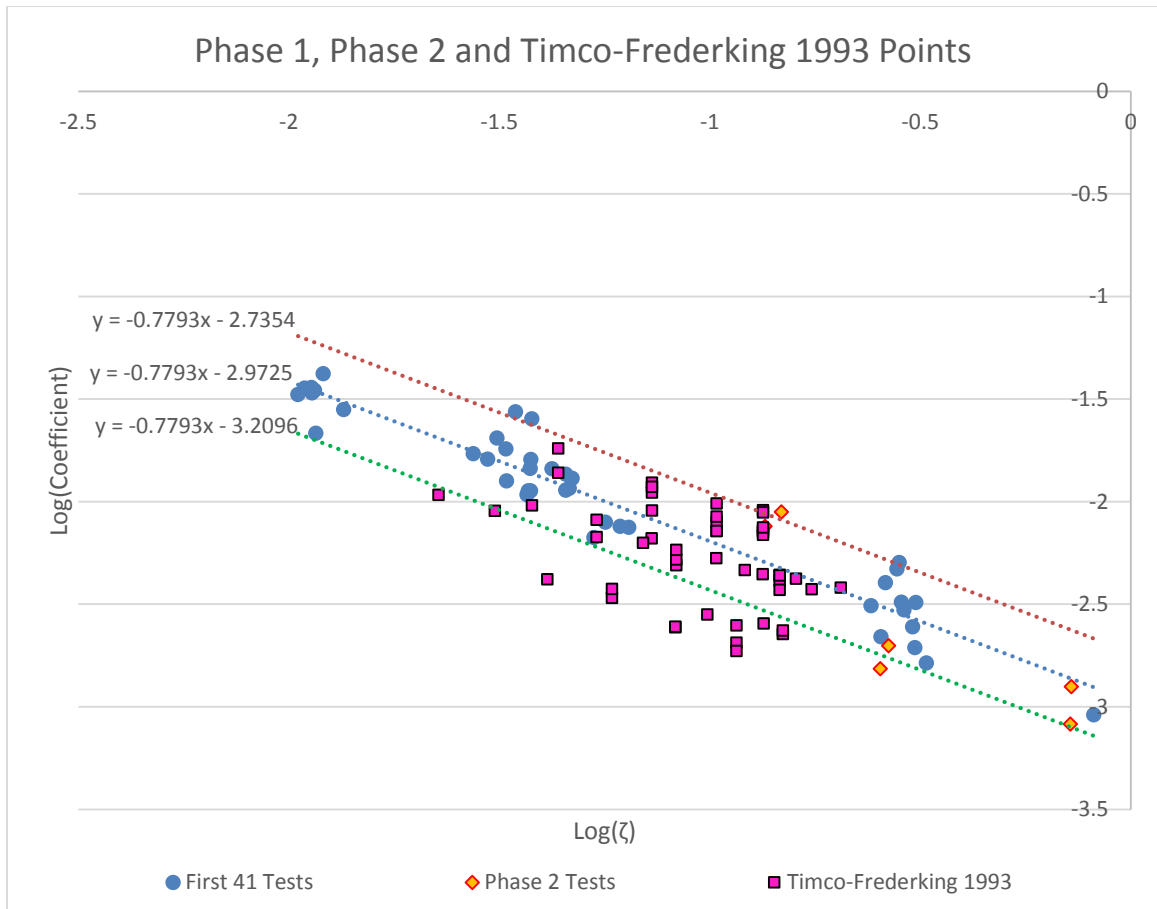


Figure 3-16. Comparison to Other Data Points Published – 100 cm ice diameter, $\sigma = 2$ MPa

Therefore it may not be possible to compare these two data sets directly due to unknowns but one conclusion that can be drawn is that the external data set (Timco-Frederking 1993) follows the same slope as the data obtained in this experimentation therefore lending better confidence in the methodology used.

Two key unknowns in the Timco-Frederking data make this comparison difficult. They are ice strength and the size (diameter) of ice sample that may be considered infinite. If the testing was repeated with high speed video, the σ term could be determined, then an ice diameter could be found to match the data with the data herein. This would give a much

better estimate of the ratio of indenter to ice confinement radius representing an infinite ice sheet.

3.11 Predicting Full Scale Loads

It must be recognized that the tests and analysis performed herein are not all encompassing, and expanding these results out for full scale load prediction may not be realistic at this stage. Nevertheless an example of possible full scale load prediction is offered for consideration and to the potential application of this methodology.

Example:

Spherical Indenter: End cap of a Rolls Royce UUC-505 azimuthing thruster, diameter = 2.44 m.

Ship: Assume a 9,800 metric ton PC5 vessel, $h_{ice} = 2.0$ m, $V = 5$ knots (2.572 m/s)

Dimensions of ice = $h_{ice} \times 2h_{ice} \times 3h_{ice}$ (*IACS POLAR CLASS Rules, 2011*)

Mass of ice = $0.9 \text{ mt/m}^3 \times 2 \text{ m} \times 4 \text{ m} \times 6 \text{ m} = 43.2 \text{ mt}$

The ice diameter is selected as being the lowest dimension 2 m, then the depth is assumed to be the next lowest, 4 m. As there is no holder, holder height is set to 0 cm. This assumption is outside the scope of the tests conducted in this experiment and is likely not realistic. These inputs and the calculated forces are shown in Table 3-10.

Table 3-10. Full Scale Prediction

Ship Mass =	9,800,000	kg
Ice Mass =	43,200	kg
Sphere Diameter =	244	cm
Ice Diameter =	200	cm
Ice Depth =	400	cm
Holder Height =	0	cm
Effective Mass =	43,010	kg
Estimated Contact Speed =	2.572	m/s
$\sigma =$	11,979,591	Pa
$\zeta' = \text{Log}[MV^2 / (4/3)\pi r^3 \sigma] =$	-2.50547	nd
Confinement Angle =	28.07	deg
Upper Bound Force =	884,767	N
Predicted Force =	512,519	N

This analysis can be compared with various guidance requirements in the marine industry. These guidance requirements primarily come from the classification societies but also can come from the Finnish-Swedish ice class rules. The class society requirements that are compared here are the ABS Guidance Notes on Ice Loads on Azimuthing Propulsion Units, the DNV Classification Notes No. 51.1 Ice Strengthening of Propulsion Machinery, and BV Rule Note NR 584 DT R00 E – Propulsors in Ice. With the additional assumptions given in Table 3-11, design loads can be estimated from the class guides.

Table 3-11. Additional Assumptions

Propeller diameter	4.2 m
Arrangement	Single propulsor on centerline
Ice Breaker	No
Ship's Mode of Operation	Bow first only
Season of operation	Summer/Autumn/Icebreaker assisted/In Open Ice

When calculated, the forces from the above mentioned requirements ranged from 2.87 MN up to 5.96 MN for this scenario. This represents a multiplier of between 3.24 to 6.74 above the upper bound force prediction presented above in Table 3-11. Re-calculating the above using the formulation from Figure 3-7 (without considering the confinement angle) gives an upper bound force of 6,323,595 N, which is very close to the majority of the requirements. This may indicate that the guidance requirements do not consider confinement in the force levels.

It is understood that the development of these requirements may have taken into account other factors that are not possible to consider herein, such as submerged effects on spalling, dynamic response in the structure, or even just simple safety factors to account for unknowns.

4 Conclusions and Recommendations

4.1 Conclusions

This work presents two new concepts, 1) a methodology for quantifying confinement of ice samples, and 2) dimensional analysis for predicting ice loads.

The methodology for quantifying confinement presented herein correlates to the physics witnessed during an ice collision. As many researchers have noted, ice tends to spall off, reducing the actual contact area. This spalling effect, and the effects circumferential confinement have on it, are captured by means of a simple angle. The angle can be visualized by imagining the steepest cone one could make from the ice sample. The angle used is the “point” of this internal ice cone. Another confinement term considered herein is the radius of ice sample relative to the radius of the indenter. This represents the volume of ice (radially) required to be fractured to create a spall. Together these terms can be used to accurately define cylindrical ice samples with a large variety of confinement scenarios.

The use of dimensional analysis is definitely not a new concept, and it has been used in relation to ice in the past. This is mostly with items such as ice breaker resistance in an ice model tow tank or ice floes in a hydraulic system such as a river or spillway. In this work the concept is used to analyze laboratory data obtained through experimentation. Then this method is used to compare other data available in the public domain and even make an academic approach at estimating loads on a full scale event. The full scale event

may be overstretching the safe limits of this methodology at this point but the analysis reveals that current industry practice may be conservative.

4.2 Recommendations

4.2.1 Recommendations for Repeat or Expanded Pendulum Testing

Sufficient details are contained within this thesis, as are the references needed to reproduce this testing, or preferably expand upon it. It is often said that the best time to conduct an experiment is after you have finished the experiments. This is true in the case of the experimentation done in this research. If testing was to be repeated the following recommendation would be made:

- 1) Add more dimensional reference points to the object to be studied in the video. During some of the later testing, pieces of adhesive measuring tapes were stuck onto different parts of the pendulum. This made it much easier and quicker to calibrate the on screen measurements.
- 2) The high speed camera used in these experiments has a looping memory. In other words it will continually record but it will record over the beginning until the user stops the recording. It is recommended that the high speed camera be the first instrument to be stopped after a test in order to reduce the risk of losing the video of the event.

- 3) Conduct testing with test apparatus within a cold space. Many samples were ruined and had to be discarded after they sat at room temperature for too long. This often happened when various inevitable difficulties arose, such as computer freezing or electrical failure.
- 4) Use and expand upon the checklist attached in Appendix 4.

4.2.2 Recommendations for Further work

In any dimensional analysis the goal is to collapse the experimental data down to a single line. This way anyone can use the formulation to accurately predict outcomes with known inputs. The scatter in the data presented herein suggest that there are variables that were not considered in the dimensional analysis. These variables may include:

- 1) The temperature of the ice sample at the time of impact, or the thermal gradient through the ice sample.
- 2) The history of the ice sample: when ice samples have experienced fluctuating temperatures it is possible that a tempering effect occurs. This seems to cause the samples to fail in a very brittle fashion, resulting in lower forces than expected.
- 3) The existence of fractures in the sample prior to test. One sample was nearly discarded due to preexisting fractures in it, but upon testing the results were well within the norm. This sample was included as test number 41. Nonetheless it is expected that pre-existing fractures will affect the results of the experiment.

In addition to expanding the analysis to include more factors, it is recommended that future testing of larger samples be conducted. Memorial University has a double pendulum that is 4 times larger than the one used in these experiments. That apparatus could be used in the same way as described in this thesis to establish much larger impact forces. This will reinforce the prediction which may possibly be expanded to genuine load estimation for things like bulbous bows or azimuthing propulsion units.

In many ice load related regulations, rules and guides used in the marine industry, the ice sheet is often considered to be infinite. In this thesis previous work by Timco-Frederking was examined. The Timco-Frederking testing could be repeated using methods developed in this thesis to establish the appropriate ratio to define an infinite ice sheet. (See 3.10 Comparison to Published Results for more details)

In reality the infinite ice sheet is typically in line with the load path. For example if a ship's bulbous bow strikes an ice sheet; the ice sheet may be considered infinite as it may cover the entire bay or river but the thickness is very finite compared to the bulb. This concept was introduced in the propulsor example given in 3.11 Predicting Full Scale Loads, but not fully expanded. The ice diameter concept presented in this thesis may or may not directly apply to the thickness of an ice block or the edge of an ice sheet. Further exploration into the effects of impact onto an ice sheet edge or a non-cylindrical specimen should be done.

1 References

Anderson, F. (2010). *Engineering Fundamentals of Threaded Fastener Design and Analysis*.

Arunachalam, a V. . (2005). Application of dimensional analysis to estimation of ice-induced pressures on rigid vertical structures. *Canadian Journal of Civil Engineering*, 32(5), 968–980.

Barrette, P., Pond, J., Li, C., & Jordaan, I. (2003). *Laboratory-Scale Indentation of Ice*. St. John's, NL.

Bruneau, S., Colbourne, B., Dragt, R., Dillenburg, A., Ritter, S., Pilling, M., & Sullivan, A. (2013). Laboratory Indentation Tests Simulating Ice-Structure Interaction Using Cone-Shaped Ice Samples and Steel Plates. In *POAC'13*. Espoo, Finland.

Bruneau, S. E., Dillenburg, A. K., & Ritter, S. (2011). Ice Sample Production Techniques and Indentation Tests for Laboratory Experiments Simulating Ship Collisions with Ice. In *ISOPE2012*.

Buckingham, E. (1914). On Physically Similar Systems; Illustrations of the Use of Dimensional Equations. *Physical Review*, 4(4), 345–376.

Clarke, G. (2012). *Ice Collision Experiments with a Pendulum Impact Apparatus*.

Memorial University.

Daley, C. (1999). ENERGY BASED ICE COLLISION FORCES. In *POAC 99*. Helsinki, Finland.

Dragt, R. C., & Bruneau, S. E. (2013). THE COLLISION OF CONE SHAPE ICE SAMPLES AGAINST STEEL PLATES OF VARYING SURFACE ROUGHNESS. In *POAC'13* (Vol. 2).

Dytran Instruments, I. (2001). Operating Guide, Series 1203V Ring Type LIVMtm Force Sensors, Hermetically Sealed.

Fourier, J. (1822). *Théorie Analytique de la Chaleur*. 1988 Éditions Jacques Gabay, Paris.

Frederking, R., Johnston, M., & Centre, C. H. (2002). *Testing the compressive strength of sea ice with a borehole jack: third season Field instructions for decayed ice strength testing spring/summer 2002*.

Gagnon, R. E. (1998). Analysis of visual data from medium scale indentation experiments at Hobson's Choice Ice Island. *Cold Regions Science and Technology*, 28(1), 45–58.

Gold, L. W., Timco, G. W., & Frederking, R. M. . (1991). Initial Response of Columnar-Grained Ice to Drop Impact. In *POAC91* (Vol. 1, pp. 515–526). St. John's, NL.

IACS POLAR CLASS Rules (2011). IACS. Retrieved from

Jordaan, I., & McKenna, R. (1988). *Ice crushing by Impact and Indentation : A literature review, a report*. St. John's, NL.

Kim, E., Golding, N., Schulson, E. M., Løset, S., & Renshaw, C. E. (2012). Mechanisms governing failure of ice beneath a spherically-shaped indenter. *Cold Regions Science and Technology*, 78, 46–63.

Kurdyumov, V. A., & Kheisin, D. E. (1976). Hydrodynamic model of the impact of a solid on ice. *Prikladnya Mekhanika*, 12(10), 103–109.

Li, C., Jordaan, I., & Barrette, P. (2004). HIGH PRESSURE ZONES AT DIFFERENT SCALES DURING ICE-STRUCTURE INDENTATION. In *OMAE 2004* (pp. 1–8).

Oldford, D., Sopper, R., & Daley, C. (2014). Impact Ice Loads on Spherical Geometries. In *ICETECH 2014* (pp. 1–7). Banff, Alberta.

Popov, Y., Faddeev, O., Kheisin, D., & Yakovlev, A. (1969). *Strength of ships sailing in ice*. Leningrad: Sudostroenie Publishing House.

Rayleigh, Lord. (1915). The Principle of Similitude. *Nature*, 95, 66.

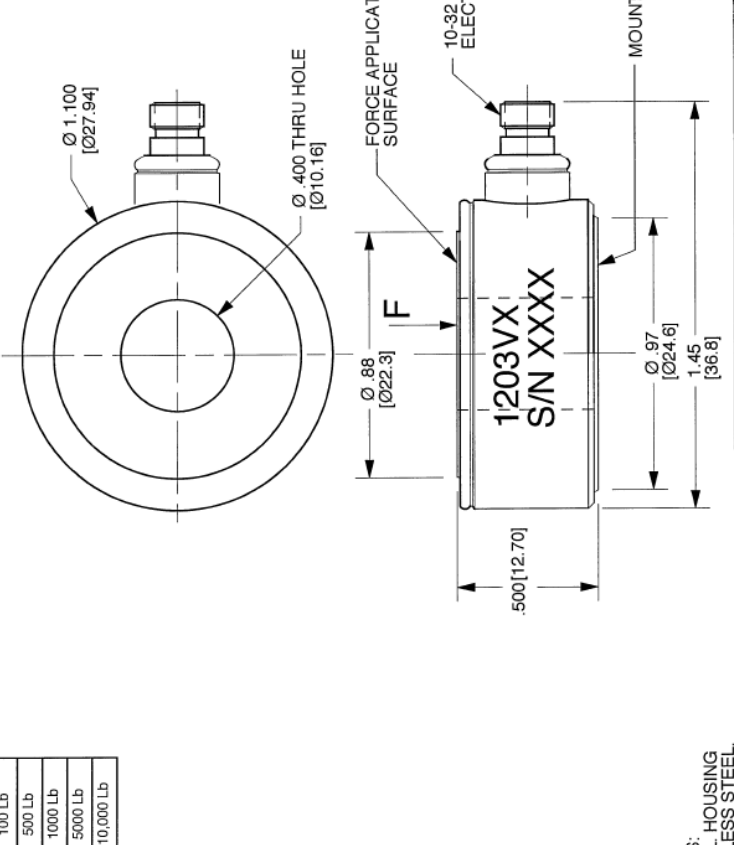
- Rosenberg, S. (2007). *Low Frequency Response and Quasi-Static Behavior of LIVM Sensors*. Chatsworth, California.
- Sharp, J. J. (1981). *Hydraulic Modelling*. London: Butterworth & Co. (Publishers) Ltd.
- Sodhi, D. S., Takeuchi, T., Nakazawa, N., Akagawa, S., & Saeki, H. (1998). Medium-scale indentation tests on sea ice at various speeds. *Cold Regions Science and Technology*, 28(3), 161–182.
- STePS2. (2013). *STePS2: Manual of Laboratory Procedures*. St. John's, NL.
- Timco, G. (1983). Confined Compressive Strength of Sea Ice. In *POAC 83* (pp. 243–253). Espoo, Finland.
- Timco, G. W., & Frederking, R. M. W. (1993). Laboratory impact tests on freshwater ice. *Cold Regions Science and Technology*, 22(1), 77–97.
- Walpole, R. E., Myers, R. H., & Myers, S. L. (1998). *Probability and Statistics for Engineers and Scientists* (6th ed.). Upper Saddle River, New Jersey: Prentice Hall Inc.
- William D. Callister, J. (1997). *Materials Science and Engineering an Introduction* (Fourth Edi). John Wiley & Sons.

Appendix 1

Drawings for Dytran 1203V Load Cells

DYTRAN PROPRIETARY AND CONFIDENTIAL THE INFORMATION CONTAINED HEREIN IS THE PROPERTY OF DYTRAN INSTRUMENTS, INC. AND ANY REPRODUCTION IN PART OR AS A WHOLE OR ANY OTHER DISSEMINATION OF THIS INFORMATION WITHOUT THE WRITTEN PERMISSION OF DYTRAN INSTRUMENTS, INC. IS PROHIBITED.		REV	ECN	DESCRIPTION	BY/DATE	CHK	APPR
A	8074	UPDATED FORMAT	RA, 11/17/11	J5			

MODEL	SENSITIVITY	TC (SEC)	RANGE F.S.
1203V1	50 mV/Lb	90	100 Lb
1203V2	10 mV/Lb	450	500 Lb
1203V3	5 mV/Lb	850	1000 Lb
1203V4	1 mV/Lb	1800	5000 Lb
1203V5	0.5 mV/Lb	1800	10,000 Lb



- WEIGHT: 50 GRAMS.
- ENVIRONMENTAL SEAL: HERMETIC.
- MATERIAL: LOAD-BEARING SURFACES: HARDENED 17-4 PH STAINLESS STEEL. HOUSING AND CONNECTOR: 300 SERIES STAINLESS STEEL.
- POLARITY: POSITIVE-GOING WITH COMPRESSION.

NOTES: UNLESS OTHERWISE SPECIFIED

UNLESS OTHERWISE SPECIFIED:
 DIMENSIONS ARE IN INCHES UNLESS OTHERWISE SPECIFIED.
 DIMENSIONS IN BRACKETS ARE IN MILLIMETERS.
 TOLERANCES ARE:
 INCHES METRIC ANGLES
 .XX ± 0.0 .XX ± 0.8 ± 1°
 .XXX ± 0.0 .XXX ± 0.25

UNLESS OTHERWISE SPECIFIED:
 INTERNAL SURFACES OF HOLES AND RECESSES SHALL BE FINISHED BY
 Y14.5M-1994 REMOVE BURRS
 COUNTERSINKS INTERNAL THDS 90° TO MAJOR DIA THD LENGTH AND DEPTHS ARE FOR THDS PER MIL-S-7742
 FINISHES APPLY AFTER FINISHING.
 ALL MACHINED SURFACES (S) TOTAL RUNOUT WITHIN .005 BREAK SHARP EDGES .005 TO .010 MACHINE FILLET RAD .005 TO .015 WELDING APPROXIMATIONS PER MIL-STD-12



MASTER
ONLY IF IN RED

DYTRAN INSTRUMENTS, INC. CHATSWORTH, CA.

SCALE: 2X	DESIGN: INC	DATE: 10-10-07	PART NO.:	MODEL SERIES 1203V
DRAWN: NC	CHECKED: R.A.	DATE: 12/17/01	MAT'L:	REV: A
APPROVED: N.C.	DATE: 08/01/06	DATE: 08/01/06	USED ON:	SERIES 1203V
TITLE: OUTLINE/INSTALLATION DRAWING, MODEL SERIES 1203V FORCE SENSORS				DWG NO. 127-1203V
				SHEET 1 OF 1

DO NOT SCALE DRAWING

Model Number 1203V5	PERFORMANCE SPECIFICATION		Doc No PS1203V5
	Force Sensors, IEPE		REV B, ECM 0751, 062012

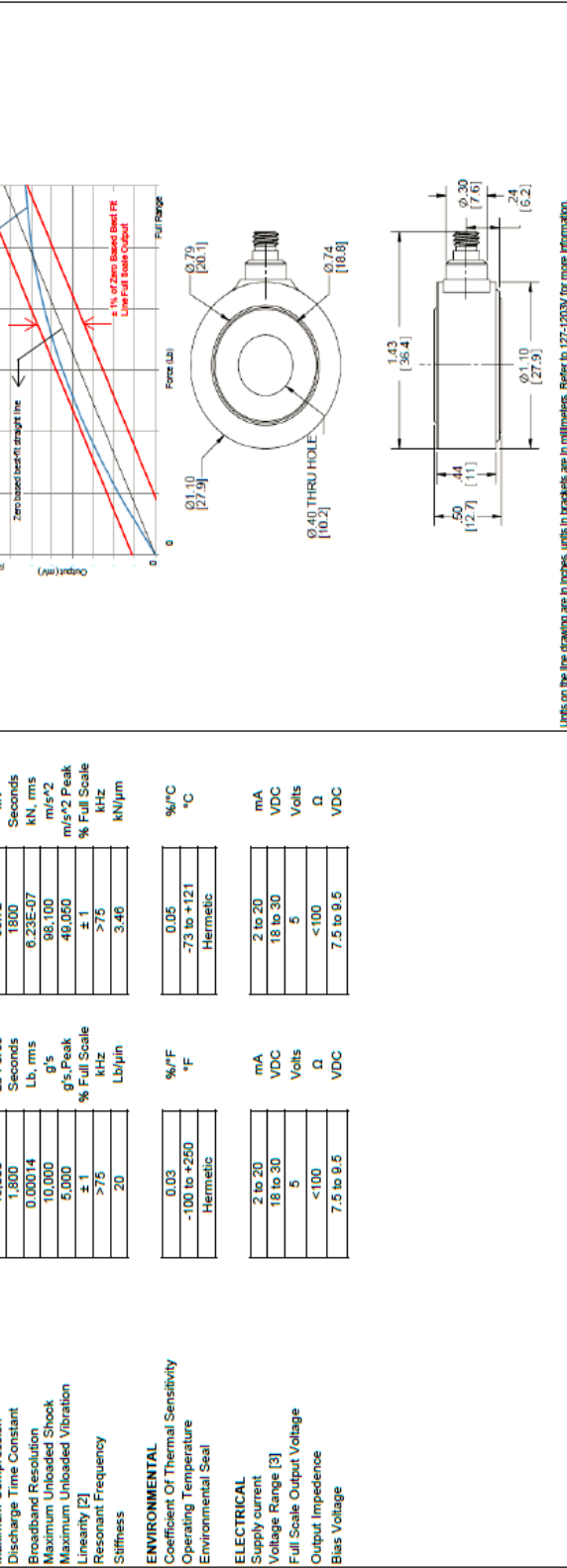
This family also includes:

Model	Sensitivity (mV/Lb)	Range (Lbs Force)	Max Force (Lbs Force)	Discharge T.C. (sec)
1203V1	50	100	200	90
1203V2	10	500	1,000	450
1203V3	5	1,000	5,000	850
1203V4	1.0	5,000	10,000	1800

Please refer to the performance specifications of the products in this family for detailed description

Supplied Accessories:
 1) Accredited calibration certificate (ISO 17025)

Notes:
 [1] Radially mounted with 10-32 receptacle micro coaxial connector
 [2] Percent of full scale or any lesser range. Zero based best-fit straight line method.
 [3] Power these instruments only with constant current type power units. Do not connect to a source of voltage without current limiting. This will destroy the integral IC amplifier.



Units on the drawing are in inches, units in brackets are in millimeters. Refer to 127-1203V for more information.

- RING STYLE FORCE SENSOR
- HERMETICALLY SEALED
- EXCELLENT LINEARITY



	ENGLISH	SI
Weight, Max.	1.75	50 grams
Connector [1]	10-32	10-32
Housing	Stainless steel	Stainless steel
Isolation	Stainless steel	Stainless steel
Material	Case grounded	Case grounded
Mode	Quartz	Quartz
	Compression	Compression

	ENGLISH	SI
Sensitivity, ± 10 %	0.5	0.12 mV/Lb
Compression Range	10,000	44.48 kN
Maximum Compression	15,000	66.72 kN
Discharge Time Constant	1,800	1800 Seconds
Broadband Resolution	0.00014	6.23E-07 kN, rms
Maximum Unloaded Shock	10,000	98.100 m/s ²
Linearity [2]	± 1	48.050 m/s ² Peak
Resonant Frequency	>75	± 1 % Full Scale
Stiffness	20	kHz
		Lb/µin
		kN/µm

	ENGLISH	SI
Coefficient Of Thermal Sensitivity	0.03	0.05 %/°C
Operating Temperature	-100 to +250	-73 to +121 °C
Environmental Seal	Hermetic	Hermetic

	ENGLISH	SI
Supply current	2 to 20	mA
Voltage Range [3]	18 to 30	VDC
Full Scale Output Voltage	5	Volts
Output Impedance	<100	Ω
Bias Voltage	7.5 to 9.5	VDC



21592 Marilla Street, Chatsworth, California 91311 Phone: 818.700.7818 Fax: 818.700.7880 www.dytran.com
 For permission to reprint this content, please contact info@dytran.com

Appendix 2

Data used for ice strength – Test No.

Time	Total Force	Frame #	Small Carriage Movement [mm]	Large Carriage Movement [mm]	Total Indentation [mm]	Radius for normal area	Nominal contact area [mm ²]	Nominal contact area [m ²]	Peak force [N]	Nominal Pressure [Pa]
19.83136	70.37	390	0.00	0.00	0.00	0.00	0.00	0.00		
19.83140	147.21									
19.83144	485.93									
19.83148	1229.39									
19.83152	2426.48									
19.83156	4373.00									
19.83160	7288.56									
19.83164	11469.07									
19.83168	14905.01									
19.83172	16443.66									
19.83176	17046.09									
19.83180	18065.83									
19.83184	18403.36									
19.83188	17618.65									
19.83192	18546.27									
19.83196	20713.09									
19.83200	21809.93									
19.83204	22475.40									
19.83208	22726.94									
19.83212	21228.91									
19.83216	20413.97									
19.83220	22119.64									
19.83224	23934.66									
19.83228	23614.08									
19.83232	22902.04									
19.83236	22322.09	391	1.84	1.43	3.27	21.90	1506.55	0.00	23935	15887098
19.83240	21625.06									
19.83244	20917.30									
19.83248	20798.50									
19.83252	21126.61									
19.83256	21604.83									
19.83260	22605.83									
19.83264	23701.49									
19.83268	23666.98									
19.83272	23836.02									

Time	Total Force	Frame #	Small Carriage Movement [mm]	Large Carriage Movement [mm]	Total Indentation [mm]	Radius for normal area	Nominal contact area [mm ²]	Nominal contact area [m ²]	Peak force [N]	Nominal Pressure [Pa]
19.83276	25267.22									
19.83280	26124.32									
19.83284	27030.66									
19.83288	27976.11									
19.83292	28357.09									
19.83296	29236.80									
19.83300	31097.15									
19.83304	32811.84									
19.83308	34341.95									
19.83312	37062.21									
19.83316	39849.97									
19.83320	40170.65									
19.83324	39814.76									
19.83328	39601.59									
19.83332	39283.98									
19.83336	39980.75	392	2.78	3.26	6.05	29.50	2734.49	0.00	40171	14690370
19.83340	42078.25									
19.83344	43365.02									
19.83348	42526.70									
19.83352	41921.16									
19.83356	42100.38									
19.83360	42346.26									
19.83364	42145.91									
19.83368	41745.21									
19.83372	41871.79									
19.83376	42192.65									
19.83380	41897.07									
19.83384	40881.02									
19.83388	40650.97									
19.83392	41396.59									
19.83396	41439.54									
19.83400	40633.61									
19.83404	40418.77									
19.83408	40669.36									
19.83412	41506.84									

Time	Total Force	Frame #	Small Carriage Movement [mm]	Large Carriage Movement [mm]	Total Indentation [mm]	Radius for normal area	Nominal contact area [mm ²]	Nominal contact area [m ²]	Peak force [N]	Nominal Pressure [Pa]
19.83416	42840.02									
19.83420	43981.31									
19.83424	43843.65									
19.83428	43978.31									
19.83432	45042.58									
19.83436	46236.47	393	3.90	3.66	7.56	32.81	3382.04	0.00	46236	13671186
19.83440	46399.35									
19.83444	45708.84									
19.83448	45444.73									
19.83452	45954.07									
19.83456	46189.03									
19.83460	45812.69									
19.83464	46352.90									
19.83468	47638.09									
19.83472	48785.78									
19.83476	49130.09									
19.83480	48647.33									
19.83484	46777.57									
19.83488	44788.92									
19.83492	44701.56									
19.83496	46101.18									
19.83500	47635.11									
19.83504	47539.00									
19.83508	45273.63									
19.83512	43082.11									
19.83516	41677.34									
19.83520	41010.01									
19.83524	41063.13									
19.83528	41183.06									
19.83532	40381.18									
19.83536	39135.55	394	4.85	4.06	8.91	35.46	3949.62	0.00	49130	12439180
19.83540	38508.33									
19.83544	38294.49									
19.83548	38589.97									
19.83552	39723.28									

Time	Total Force	Frame #	Small Carriage Movement [mm]	Large Carriage Movement [mm]	Total Indentation [mm]	Radius for normal area	Nominal contact area [mm ²]	Nominal contact area [m ²]	Peak force [N]	Nominal Pressure [Pa]
19.83556	40663.01									
19.83560	40674.53									
19.83564	40056.64									
19.83568	39894.43									
19.83572	39686.40									
19.83576	39499.38									
19.83580	39839.50									
19.83584	40208.17									
19.83588	40091.14									
19.83592	38971.43									
19.83596	36788.40									
19.83600	35104.38									
19.83604	35037.08									
19.83608	34925.19									
19.83612	34252.39									
19.83616	33007.27									
19.83620	31414.76									
19.83624	29537.48									
19.83628	28379.69									
19.83632	28044.34									
19.83636	27905.64	395	5.57	4.69	10.26	37.87	4505.34	0.00	40675	9028066
19.83640	28114.23									
19.83644	28087.71									
19.83648	27613.96									
19.83652	26969.59									
19.83656	26588.34									
19.83660	26583.09									
19.83664	27264.61									
19.83668	28282.02									
19.83672	28804.46									
19.83676	29079.98									
19.83680	29543.90									
19.83684	30089.76									
19.83688	30106.41									
19.83692	30219.95									

Time	Total Force	Frame #	Small Carriage Movement [mm]	Large Carriage Movement [mm]	Total Indentation [mm]	Radius for normal area	Nominal contact area [mm ²]	Nominal contact area [m ²]	Peak force [N]	Nominal Pressure [Pa]
19.83696	30630.52									
19.83700	30746.91									
19.83704	30472.46									
19.83708	29992.74									
19.83712	29159.23									
19.83716	28160.60									
19.83720	27568.31									
19.83724	27108.14									
19.83728	26343.52									
19.83732	25168.88									
19.83736	24025.92	396	5.79	5.68	11.47	39.85	4990.04	0.00	30747	6161652
19.83740	22941.59									
19.83744	22011.81								Average pressure:	1197959 2

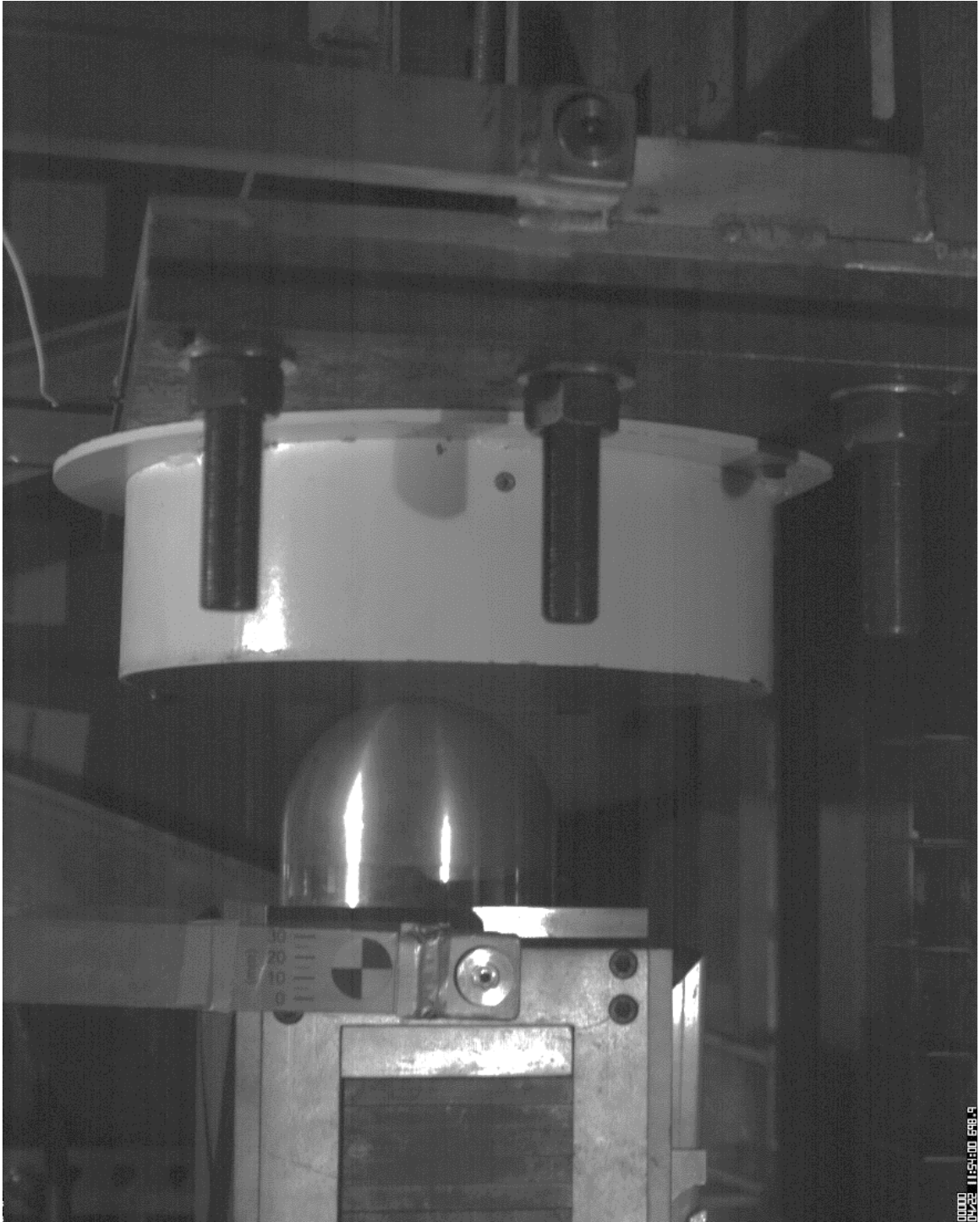


Figure A2-1. Test No. 24 - Frame 389

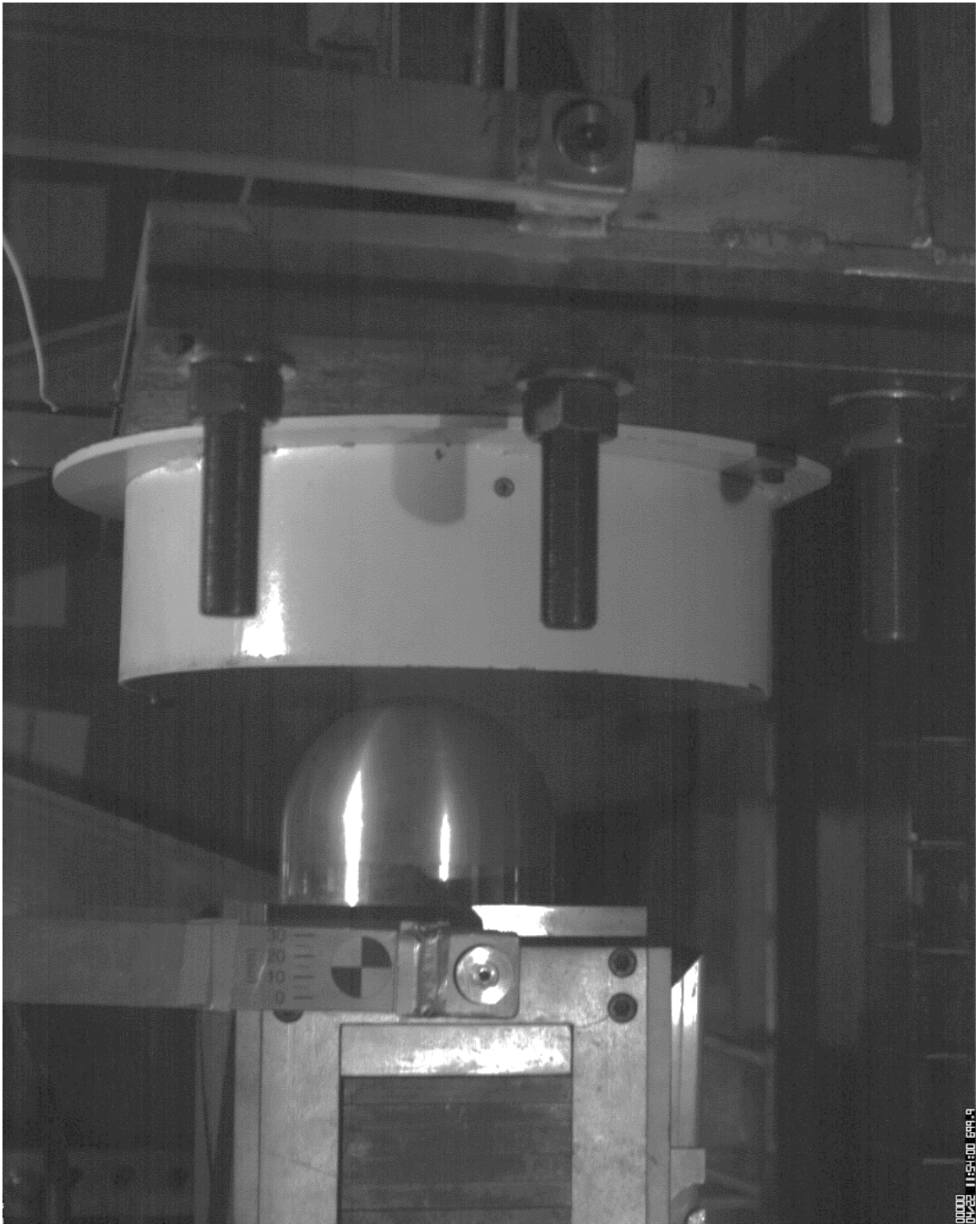


Figure A2-2. Test No. 24 - Frame 390

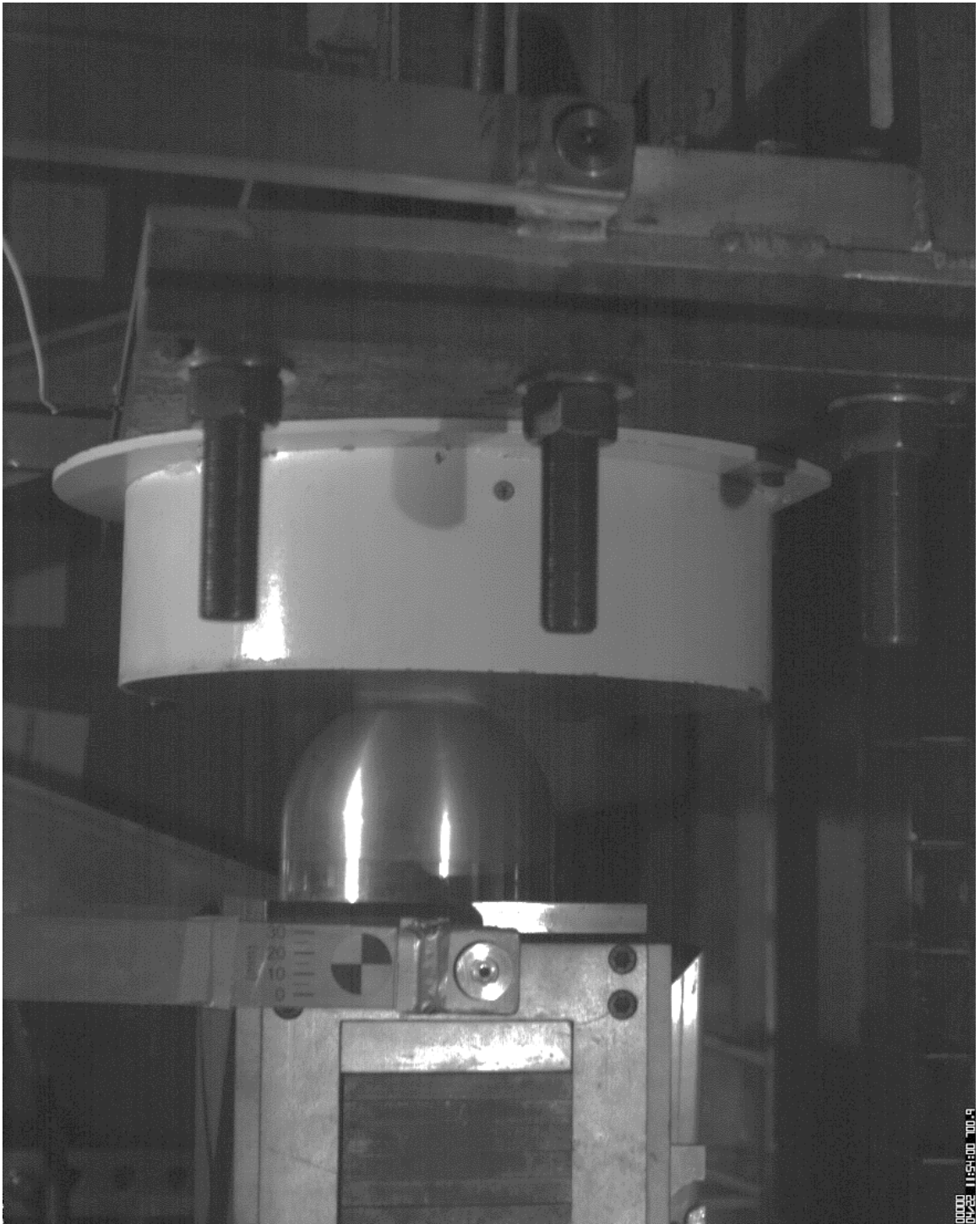


Figure A2-3. Test No. 24 - Frame 391

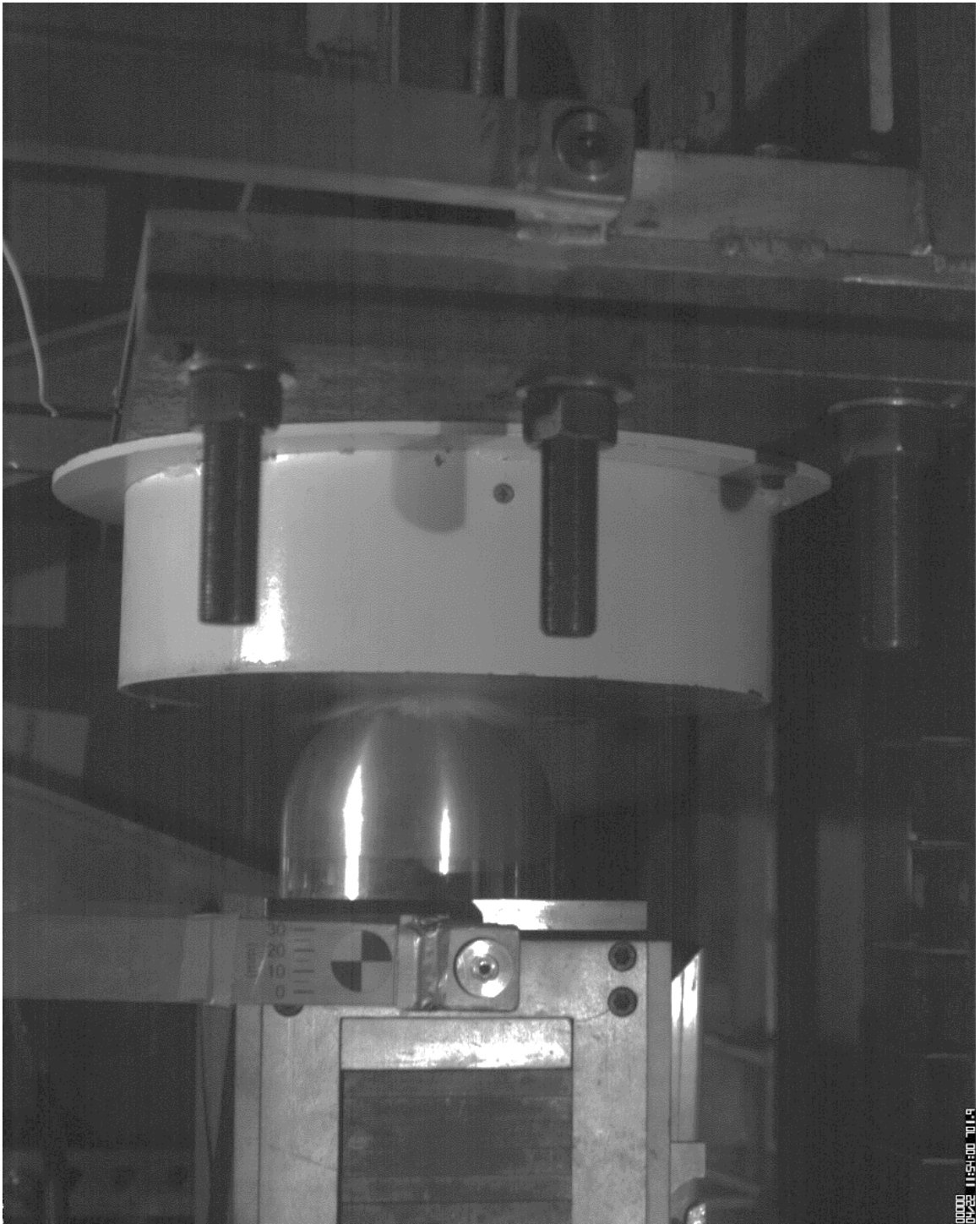


Figure A2-4. Test No. 24 - Frame 392

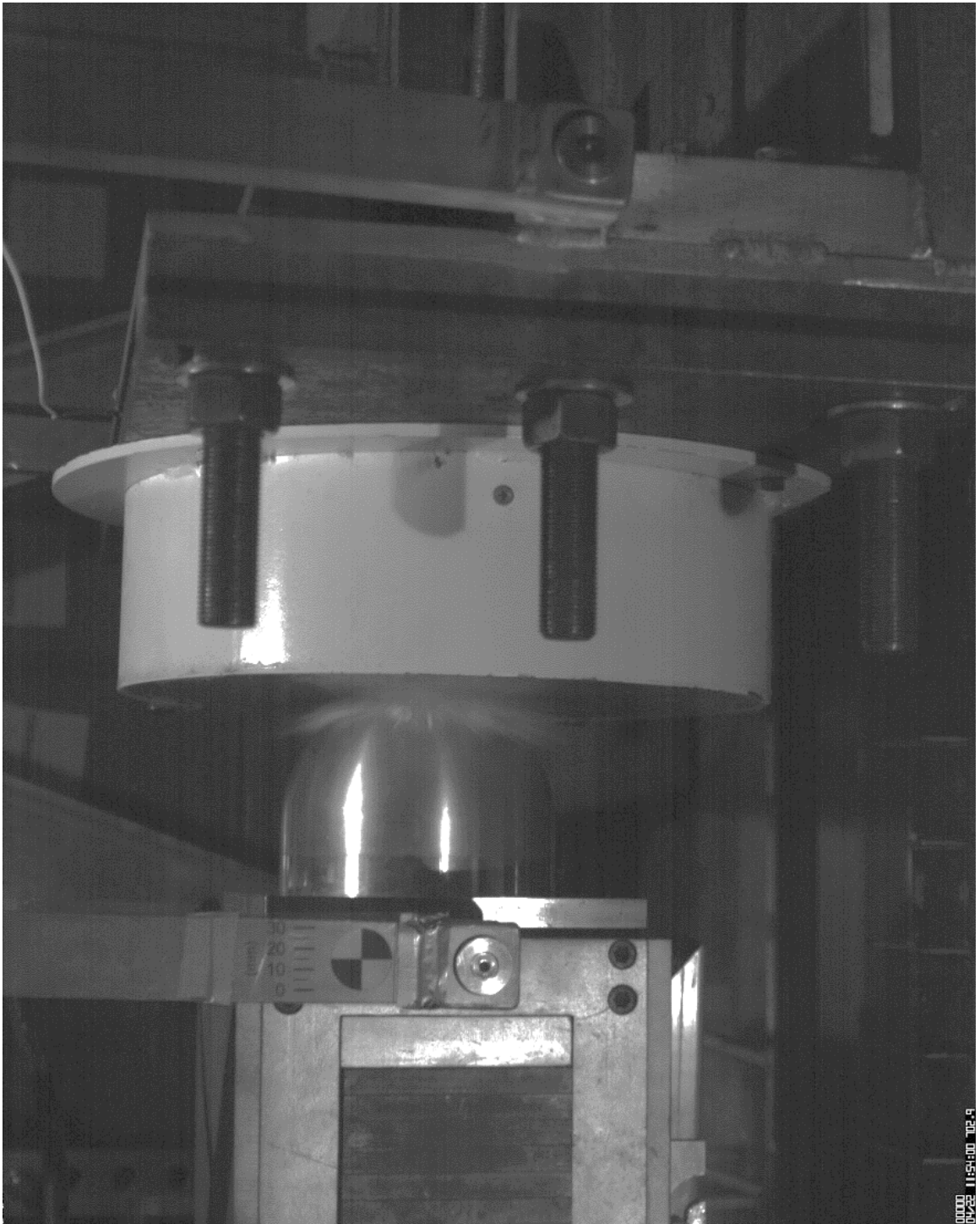


Figure A2-5. Test No. 24 - Frame 393

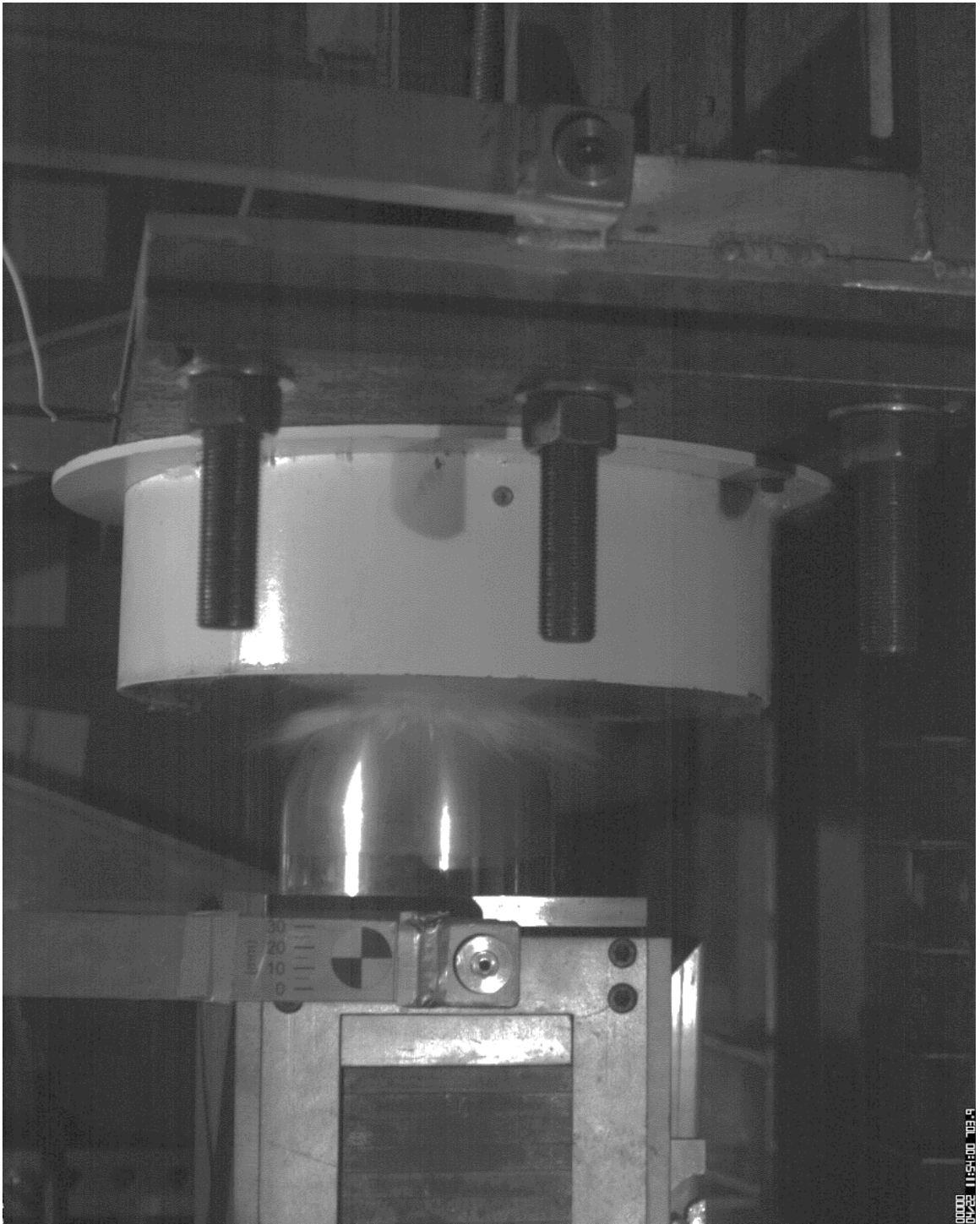


Figure A2-6. Test No. 24 - Frame 394

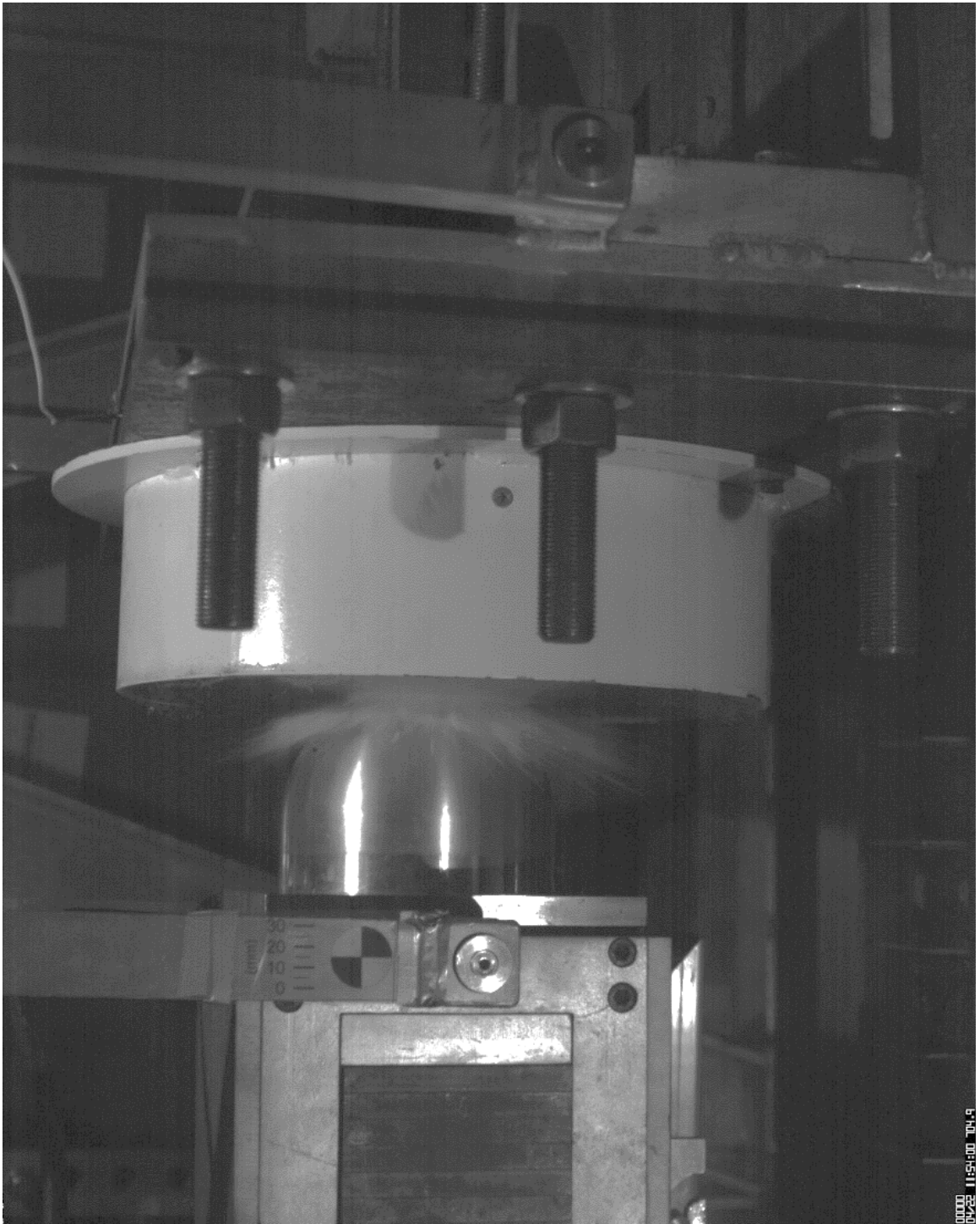


Figure A2-7. Test No. 24 - Frame 395

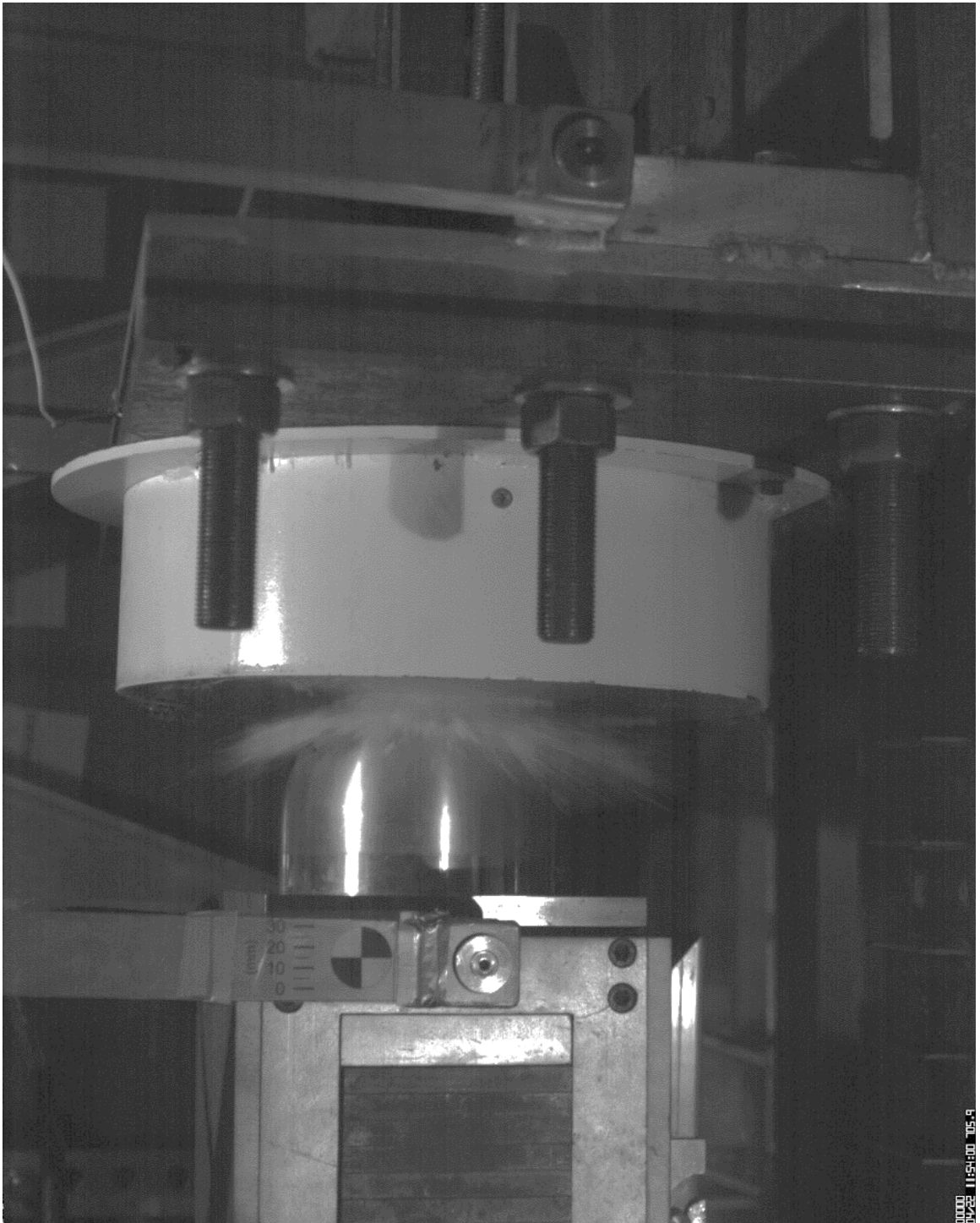


Figure A2-8. Test No. 24 - Frame 396

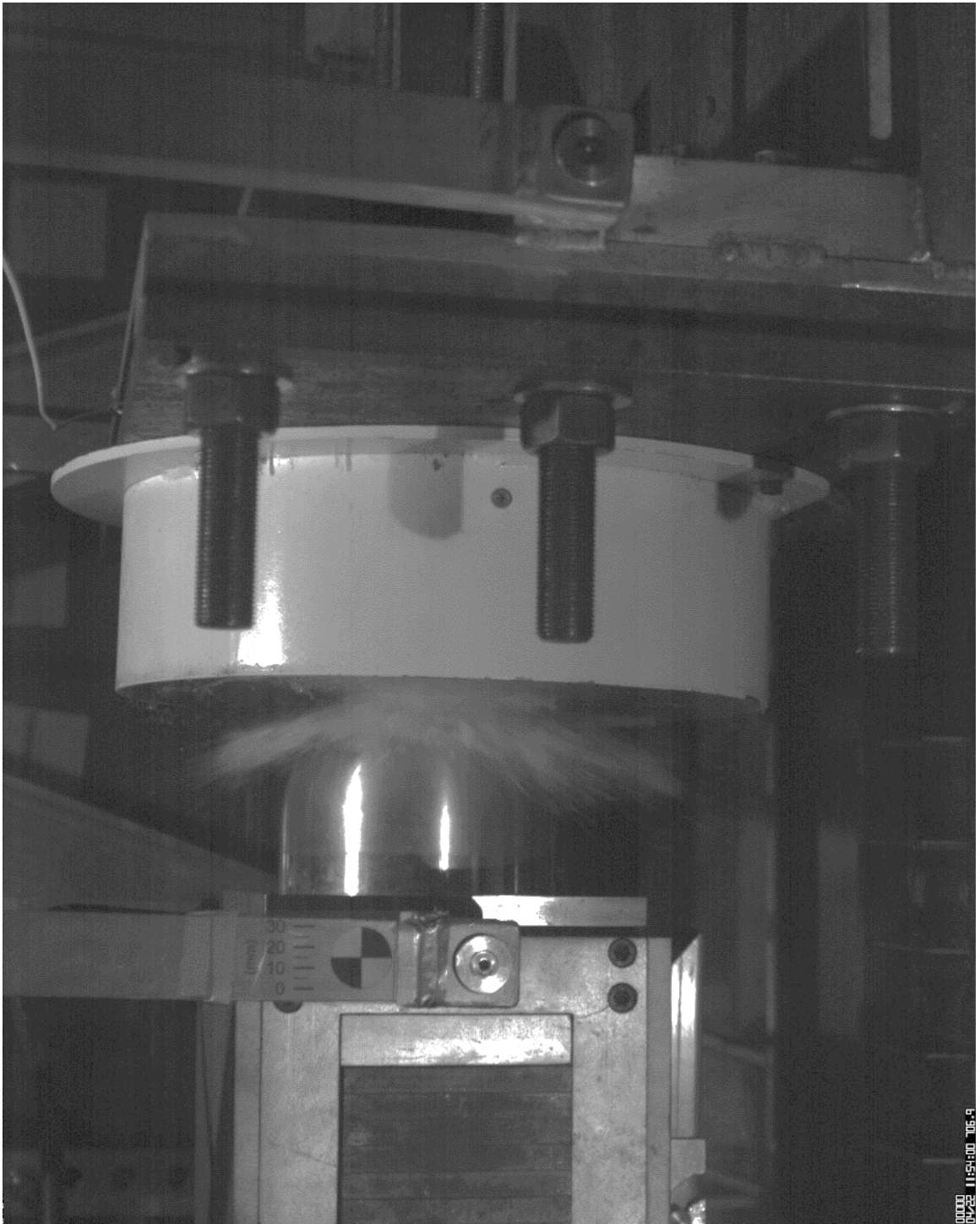


Figure A2-9. Test No. 24 - Frame 397

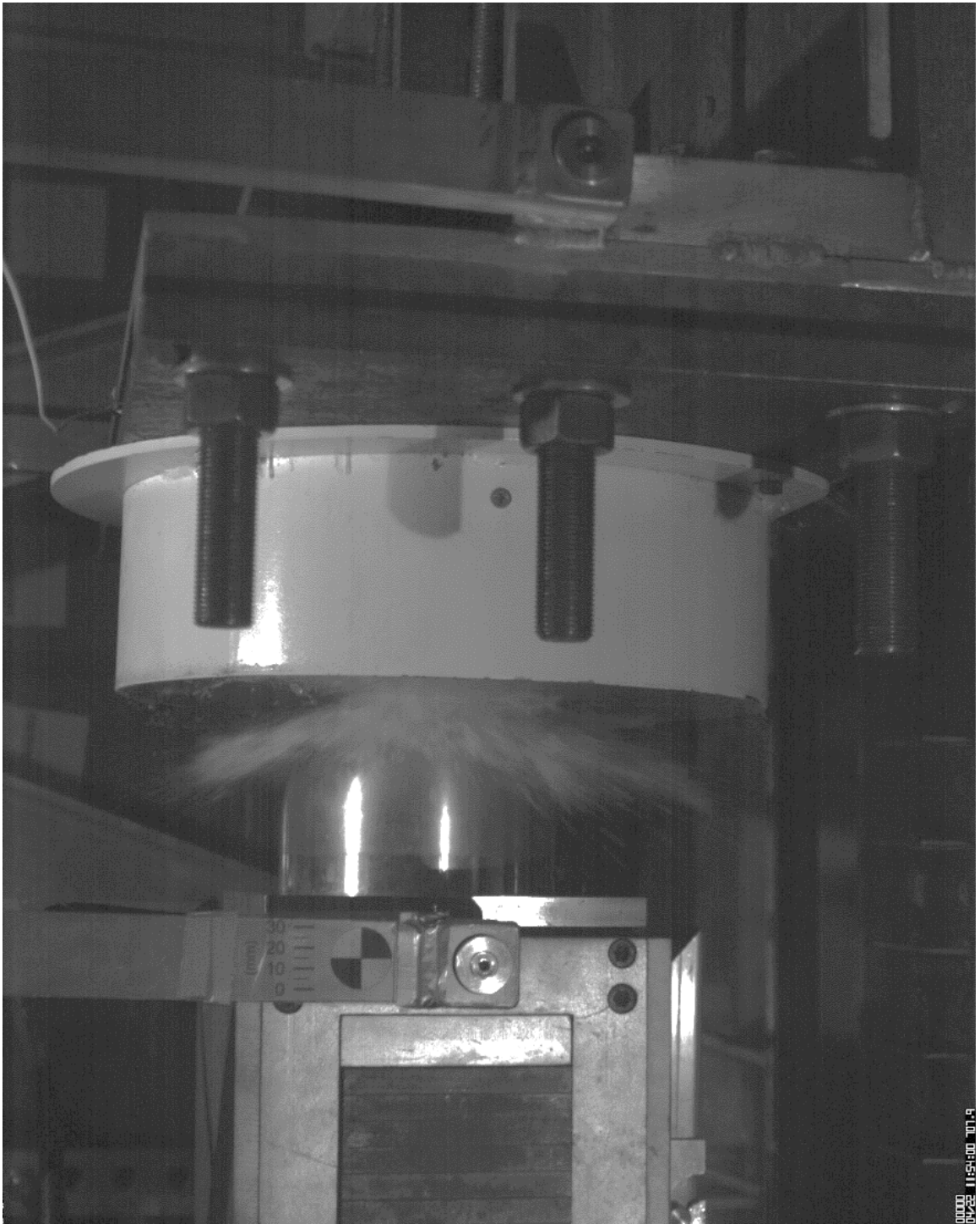


Figure A2-10. Test No. 24 - Frame 398

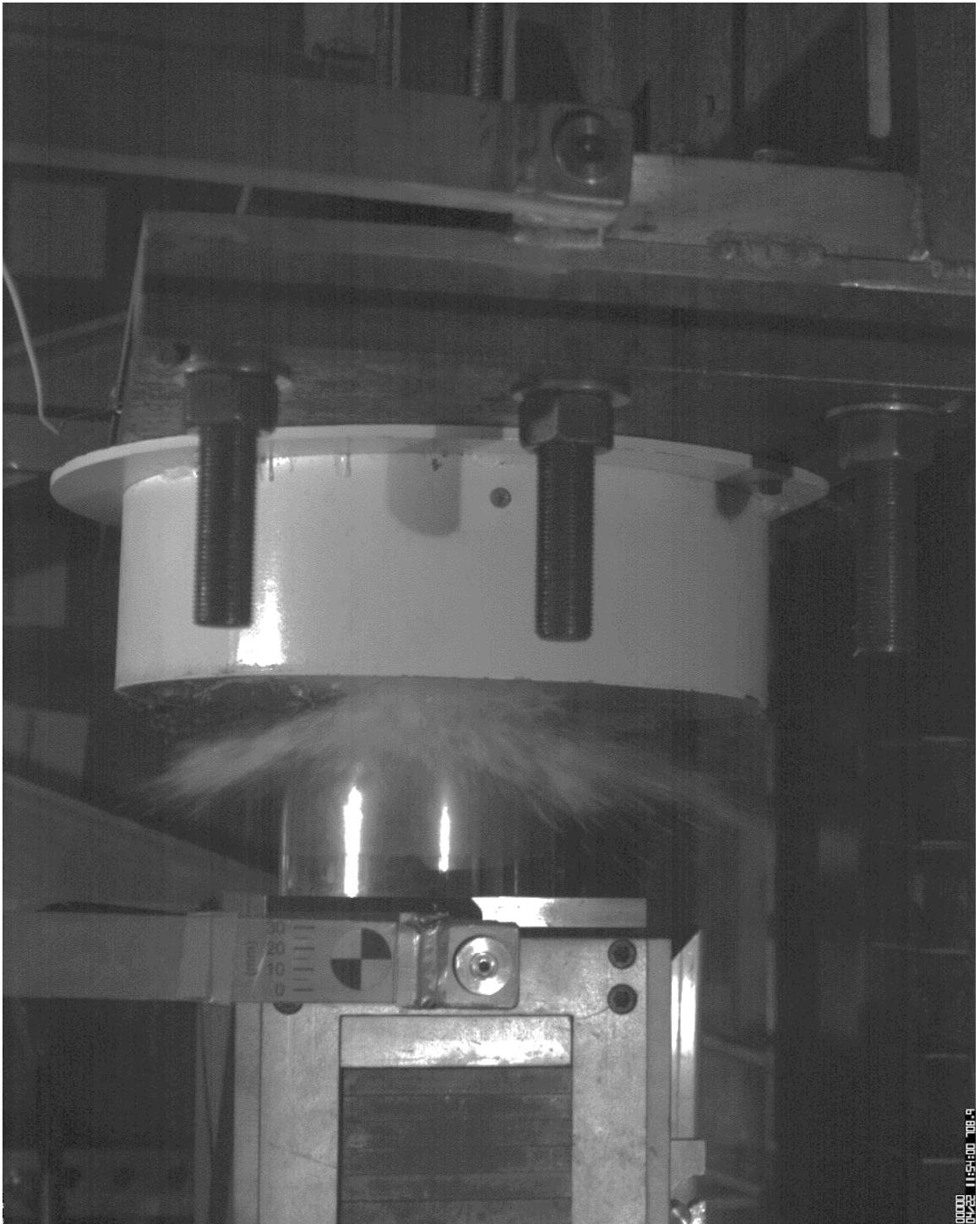


Figure A2-11. Test No. 24 - Frame 399

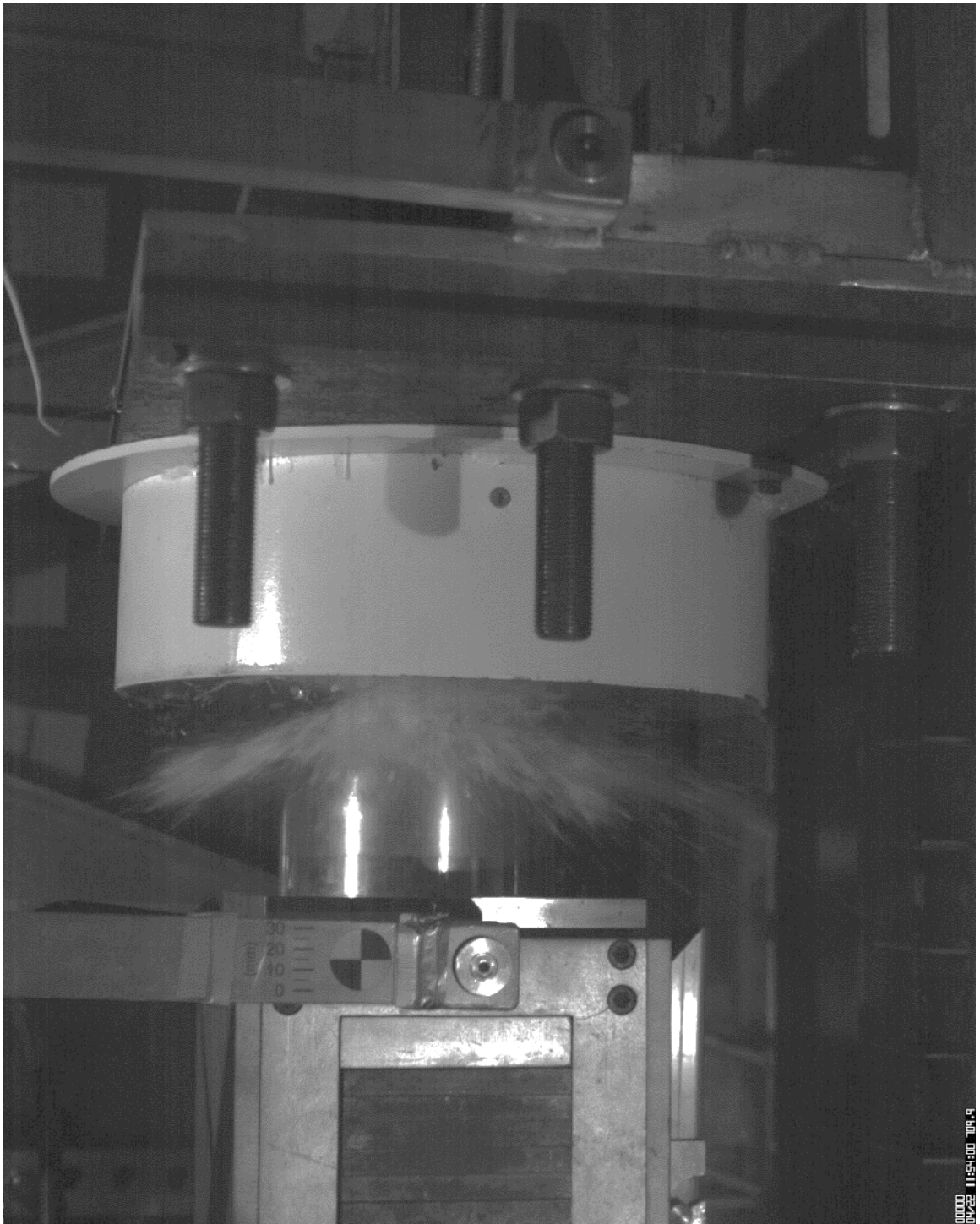


Figure A2-12. Test No. 24 - Frame 400

Appendix 3

High Speed Video – Velocity estimation

Processing the video is done in several steps:

- 1) Identify the point of contact. This often occurs between two frames in which case the last frame with no contact is used as the end frame for velocity calculations. This is illustrated below in Figure A3-1 and Figure A3-2. Frame 361 shows no signs of contact whereas 362 clearly shows contact.



Figure A3-1. Test No. 44 - Frame 361

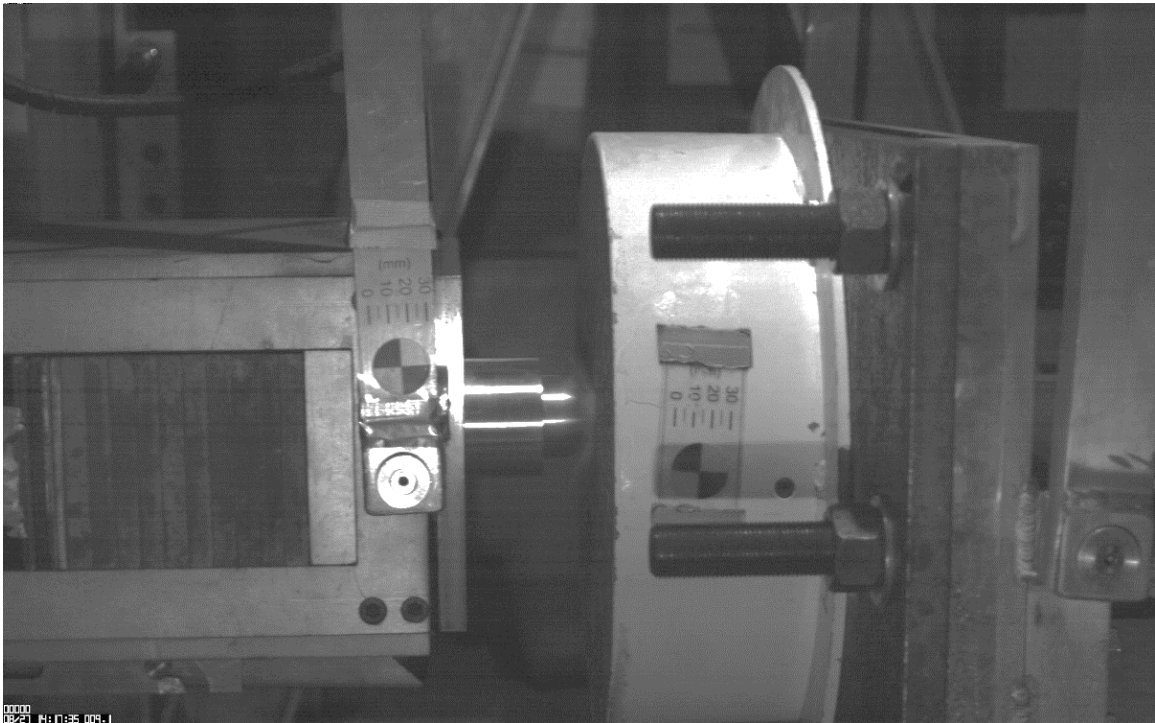


Figure A3-2. Test No. 44 - Frame 362

- 2) A scale is set using scales that are adhered to the pendulum. Then the video is reversed to several frames before contact. Using the pixels in the video a displacement is established.

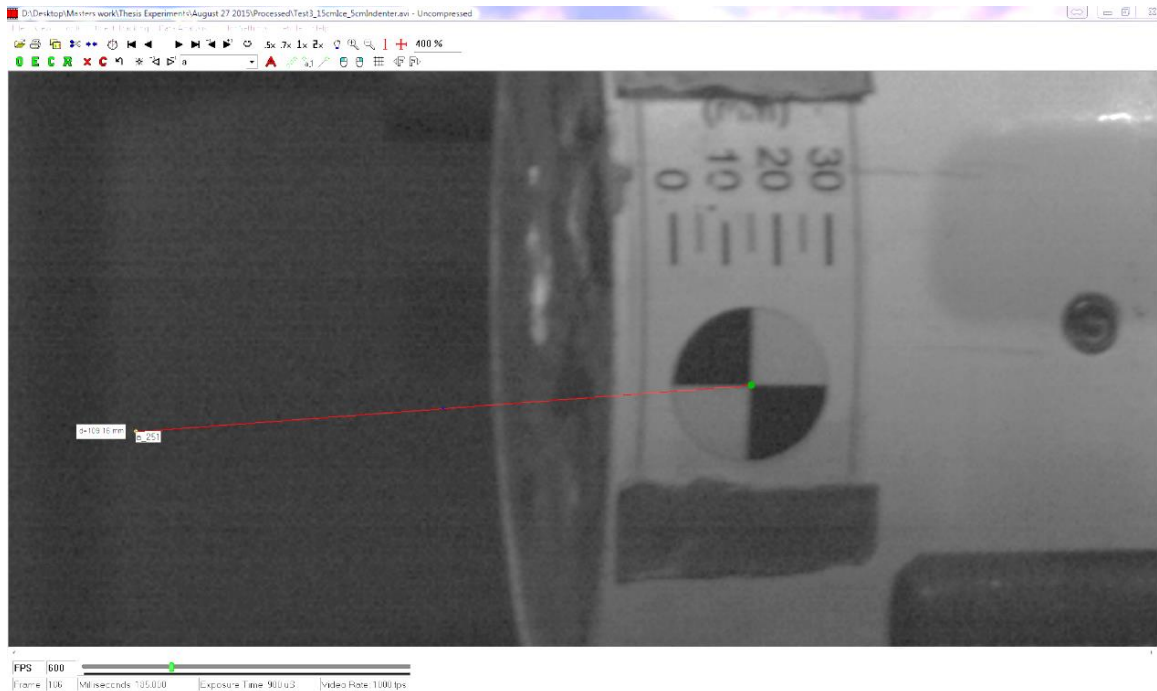


Figure A3-3. On Screen measurement

Knowing the camera film rate (1,000 FPS) and the distance moved over the number of frames counted, a velocity for each carriage just before impact can be estimated. The two estimates are added together to get the contact velocity.

Appendix 4
Laboratory check sheet

Test Set-up

Weight of ice samples known?

- T1: 35cm \varnothing X 30cm = ~33 kg
- T2: 35cm \varnothing X 11cm (tall holder) = ~14.817 kg
- T3: 35cm \varnothing X 11cm (short holder) = ~13.87 kg
- T4: 25cm \varnothing X 30cm = ~22.479 kg
- T5: 25cm \varnothing X 11cm (tall holder) = ~11.863 kg
- T6: 25cm \varnothing X 11cm (short holder) = ~9.797 kg
- T7: 15cm \varnothing X 30cm = ~8.015 kg
- T8: 15cm \varnothing X 11cm (tall holder) = ~4.416 kg
- T9: 15cm \varnothing X 11cm (short holder) = ~3.763 kg

Ensure Cannon camera is charged and on tri-pod

Get electro magnet driver and plugged in

Get High Speed Camera and tri-pod

Get HS Camera red cable

Get 2 LED construction lights

Install sphere

Check HS camera

- Fstop: 2.8
- Zoom out all the way
- Focus on position circle @ 400% zoom, adjust focus until clear, reset to 50% zoom.
- Speed: 1000 fps
- Exposure time: 900 μ s
- Gain: 900
- Offset: 8

Check data acquisition system

Pre-test checklist

- Download camera video from previous test and check
- Weights adjusted according to test
- T1: 35cm Ø X 30cm = 0 kg
 - T2: 35cm Ø X 11cm (tall holder) = +~18.183 kg
 - T3: 35cm Ø X 11cm (short holder) = +~19.13 kg
 - T4: 25cm Ø X 30cm = +~10.521 kg
 - T5: 25cm Ø X 11cm (tall holder) = +~21.137 kg
 - T6: 25cm Ø X 11cm (short holder) = +~23.203 kg
 - T7: 15cm Ø X 30cm = +~24.985 kg
 - T8: 15cm Ø X 11cm (tall holder) = +~28.584 kg
 - T9: 15cm Ø X 11cm (short holder) = +~29.237 kg
- Open pendulum to widest brake position and disengage magnets
- HS Camera positioned and focused.
- HS Camera is set and ready to trigger.
-
- Get ice and install
-
- Place ice side position indicating circle
- Pendulum carriages at 45 degrees (by Phone).
- Data acquisition system running
- HS Camera lens cap is off.
- Safety latches released
- DAC recording, (wait for confirmation)
 - Cannon camera recording in slow motion.
 - HS camera triggered

Notes:
